A THEORETICAL STUDY OF THE REACTION $N^+ + H_2 = NH^+ + H$

by

Martin Andrew Gittins

This dissertation is submitted in fulfilment of the requirements of the degree of Doctor of Philosophy of the University of Warwick.

The research presented here was performed in the School of Molecular Sciences, University of Warwick.

March 1978

ACKNOWLEDGEMENTS

I wish to thank my supervisor, Dr. D.M.Hirst, for his help and advice during my period of study. I also wish to thank various members of the School of Molecular Sciences, both past and present, for helpful discussions and advice, the University of Warwick Computer Unit for the provision of computing facilities and for use of a Qume printer on which this dissertation was produced. The provision of a studentship for myself, and grants of computer time at the Rutherford Laboratory to my supervisor, by the Science Research Council, is gratefully acknowledged. Finally I wish to thank my wife for her support and encouragement, without which this dissertation would not have been completed.

DECLARATION

The work described here has not been submitted previously in respect of any degree or qualification. Some of the configuration interaction energies used in the diagrams and included in Appendix B were calculated by Drs. D.M.Hirst and M.F.Guest.

Table of Contents

List of Figures

The figures are bound following the pages indicated.

List of Tables

The tables follow the pages indicated

List of Tables

The tables follow the pages indicated

ABSTRACT

The research described in this dissertation is an attempt to investigate the triatomic ion-molecule reaction $N^+(H_2,H)NH^+$ using current theoretical techniques. The aim of the work is twofold: to evaluate the current techniques for an ion-molecule reaction; and to clarify some aspects of this interesting reaction.

The investigation consists of three main areas. the calculation of a potential energy surface, the fitting of an analytical function to that surface, and calculation of the reaction dynamics using the function fitted.

The potential energy surface was calculated by both Unrestricted Hartree Fock (UHF) method and a configuration interaction (CI) method. The results of these calculations show that a route is available to the deep potential well which involves no potential barrier. The method of diatomics - in - molecules (DIM) is used to try to reproduce the CI results, with poor success.

Various methods of surface fitting are discussed, as well as the functional forms used. It is shown that one method (Marquartd's) yields a good fit with the function proposed by Sorbie and Murrell [101]. The problems involved in the use of spline interpolation are described.

Finally the results of classial trajectory calculations using the best surface obtained are presented, and qualitative agreement with the experimental results of Fair and Mahan [27] obtained. This suggests that the conical intersection which occurs for NH_2^+ may not be as important as Fair and Mahan suggest.

CHAPTER 1.

Introduction and Experimental results

1.1 INTRODUCTION

One of the ultimate aims of theoretical chemistry is to describe chemical reactions accurately. In recent years, a great deal of development has taken place in this area with the introduction of theoretical techniques for calculating reaction dynamics. This has been enhanced by the enormous increase in computing power available, and it is now possible to compute potential energy hypersurfaces to reasonable accuracy. However, accurate ab initio surfaces with more than three dimensions are still beyond present day capabilities.

Coupled with this there has been an increase in the range and refinement of experimental techniques, especially in the area of molecular beams.

In order to calculate the dynamics of a chemical system it is first necessary to calculate the potential energy hypersurface for the processes involved. To do this to "chemical accuracy", i.e. close to Hartee-Fock limit and full configuration interaction (CI), requires a great deal of computer time, and only recently have such calculations become possible. The pointwise surface generated in this way can not be used directly, but must either be reproduced by some analytical function, or some interpolation scheme used. This is necessary in order to be able to calculate the potential and derivatives at any point on the surface. Some techniques for performing this, sometimes difficult,

feat are discussed in Chapter 3. The final stage is actually to calculate the dynamics on this surface. The Schrodinger equation is not solvable for reactive scattering except for very unrealistic potentials. and so approximations and/or numerical methods are used. For "averaged" quantities such as total cross section, the use of classical mechanics has proved very successful. A wide range of systems have been studied using classical trajectory methods, including $H+H_2$ [39,53,48 and many others], H^++H_2 [56], H^++D_2 [107], $F+H_2$ [75,50,87, 76,74], $F+D_2$ [5], $Cl+H_2$ [1], $Ar+H_2$ [7], Li^++H_2 [59], Ar^++H_2 [109], $H+HF$ [115], $H+Br_2$ [9], $D+F_2$ [116], H_2^++He [114], Cl_2+HCl [1], $Cl+HI$ [80], $K+NaCl$ [58], $Na+Li_2$ [113], HeH^++H_2 [73], $Ar+CO_2$ [39], Br+M+Br [18,19], I_2^* [104], $K+CH_3I$ [60,52].

The aim of the work described in this dissertation was to evaluate the application of current techniques to a simple three atom ion-molecule reaction. The reactions considered for close study, apart from $N^+(H_2,H)NH^+$, included such reactions as $H^+(H_2,H)H_2^+$, $O^+(N_2,N)NO^+$, $Ar^+(H_2$ and $H)ArH$, $C^+(H_2,H)CH^+$. The $N^+(H_2,H)NH^+$ reaction was chosen for two reasons. Firstly it had been studied experimentally [34], and appeared to show interesting kinetics. Secondly the fact that NH_2^+ is a stable gaseous ion, isoelelectronic to carbene (CH_2^+), means that the potential surface is intrinsically interesting.

Ion molecule reactions have some unique features that may or may not be adequately handled by classical trajectory techniques. Of these the main feature is that they usually have no activation barrier, and frequently proceed via a meta-stable intermediate (i.e. a long-lived collision complex). It was not known if this was the case for NH_2^+. They also, of course, have long-range attractive forces that tend to make the reaction cross section larger, at low relative energies, than comparable neutral reactions.

1.2 EXPERIMENTAL RESULTS

The simplest form of molecular beam experiment consists of two molecular beams arranged so that the beams intersect, and a detector sensitive to one or more of the reactant or product species. The detector is mobile, so that the distribution of scattered particles may be determined. The entire apparatus is maintained at high vacuum (typically 10^{-7} torr). In practice some form of velocity selection is nearly always used for at least one of the beams. Increasingly, the reactant molecules in the beams are being selected to be in very precise states. Also the electronic state of the product is occasionally determined, see for example Cruse et al.[21].

For the case of NH_2^+ the experimental technique used by Gislason et al.[34] was somewhat different from that described above. The primary beam consisted of N^+ ions, but the secondary beam consisted of a scattering cell containing hydrogen gas. The N^+ ions were produced by electron impact on N_2, giving predominantly the ^3P state. The product ions, NH^+, were detected by an electrostatic energy analyzer with a quadrupole mass filter and an ion-counter.

The experiment was carried out at twelve relative energies ranging from 2.52 to 8.18 eV. The velocity spectra of the product ions were measured in the initial direction of the ion beam. At all energies two velocity peaks were found, an intense peak at a velocity greater than the centre of mass, and a small peak at a velocity below that of the centre of mass. The intense peak corresponds to forward scattering, and the small peak to backward scattering. For two energies, 3.98 and 5.01 eV, complete velocity vector distributions were measured, and from these contour maps produced showing product intensity in centre-of-mass

co-ordinates. This showed that the differential cross sections are strongly peaked in the forward direction.

This type of behaviour indicates that the reaction proceeds via a direct mechanism rather than a collision complex. Gislason et al. also note that the reaction cross section, although not explicitly measured, seemed smaller than the comparable reaction: $Ar^+(D_2,D)ArD^+$.

Fair and Mahan [27] later investigated the lower-energy , and more interesting , dynamics. They performed a number of experiments with relative energies ranging from 0.79 eV to 2.8 eV. Full velocity vector distributions were determined at all energies, and six of these are reproduced in their paper. At 2.8 eV the reaction is strongly forward peaked, as has been previously observed. However, as the relative energy is reduced, this peak moves away from the forward direction until, at 0.79 eV, the scattering is virtually symmetric, with the product intensity peak occuring at the centre of mass velocity. They tentatively suggest that this is due to the reaction proceeding via a long-lived collision complex at low-energies. This argument is supported by a correlation diagram showing the expected deep well for the $^3B_1$ state of NH_2^+. They also point out that a conical intersection is to be expected for the $^3B_1$ and $^3A_2$ states, and that the direct mechanism observed at higher energy may be due to transitions occuring to the higher surface.

In a third paper Farrar, Hansen and Mahan [28], used a microwave discharge to produce the N^+ ions. This is known to produce only 3 % of N^+ in excited states, as opposed to the electron impact method used previously which produced significant amounts of ^1D and ^1S states. Using more sensitive apparatus, the electron-impact spectrum was shown to be less symmetric than before, and to consist of two peaks,

one symmetric and the other peaked in the forward direction. Using microwave discharge (at 0.72 eV) the forward peak disappeared completely leaving a totally symmetric distribution.

The question then arises as to how much of the asymmetric distribution is caused by diabatic effects and how much by the dynamics of the lower adiabatic surface.

CHAPTER 2.

Potential Energy Surface for NH_2^+.

2.1 QUALITATIVE SURFACE FOR NH_2^+

2.1.1 Introduction

To understand the dynamical surface for NH_2^+ fully it is necessary to consider in detail the electronic states of the atoms and diatomics involved, not only because these constitute the asymptotic limits of the surface, but also because some methods of calculation use the diatomic states as a basis for calculating the triatomic surface (see section II.4).

For this reason this section is divided into three parts: the atomic states, the diatomic states, and, finally, the triatomic states.

2.1.2 Atomic States

The most important atomic constituent in the NH_2^+ surface is the nitrogen cation (N^+). The ground state of this cation is a ^3P state. Two other states are of sufficiently low energy to be important, the ^1D and ^1S. The relative energies of these states are given in table II.1.1.

Similarly, there are two low lying states of atomic nitrogen. The ground state being a ^4S state, the atomic energies relative to $N^+(^3P)$ are shown in table II.1.1.

The energy difference between N and N^+ is, of course, the

Table II.1.1

Atomic energies for N and N^+.

$N^+(^3P)$	-	0.0
$N^+(^1S)$	-	0.08937
$N\ (^4S)$	-	-0.51584
$N\ (^2D)$	-	-0.41671

(all energies in a.u.)

ionization potential and the experimental value of this is [72]:

0.53436 (a.u.) [117,345 cm^{-1}]

For hydrogen only the ground state, (^2S), is of sufficiently low energy to be of importance.

2.1.3 Diatomic States

Four diatomics are of interest, viz: NH, NH^+ , H_2 , H_2^+ .

2.1.3.1 NH

NH has to combine with a proton to form NH_2^+ . Therefore, since the proton can not affect the electronic spin state, and we are only interested in the triplet states of NH_2^+, only the triplet states of NH are discussed here.

Following the normal rules [61, page282] one predicts a $^3\Sigma$ from the ^4S state of N, a $^3\Delta$, $^3\Pi$, and $^3\Sigma^-$ from the ^2D, and a $^3\Pi$ and $^3\Sigma^+$ from the ^2P. A correlation diagram for these states is shown in fig. II.1.1.

2.1.3.2 NH^+

Since this combines with a hydrogen radical to form NH_2^+, we are interested in doublet and quartet states of NH^+. Both states formed from N + H^+ and N^+ + H must be considered. A list of the low-lying states of NH^+ is given in table II.1.2., and a correlation diagram in fig. II.1.2.

2.1.4 Triatomic States

The potential energy surface for any triatomic system is

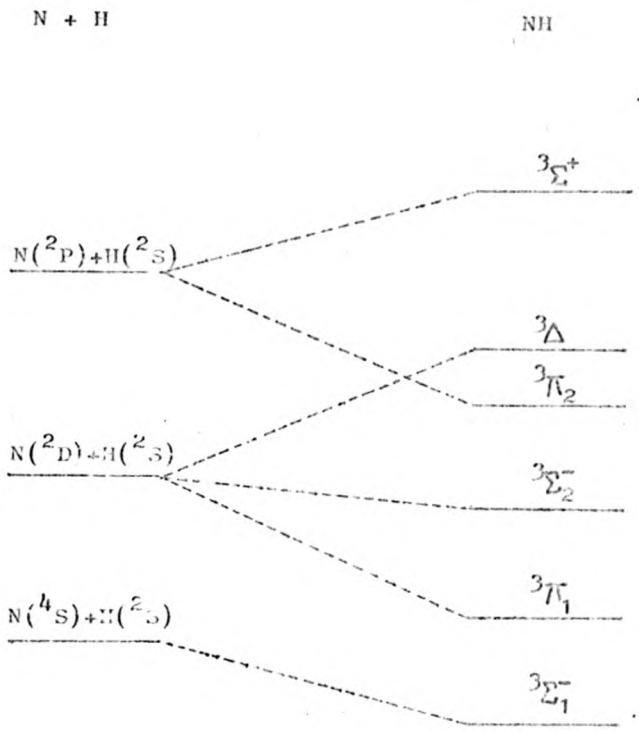

FIG. II.1.1. Correlation diagram for low lying triplet states of NH.

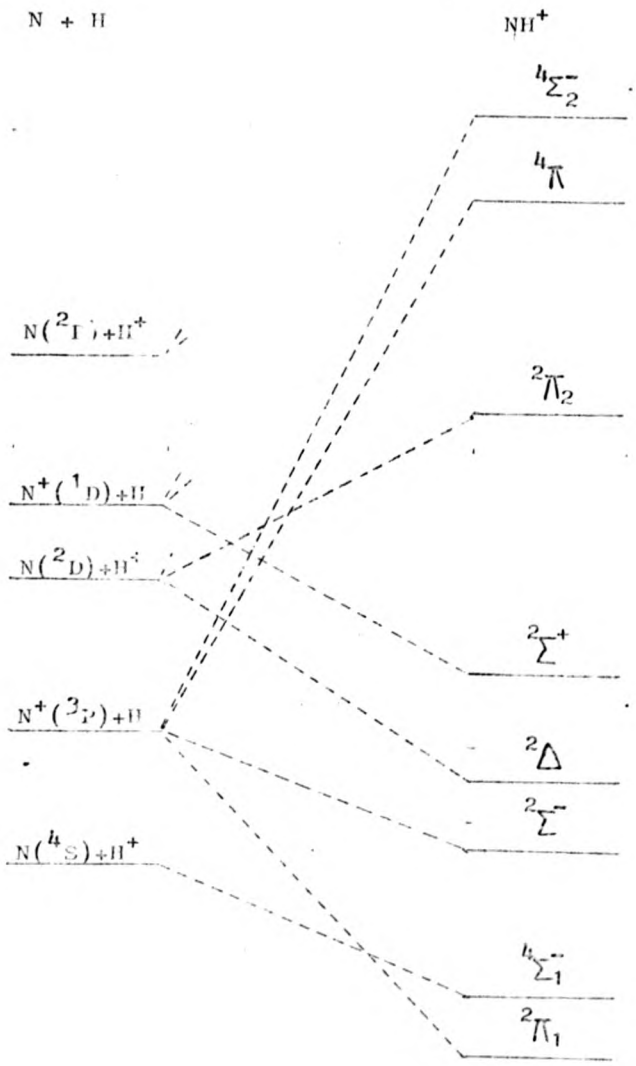

FIG. II.1.2. Correlation diagram for low-lying states of NH^+.

Table II.1.2

Low-lying states of NH^+

State	N	H
$a\,^4\Sigma^-_1$	$N(^4S)$	H^+
$X\,^2\Pi_1$	$N^+(^3P)$	$H(^2S)$
$A\,^2\Sigma^-$	$N^+(^3P)$	$H(^2S)$
$B\,^2\Delta_1$	$N(^2D)$	H^+
$C\,^2\Sigma^+$	$N^+(^1D)$	$H(^2S)$
$D\,^2\Pi_2$	$N(^2D)$	H^+
$E\,^4\Sigma^-_2$	$N^+(^3P)$	$H(^2S)$
$^4\Pi$	$N^+(^3P)$	$H(^2S)$
$^2\Pi_3$	$N(^2P)$	H^+
$^2\Delta_2$	$N^+(^1D)$	$H(^2S)$
$^2\Pi_3$	$N^+(^1D)$	$H(^2S)$
$^4\Sigma^-_3$	$N^+(^5S)$	$H(^2S)$

complicated by the various symmetries involved. A triatomic system can assume configurations that belong to four possible point groups, i.e. $D_{\infty h}$, $C_{\infty v}$, C_{2v} and C_s.

In triatomic calculations most workers concentrate mainly on the C_{2v} and $C_{\infty v}$ symmetries, mainly because they show the most interesting behaviour. However, from a dynamic point of view, the C_s symmetry is the most important as any real system will belong only transiently to another point group .

For C_{2v} geometries the approach of a nitrogen ion in the (^3P) state to a hydrogen molecule gives rise to three triplet states, viz: $^3B_1$, $^3B_2$, $^3A_2$. These arise from the three possible orientations of the ^3P state of N^+ relative to the hydrogen molecule. As the N^+ approaches the hydrogen these states separate in energy.

The relationship of these states is best understood by means of a correlation diagram linking the united and separated atoms. Such a diagram is shown in fig. II.1.3. The configurations of the three asymptotic states are shown. It is apparent that the $^3B_1$ and $^3B_2$ states are predicted to be repulsive due to the occupation of the $4a_1$ orbital and the $^3A_2$ state is predicted to be attractive.

Although, from this diagram, it would appear that the $^3A_2$ state is the ground state, the b_2 orbital is predicted to be lower in energy, at short internuclear distances, than the $3a_1$. Thereby giving rise to a $^3B_1$ ground state with the configuration:

$$1a_1^2\ 2a_1^2\ 1b_2^2\ 3a_1^1\ 1b_1^1 \qquad [II.1.1]$$

This state correlates with the $N^+(^2D) + H_2(^2\Sigma_g^+)$ at infinite separation. Therefore, for C_{2v} symmetry the equilibrium ground state is

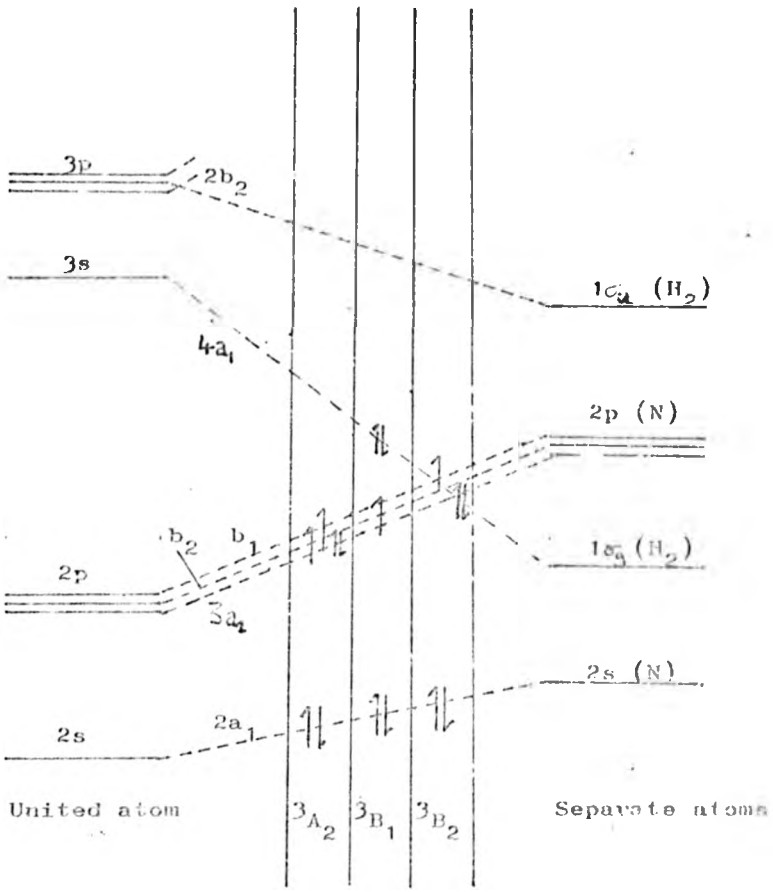

FIG. II.1.3. Correlation diagram of separated and united orbitals for NH_2^+, C_{2v} geometries. (configurations of lowest triplet triatomic states are also shown.)

Fig. II.1.4. Correlation of NH_2^+ triplet states, for various geometries. (dotted lines denote behaviour for C_s geometries.

only accessible via an avoided crossing of two $^3B_1$ states.

If the symmetry is now changed to C_s, the B_1 and A_2 states both become $^3A''$. This means that, at the point where the $^3B_1$ and $^3A_2$ states cross, under C_s symmetry this is an avoided crossing, i.e. this is a conical intersection. As observed above, in a real system it is the C_s symmetry that dominates the dynamics. Therefore any feasible route to the equilibrium configuration is likely to follow a path around this conical intersection.

When the nitrogen is at the mid point of the two hydrogen atoms, then the molecule becomes linear with a symmetry of $D_{\infty h}$. Then the a_1, and $1b_1$ orbitals become a degenerate 1π, and the $^3B_1$ state becomes a $^3\Sigma_u^-$, the configuration of which is given by eqn. [II.1.2].

$$1\sigma_g^2\ 2\sigma_g^2\ 3\sigma_u^2\ 1\pi_x^1\ 1\pi_y^1 \qquad \text{[II.1.2]}$$

If one hydrogen atom is now displaced, the configuration becomes $^3\Sigma^-$. However, this configuration correlates with $NH + H^+$, rather than $NH^+ + H$, which correlates with the configuration given by eqn [II.1.3].

$$1\sigma^2\ 2\sigma^2\ 3\sigma^1\ 4\sigma^1\ 1\pi_u^1\ 1\pi_g^1 \qquad \text{[II.1.3]}$$

This lack of correlation becomes important when performing configuration interaction calculations.

The other possible symmetry for approach of N^+ to H_2 is a linear $C_{\infty h}$ conformation (NHH). For this case, the symmetries and configurations are the same as the HNH conformation, although the energies should be higher.

A correlation diagram for the various triplet states is shown in Fig. II.1.4. This is largely derived from that given by Fair & Mahan [27].

2.2 QUANTITATIVE SURFACE FOR NH_2^+ (Unrestricted Hartee Fock)

2.2.1 Introduction

Two sets of calculations were performed for NH_2^+. Firstly, a mesh of points was generated to cover the entire reactive surface, and the energy calculated at each point using the unrestricted Hartree Fock method (UHF), Then specific sections of the surface were selected, and configuration interaction (CI) calculations performed for these sections. The UHF calculations were performed using the ATMOL 2 program [42], and the CI calculations using ATMOL 3 and MUNICH CI programs as implemented at the Atlas Computing Division of the Rutherford Laboratory. The help of Dr. M.F.GUEST with the CI calculations is gratefully acknowledged.

2.2.2 Theory

The unrestricted (UHF) version is formally the simplest form of Hartree Fock theory, and is an open shell method which includes some correlation energy. In UHF theory the molecular wavefunction, M, is constructed from a Slater determinant of one electron spin orbitals, P_i.

$$M = | P_1 P_2 .. ..P_n | \qquad [II.2.1]$$

The desired wavefunction is obtained by minimising eqn [II.2.2].

$$E_o = < M | H | M > / < M | M > \qquad [II.2.2]$$

with respect to changes in the P_i.

From this condition, and considering infinitesimal changes in

the P_i, it is possible to derive the Hartree Fock equation [II.2.3]. See for instance Hurley [49].

$$F_o \cdot P_i = e_i \cdot P_i \qquad \text{[II.2.3]}$$

where F_o is the Fock operator given by eqn [II.2.4].

$$F_o = -0.5 \cdot \nabla^2 - \sum_a z_a/r_a + \sum_{i=1}^{n}(J_i - K_i) \qquad \text{[II.2.4]}$$

where J_i and K_i are the standard Coulomb and Exchange integrals respectively.

Eqn [II.2.3] does not however offer a one step solution because the Fock operator is itself a function of the P_i. The normal practice is to generate an approximate solution, P_i^o, apply the Fock operator to obtain an improved solution, P_i^1, and repeat the process until some convergence criterion is satisfied.

Eqn [II.2.3] applies to the alpha and beta spin orbitals separately in the unrestricted theory. This means that the spatial components of the resulting orbitals are different for the alpha and beta spin. Therefore the resulting molecular wavefunction is not, in general, an eigenfunction of the S^2 operator. If spin eigenfunctions are desired then the normal practice is to annihilate the higher spin states. This has not been performed for any of the UHF calculations described here. This disadvantage is more than offset by the fact that UHF wavefunctions do not dissociate incorrectly, as is the case for many RHF wavefunctions. The different spatial components also means that some correlation energy is recovered.

In ATMOL2 and 3 UHF program the Fock matrices, for alpha and beta spin, are modified before diagonalization.

This modification involves multiplying those elements that

connect occupied and virtual orbitals by a constant (damping factor). Similarly those concerned only with virtual orbitals have a constant added to them (level shifter). These modifications are designed to enhance the convergence properties of the UHF equations. It can be shown that, for sufficiently large values of the level shifters, convergence can be guaranteed [97].

2.2.3 Basis set

The choice of basis set for an ab-initio calculation is quite critical ,especially if the computer power available is limited. The ATMOL program uses a contracted Gaussian basis set, and there are four possibilities for the selection of the set. These are,

a) use the provided expansion of Slater type orbitals (STO's),

b) use some published contraction,

c) use a unique contraction optimised for the problem at hand,

d) use the provided Slater orbitals. Of these possibilities the last was rejected because of the time required to generate such an optimised set, and the aim was not to produce the best possible basis set. The best published small basis set for nitrogen and hydrogen would appear to be those of Dunning. The basis set chosen has a 9s5p/4s2p contraction for nitrogen, and a 4s/3s contraction for hydrogen.[124]

A limited comparison was made between this basis set and the ATMOL STO basis using a 12s5p/2s1p contraction for nitrogen, and 4s/1s for hydrogen. The STO basis, therefore, had more primitive functions, but was markedly more contracted. The results for two typical points are shown in table II.2.1. It was soon apparent that the greater flexibility of the Dunning basis was vastly superior to a STO basis of this size. The Dunning basis was therfore used.

Table II.2.1

Comparison of Dunning and Atmol STO basis sets.

$R(NH_a)$	$R(NH_b)$	HH	E(D)	E(STO)	Δ
2.0	3.0	5.0	-55.12336	-54.98442	0.13894
3.0	3.0	6.0	-55.04174	-54.90065	0.14109

Where E(D) = Calculated potential energy using Dunning basis,

E(STO) = Calculated potential energy using STO basis,

Δ = E(STO)-E(D).

All values are in a.u..

Table II.2.2

Energy of NH_2^+ with $R(NH_a)$=4, R(HH)=5

$R(NH_b)$	E	Charges:N	H_a	H_b
3.9	-54.93673	+.28	+.06	+.66
4.0	-54.91905	+.03	+.49	+.49
4.1	-54.93328	+.28	+.67	+.05

One failing of the basis set used was the lack of polarization functions. A limited investigation into the use of polarization functions was made, and the improvement in energy did not appear to warrant the overheads involved. Recently, other workers have shown that polarization functions can have a marked effect on the form of the resulting potential surface[81], but this was not appreciated at the time.

2.2.4 Results

2.2.4.1 CONFIGURATIONS STUDIED

The UHF surface was calculated with the intention of providing a starting point for trajectory calculations. The question then arose as to what distribution of points should be used to give the most suitable set of points for a fitting procedure or interpolation. The scheme chosen was to calculate the energy at all points satisfying the following conditions:

$R(NE_b), R(NE_e)$ = 1,2,3,4,5,6,7, or 8 a.u.

$R(HF)$ = 1, 1.5, 2, 3, 4, 5, 6, 7, or 8 a.u.

Minimum [$R(NE_e)$, $R(NE_b)$, $R(HF)$] < 5.5 a.u.

Plus any additional points deemed necessary or of particular interest.

The energies obtained are listed in Appendix A. The disadvantage of this scheme is that sections through the surface are rather poorly defined. However the distribution is reasonable over the entire reactive part of the surface, and not biased to lines of C_{2v} symmetry, or similar areas. This is highly desirable if the resulting set of energies is to be used for optimizing an analytical function or interpolation.

2.2.4.2 INTERPRETATION OF RESULTS

The complete set of UHF results obtained is given in Appendix A. The expectation value of the S^2 operator, and the symmetry type under C_s point group are shown along with the energy.

During the course of the calculations, stationary energies were frequently obtained which did not correspond to the ground state. These excited states, whilst of dubious quantitative accuracy, are extremely interesting, and are included both in the following discussion and appendix A.

The collinear approach of $N^+(^3P)$ to $H_2(^1\Sigma_g^+)$ is shown in Fig. II.2.1. for H-H distance of 2.0 a.u., As can be seen the curve has a shallow minimum at about 2.0 a.u. as would be expected. Similarly, the departure of H^+ from NH^+ also shows a shallow minimum (see fig II.2.2).

For C_{2V} symmetry the approach of N^+ is shown in fig. II.2.3. The splitting into the three separate states can be seen clearly in this diagram, and it is fairly apparent that only the $^3A_2$ state is attractive.

The situation, however, is made rather more complex if the variation of energy with H-H distance is considered. The behaviour of the $^3A_2$ and $^3B_2$ surfaces is shown in fig. II.2.4. It is apparent from this that there are two low-lying $^3A_2$ states. One of these, labelled IA_2 in the figure, correlates with $N^+(^3P)+H_2$, while the other, IIA_2, correlates to $N\ (^4S)+H_2^+$. The two states are shown as crossing in the diagram, whereas of course such a crossing is forbidden. As would be expected, the curve IIA_2 is very similar to the H_2^+ curve shown in fig. II.4.3. However, the IA_2 curve does not correspond to the true

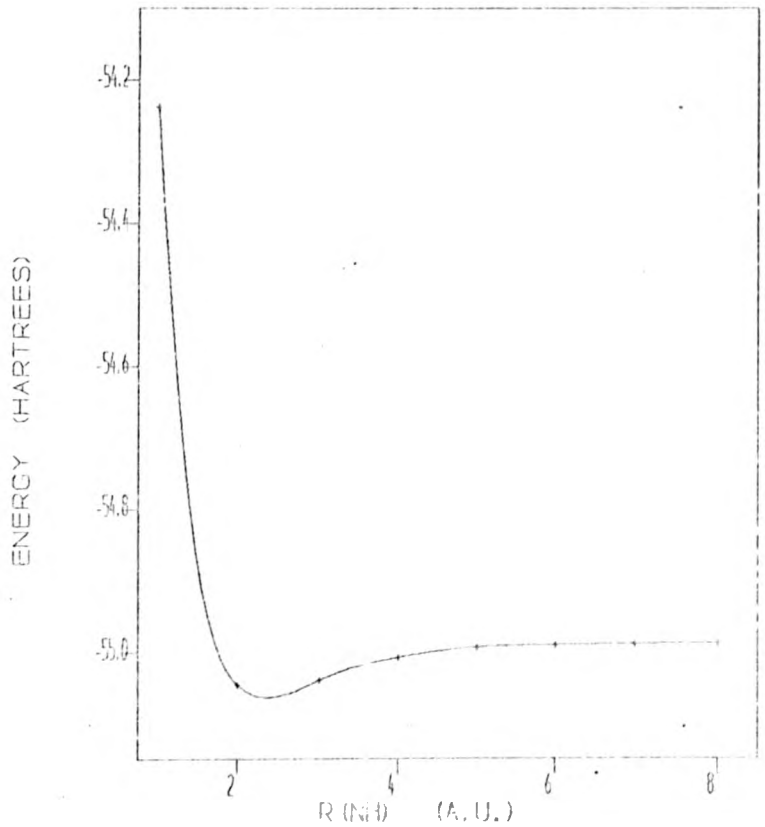

FIG. II.2.1. $E(NH_2)$ UHF VS. R(NH).
LINEAR N-H-H , H-H DISTANCE = 2.0 A.U.

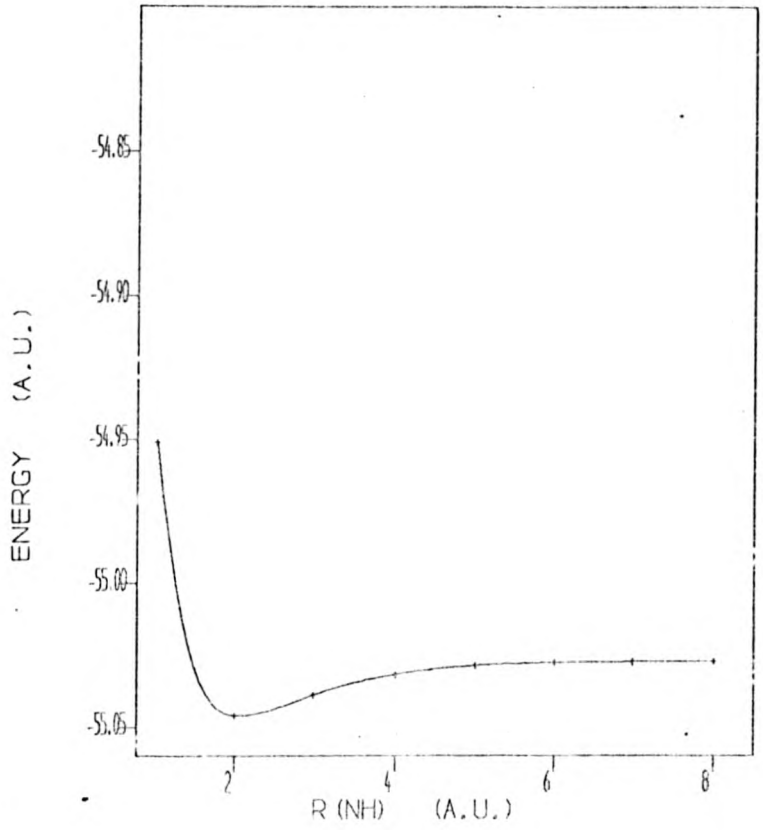

FIG. II.2.2 $E(NH_2')$ UHF VS. R (NH) ;

LINEAR H-H-N ; N-H DISTANCE = 2.0 A.U.

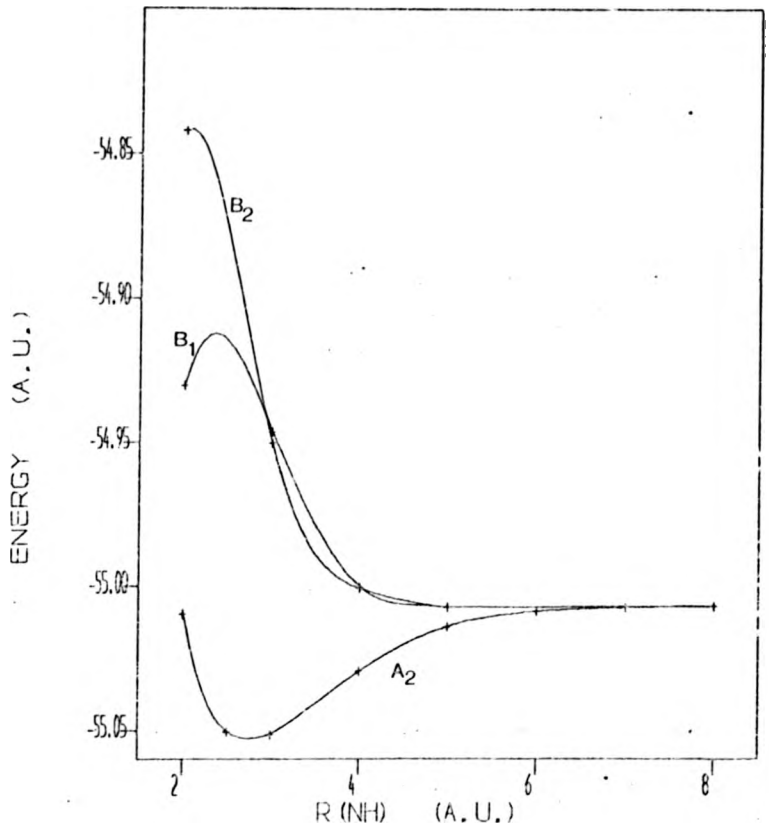

FIG. II.2.3 E(NH_2^*) UHF VS. R(NH); C_{2v} SYMMETRY; H-H DISTANCE = 2.0 A.U.

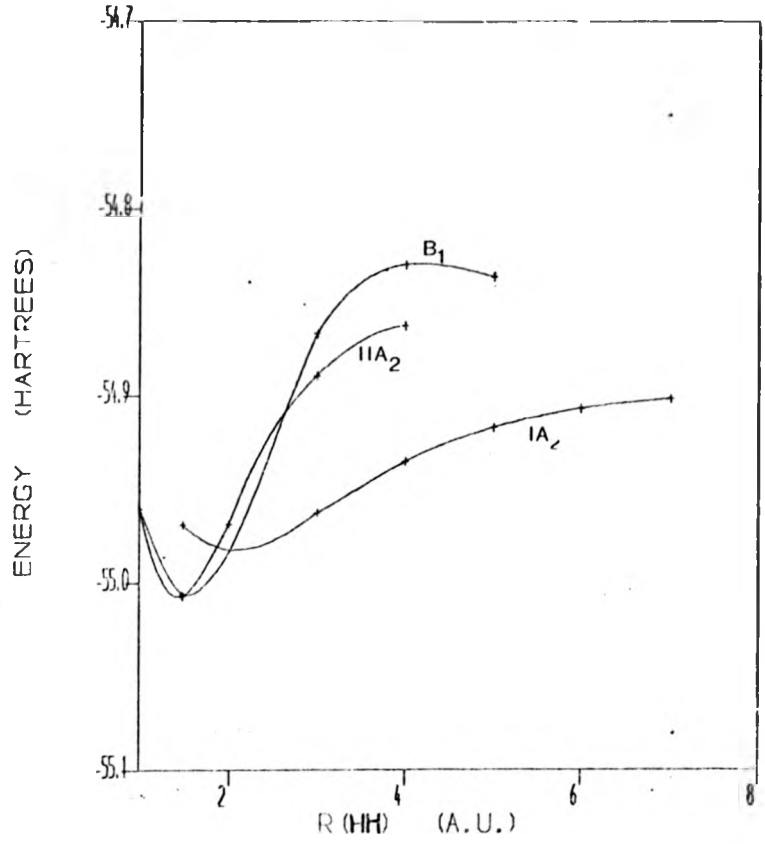

FIG. II.2.4 E (NH_2^+) UHF VS. R (HH) ; C_{2v} SYMMETRY ; N-H DISTANCE = 8.0 A.U.

dissociation of H_2 due to the failure of Hartee Fock theory. Estimation of the charge on the nitrogen from the population analysis reflect the different asymptotic states, with IA_2 having a nitrogen charge close to unity, and IIA_2 close to zero.

The net result is that at large NH distances an increase in the H-H distance causes massive charge transfer from the nitrogen.

As the N-H distance deceases, there is little change in the energy of the states until the N-H distance reaches about 4.0 a.u. At this point the IA_2 and IIA_2 states start to become indistinguishable for UHF calculation, and a new $^3B_1$ states appears at large H-N-H angles The situation is shown in fig. II.2.6, for N-H distance of 4.0 a.u.

It is in this region that one of the major failings of single determinant wavefunctions become apparent.

Consider the geometry with H-H and one N-H distance fixed at 5.0 and 4.0 a.u. respectively, and the other N-H distance varying either side of 4.0 a.u. Three points of this type are shown in Table II.2.2.

It is apparent that the energy at $R(NH_b)$=4.0 a.u. is approximately 0.016 hartrees higher than the adjacent C_s points. Looking at the approximate charges shown the reason is fairly apparent. For C_{2V} symmetry the single determinant is constrained to reflect that symmetry, and the two hydrogens must be equivalent. They therefore carry the same charge. For non-C_{2V} symmetry this does not apply and the charge can be distributed in a more reasonable manner. This problem does not occur, however, for configuration interaction calculations. Those points that were believed to suffer from this failing were not included in the surface fitting described in Chapter III.

This type of effect has been noted before by Walker [111], and has been shown by him to be due to the energy of open-shell single determinant wavefunctions being invariant with respect to a unitary transformation of the orbitals. Walker gives as an example BF_3^+, which at D_{3h} symmetry gives lower energy than at adjacent C_{2V} symmetries. Gregory [40], discusses a more general case where discontinuities are found in surfaces due to a change in configuration. Such discontinuities may occur in closed shell, a well as open-shell calculations.

At short NH distances the situation is completely different. Here the $^3A_2$ state is no longer the lowest in energy due to a deep well in the $^3B_1$ state around the linear H-N-H geometry. The variation of energy with H-N-H angle is shown in fig. II.2.5. This shows clearly the formation of meta-stable $[HNH]^+$ ions, analagous to the isoelectronic carbene (CH_2). Like carbene it is very difficult to decide if the equilibrium geometry is linear or slightly bent, given the very flat nature of the potential at large angles. The lowest potential calculated was in fact the linear geometry. However, no attempt was made to locate the equilibrium point accurately.

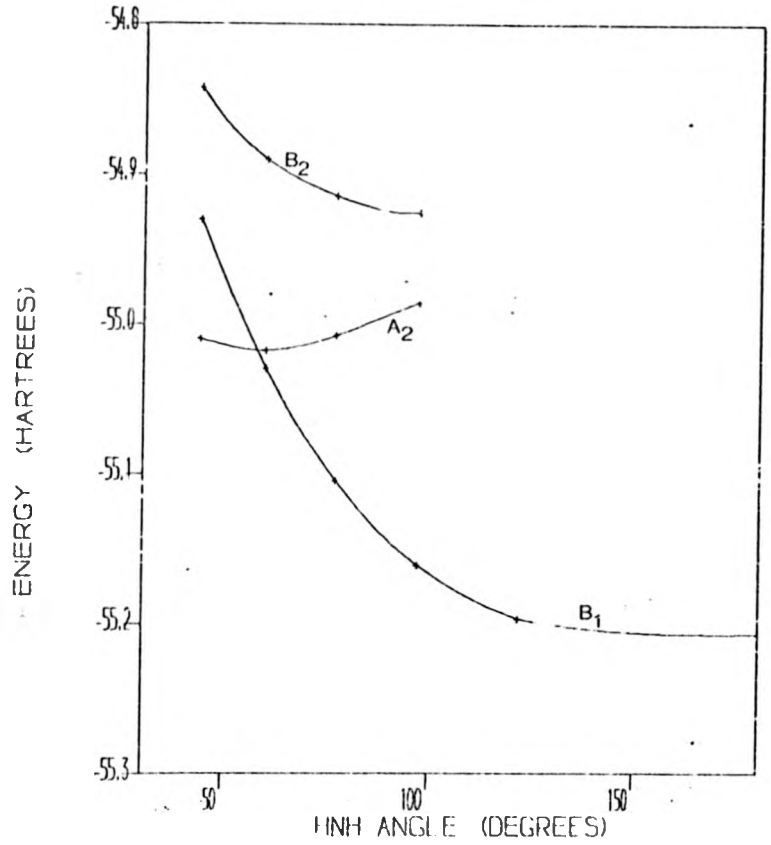

FIG. 11.2.5. $E(NH_2^+)$ VS. HNH ANGLE.

C_{2v} SYMMETRY , N-H DISTANCE = 2.0 A.U.

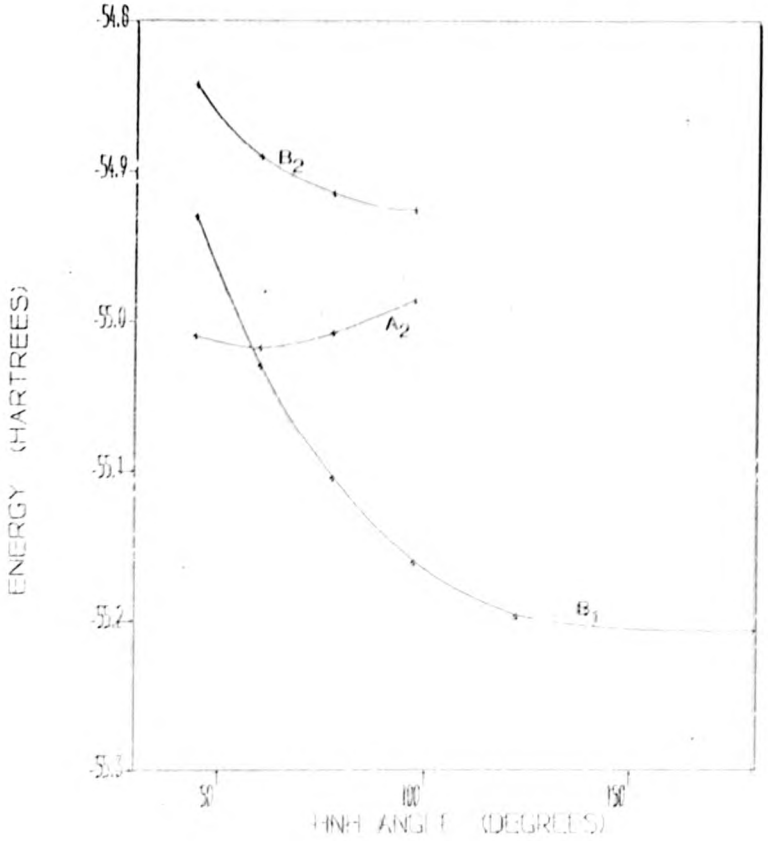

FIG. II.2.5. E(NH_2) VS. HNH ANGLE.

C_{2v} SYMMETRY, N-H DISTANCE = 2.0 A.U.

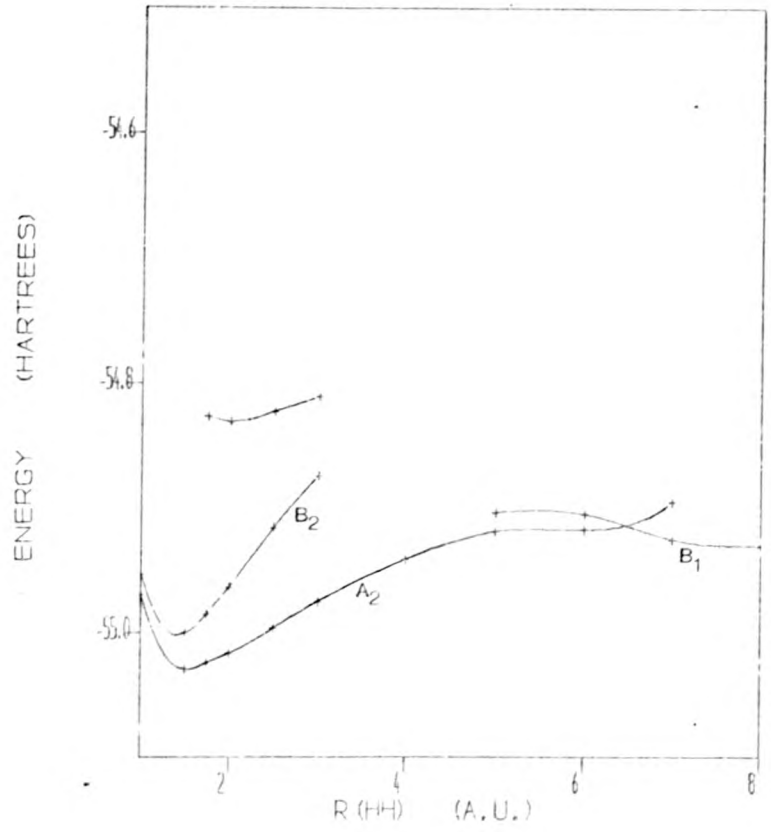

FIG. II.2.6 $E(NH_2^+)$ UHF VS. R(HH), C_{2v} SYMMETRY, N-H DISTANCE = 4.0 A.U.

2.3 QUANTITATIVE SURFACE FOR NH_2^+ (CI)

2.3.1 Introduction

In order to gain a better understanding of the various states involved in the NH_2^+ surface, as well as more accurate values for the potential energy changes involved, a series of calculations involving configuration interaction (CI) were performed. These calculations were performed in conjunction with Dr. M.F.Guest.

The aim of the CI calculations was somewhat different from the UHF as it was not intended to generate a grid of points suitable for fitting with some optimization technique, but rather to investigate specific features of the NH_2^+ surface.

Due to the lack of a readily available CI package at the time these calculations were planned some work was done on a CI computer program to interface with ATMOL2. This was advanced to the point at which small calculations could be performed. However the algorithms used were rather slow, particularly the integral transformation (see [23] for how it should be done). When a suitable CI package became available work was stopped, and all calculations were performed using the SPLICE suite.

2.3.2 Theory

The SPLICE system at the Rutherford Laboratory, performs CI calculations using bonded functions. If a bonded pair is defined by eqn [II.3.1].

$$[\phi_i,\phi_j] = \phi_i(1)\phi_j(2)[\alpha(1)\beta(2)-\alpha(2)\beta(1)].2^{-1/2} \qquad [II.3.1]$$

2.3 QUANTITATIVE SURFACE FOR NH_2^+ (CI)

2.3.1 Introduction

In order to gain a better understanding of the various states involved in the NH_2^+ surface, as well as more accurate values for the potential energy changes involved, a series of calculations involving configuration interaction (CI) were performed. These calculations were performed in conjunction with Dr. M.F.Guest.

The aim of the CI calculations was somewhat different from the UHF as it was not intended to generate a grid of points suitable for fitting with some optimization technique, but rather to investigate specific features of the NH_2^+ surface.

Due to the lack of a readily available CI package at the time these calculations were planned some work was done on a CI computer program to interface with ATMOL2. This was advanced to the point at which small calculations could be performed. However the algorithms used were rather slow, particularly the integral transformation (see [23] for how it should be done). When a suitable CI package became available work was stopped, and all calculations were performed using the SPLICE suite.

2.3.2 Theory

The SPLICE system at the Rutherford Laboratory, performs CI calculations using bonded functions. If a bonded pair is defined by eqn [II.3.1].

$$[\phi_i,\phi_j] = \phi_i(i)\phi_j(j)[\alpha(i)\beta(j)-\alpha(j)\beta(i)].2^{-1/2} \qquad [II.3.1]$$

$$\text{if } \phi_i \neq \phi_j$$

$$= \phi_i(1)\phi_j(j)a(i)\beta(j) \quad \text{if } \phi_i = \phi_j \ \ldots$$

where a(i) and b(i) are the alpha and beta spin orbitals. and an unpaired orbital by eqn [II.3.2]:

$$[\phi_i = \phi_i(1)\ a(i) \qquad \text{[II.3.2]}$$

Then a bonded function is described by eqn [II.3.3], where n is the number of electrons, p the number of unpaired orbitals, and A the antisymmetrizer.

$$M = A.[\phi_1,\phi_2][\phi_3,\phi_4]\ldots\ [\phi_{n-p-2},\phi_{n-p-1}][\phi_{n-p}\ldots[\phi_n \qquad \text{[II.3.3]}$$

This bonding technique is equivalent to the method of Rumer diagrams [93], and a linearly independent set can be generated by following the rules for constructing such diagrams.

Using bonded funnctions in this form the program goes through the normal stages of a CI calculation; generation of single and double excited states from the root function; calculation of the matrix elements; computing the eigenvalues and vectors; and finally analysing the results. Details of the methods used are given in the SPLICE manual [42].

2.3.3 Results

The results of all points on the potential surface are listed in Appendix B. They are listed according to the point group to which they belong. Some of the points listed here were calculated by Dr. D.M.Hirst or Dr. M.F.Guest.

2.3.3.1 C_{2v} GEOMETRIES

This is by far the most interesting point group, and a large number of calculations were made to elucidate the nature of the C_{2v}

surface.

For the $^3B_2$ state a root function of: $1a_1^2\ 2a_1^2\ 3a_1^2\ 1b_2^1\ 4a_1^1$ was used, giving 546 configurations, For $^3A_2$: $1a_1^2\ 2a_1^2\ 3a_1^2\ 1b_1^1\ 1b_2^1$ giving 505 configurations. For the $^3B_1$ state two root functions are required because the equilibrium state does not correlate with the reactants directly, but rather with $N(^2D) + H_2^+$. The two functions were the ground state:

$$1a_1^2\ 2a_1^2\ 1b_2^2\ 3a_1^1\ 1b_1^1$$

and the function which correlates with the reactants:

$$1a_1^2\ 2a_1^2\ 3a_1^2\ 1b_1^1\ 4a_1^1$$

giving a total of 659 configurations.

A cross-section of the entrance channel for C_{2v} geometries, is shown in fig. II.3.1. Compare this with the corresponding diagram for the UHF surface, fig. II.2.4. The two $^3A_2$ states apparent previously now only show as one state. Only the lowest eigenvalue was calculated for each symmetry representation, and so the behaviour of the higher $^3A_2$ state is unknown. The $^3A_2$ state will of course correlate to the $N^+(^3P)+ H_2$ state at infinite separation, but will consist of a high component of the $N(^4S)+ H_2^+$ state at large N-H distances. As the lowest states of all three representations correlate with $N^+(^3P)+ H_2$, the closeness of the potentials is to be expected.

A cut through the surface with R(HH) at 1.5 a.u., for C_{2V} symmetry is shown in fig.II.3.2. Here the behaviour is very similar to the UHF surface, with the $^3A_2$ state being attractive without any barrier, and the $^3B_1$ and $^3B_2$ states being repulsive. The $^3B_2$ state is repulsive for all N-H distances with only a slight distortion at an N-H distance of 2.1 a.u. to indicate a possible avoided crossing. The $^3B_1$ state however, has a marked avoided crossing with an attractive state of

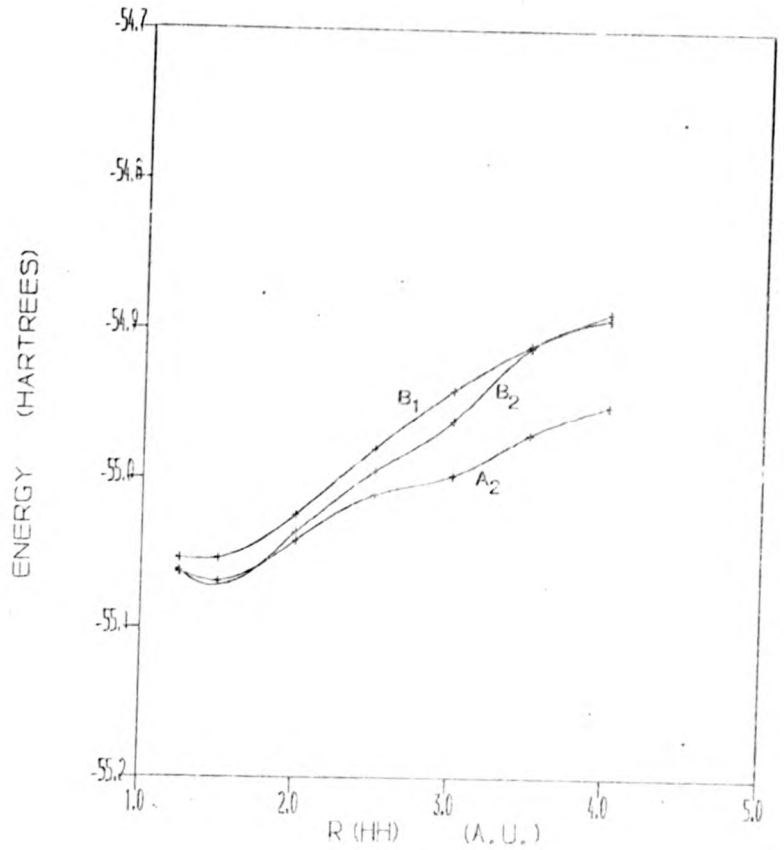

FIG. II.3.1. $E(NH_2^+)$ CI VS. R(HH), C_{2v} SYMMETRY, N-H DISTANCE = 6.0 A.U.

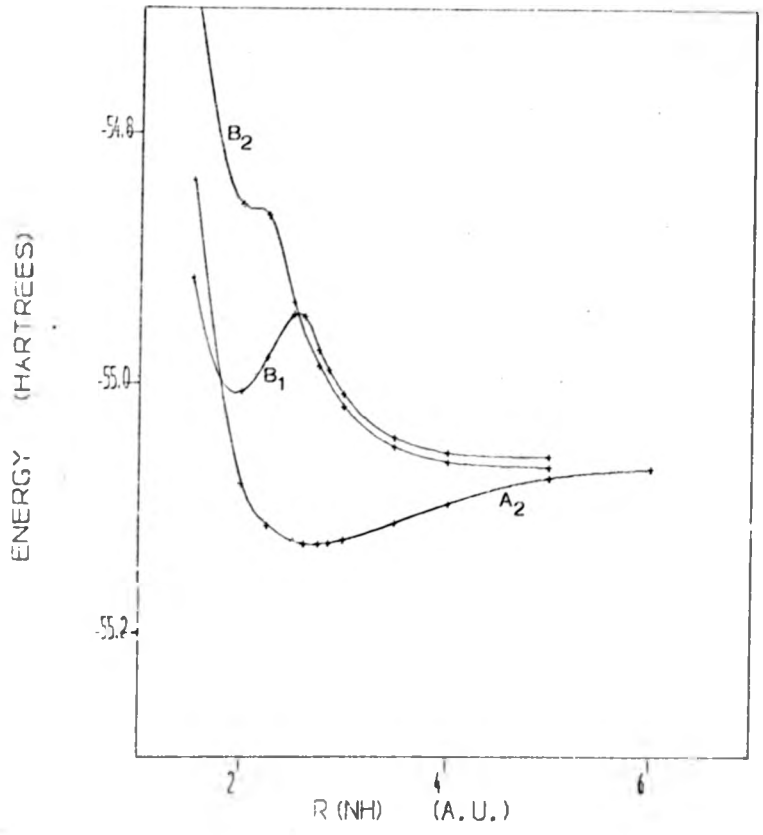

FIG. II.3.2. $E(NH_2^+)$ CI VS. R(NH), C_{2v} SYMMETRY, H-H DISTANCE = 1.5 A.U.

higher energy. This is the state that becomes the equilibrium state at larger H-H distances, and correlates with $N(^2D) + H_2^+$. Some of the UHF results indicated this crossing.

Increasing the H-H distance to 2.0 a.u. gives a similar result (see fig. II.3.3). The distortion of the $^3B_2$ state is now more pronounced, and the local minimum of the $^3B_1$ state has now deepened so as to be almost lower than the $^3A_2$ state.

A contour diagram of the $^3A_2$ state is shown in fig. II.3.4. As can be seen the shallow minimum occurs at approximately: R(NH)=2.6 a.u., R(HH)=1.75 a.u.. The lowest point actually calculated is at R(NH)=2.649 a.u., R(HH)=1.75 a.u. with an energy of -55.13183 hartrees. This is approximatly 0.064 hartrees below the corresponding energy of the separated $N^+ + H_2$. This well depth is considerably less than that reported by Bender et al.[3] (3 e.v= 0.110 hartrees, at R(NH)=2.649, R(HH)= 1.8 a.u.) Futher work by Hirst [121] has shown this difference to be due to the inclusion of polarization functions in the basis set of Bender et al.

The $^3B_1$ state is shown in fig II.3.5. The major feature is the deep well at N-H distance = 2.0 a.u., H-H distance = 4.0 a.u. This is in fact the lowest point calculated with an energy of -55.27439 hartrees, which is some 0.207 hartrees below the corresponding energy of $N^+ + H_2$. The variation of energy with angle is shown in fig II.3.6. As for the UHF surface, the well is very flat at large angles and the true equilibrium position is probably not linear. Bender et al. do not report any attempt to locate the minimum for $^3B_1$. The barrier to this well can be clearly seen in Figs. II.3.2, II.3.3 and II.3.5.

The other major feature, apparent from figs II.3.1 and II.3.2, is the large potential barrier to the well of the surface. This barrier

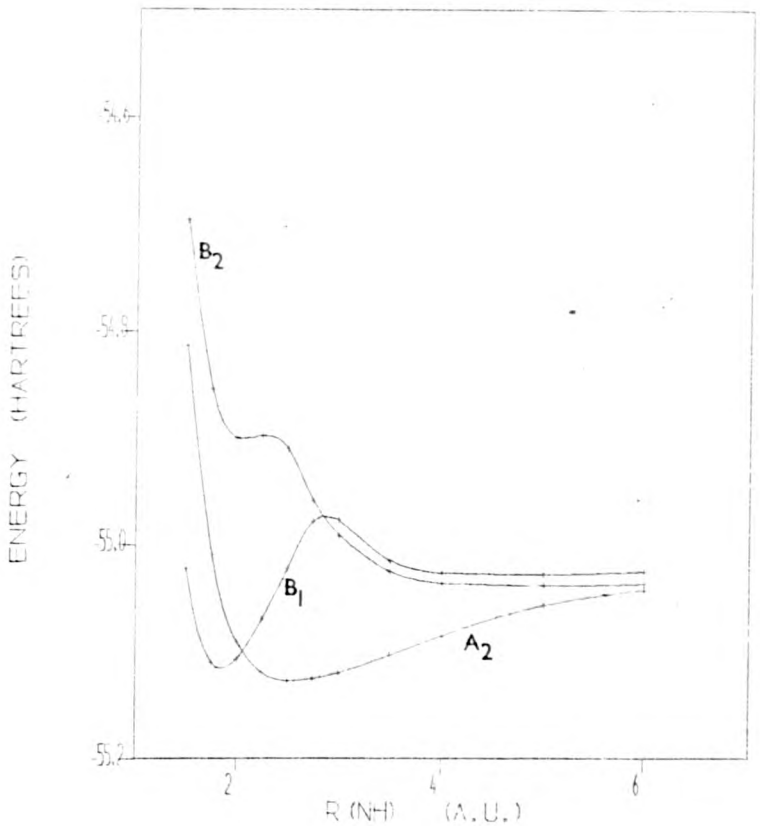

FIG. II.3.3 $E(NH_2)$ CI VS. R(NH)

C_{2v} SYMMETRY ; H-H DISTANCE = 2.0 A.U.

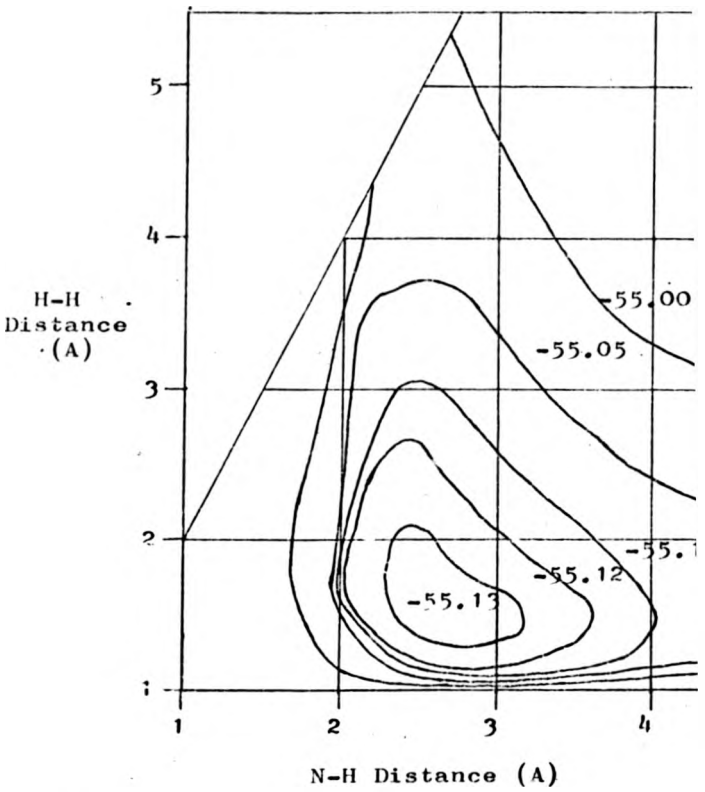

FIG. II.3.4. CI Energy for NH_2^+; Contour d

state; C_{2v} geometries.

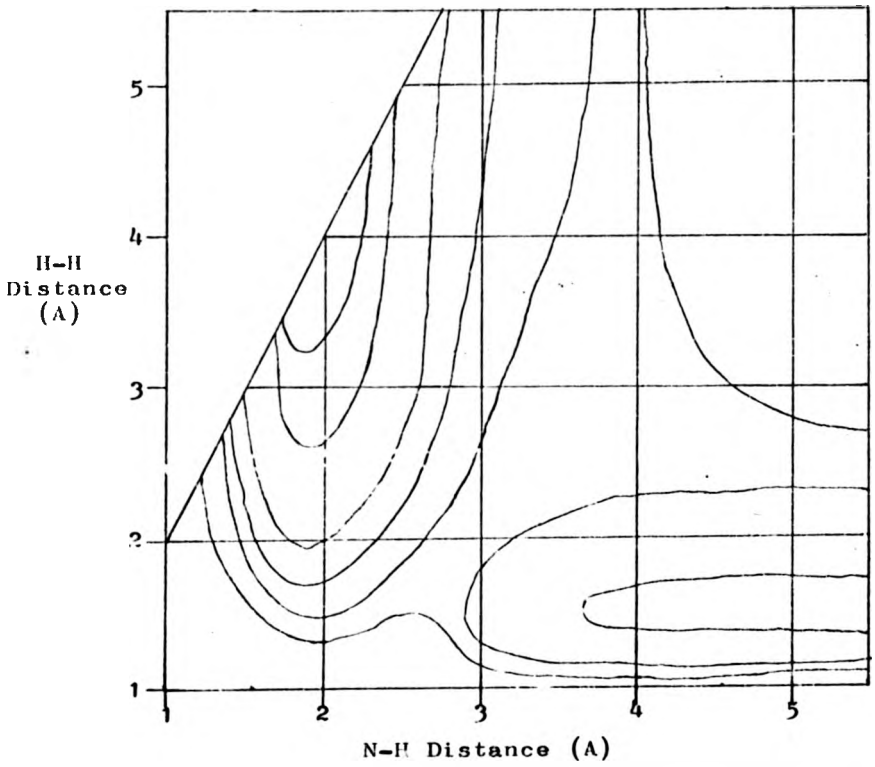

FIG. II.3.5. CI Energy for NH_2^+; Contour diagram for $^3B_1$ state; C_{2v} geometries.

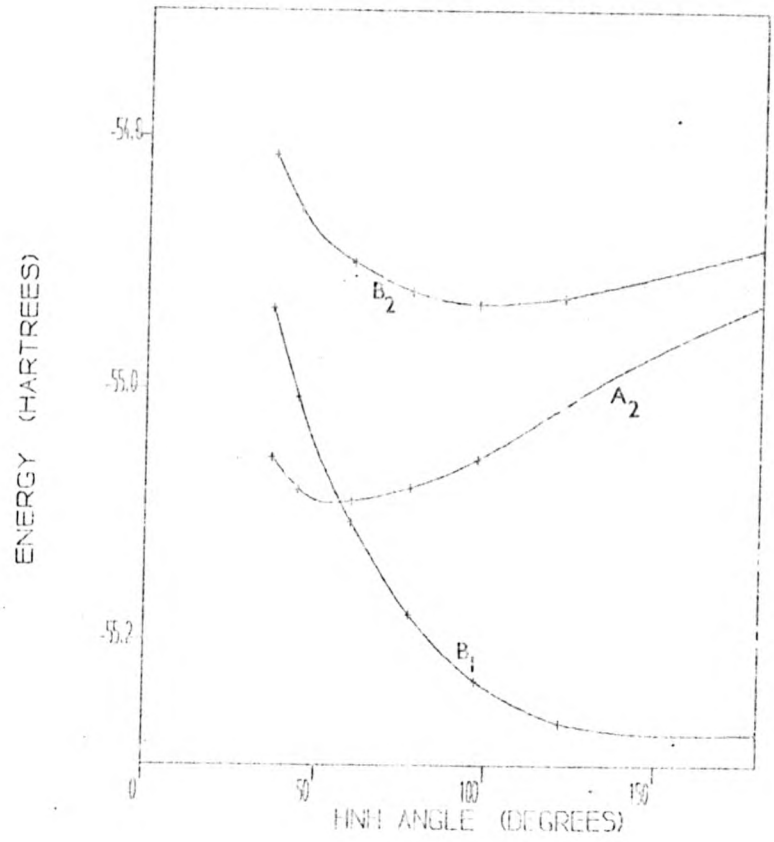

FIG. II.3.6 $E(NH_2^+)$ CI VS. HNH ANGLE.
C_{2v} SYMMETRY, N-H DISTANCE = 2.0 A.U.

is to be expected, as the insertion of carbon into an H-H bond is forbidden by the Woodward- Hoffmann rules [117].

2.3.3.2 LINEAR GEOMETRIES

For linear geometries of $[N-H-H]^+$ two states are of interest viz: $^3\Sigma^-$ and $^3\Pi$.

For $^3\Sigma^-$ the root functions taken were:

$1\sigma^2\ 2\sigma^2\ 3\sigma^2\ 1\pi_x^1\ 1\pi_y^1$

and

$1\sigma^2\ 2\sigma^2\ 3\sigma^1\ 4\sigma^1\ 1\pi_x^1\ 1\pi_y^1$

the second configuration is included because the RHF wavefunction does not dissociate correctly to $NH^+(^4\Sigma^-)+H$, instead it dissociates into $NH(^3\Sigma^-)+H^+$. These gave rise to 1293 configurations.

For the $^3\Pi$ state the root functions used were:

$1\sigma^2\ 2\sigma^2\ 3\sigma^2\ 1\pi^1\ 4\sigma^1$

and

$1\sigma^2\ 2\sigma^2\ 3\sigma^1\ 1\pi^1\ 4\sigma^2$

The resulting points for H-H distance = 1.5 a.u. are shown in fig II.3.7. As for the UHF surface the $^3\Sigma^-$ state has no barrier to a shallow well of approximately 0.58 hartrees(1.6eV) depth. The $^3\Pi$ state is repulsive at all internuclear distances with no local maxima or minima.

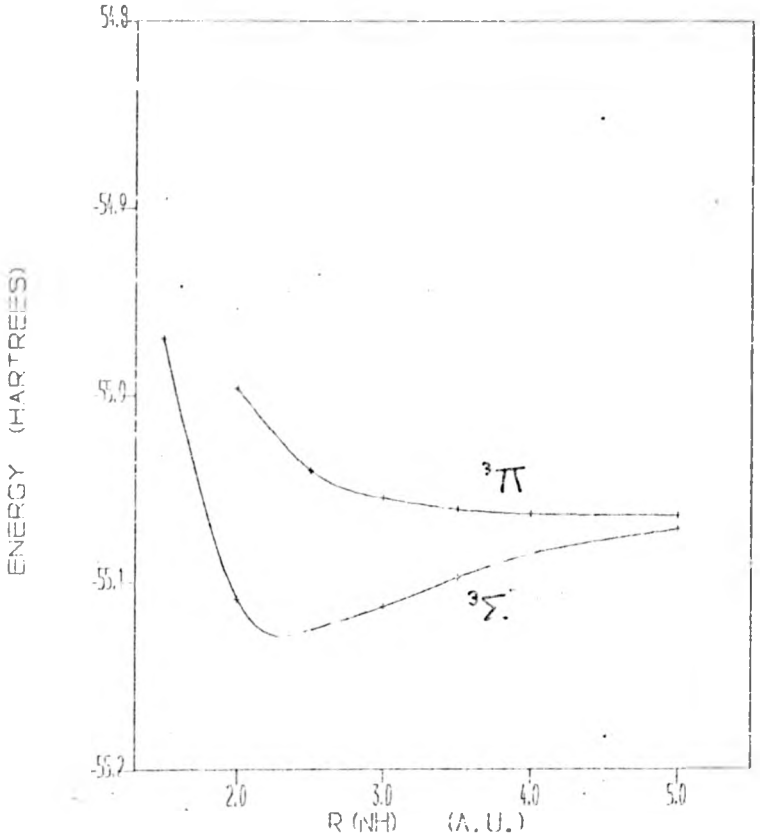

FIG. II.3.7. E(NH$_2$) CI VS. R(NH) ; LINEAR N-H-H ; H-H DISTANCE = 1.5 A.U.

2.4 DIATOMICS IN MOLECULES

2.4.1 Introduction

The method of Diatomics in molecules was first proposed by Ellison in 1963 [25], and subsequently used by him and his co-workers on a number of triatomic systems and H(n)+ clusters [26,118,86].

The method was reformulated by Kuntz and Roach [57] in matrix notation, further expanded by Tully [108], and, more recently, by Baker and Parr [24].

Diatomics in molecules has a number of attractive features for theoretical chemical dynamics. It is essentially a valence bond theory and hence the behaviour in the diatomic limits is correct. Also because the basis is in terms of the diatomic potentials, accurate relative energies are easier to obtain than from an ab-initio technique. This means the method is very fast in terms of computer time, and so can be used directly in a trajectory study. The first derivatives of the energy (i.e. forces) , which are required for trajectory calculations are also comparatively easy to obtain by means of the Hellman-Feynmann theorem.

2.4.2 General theory

2.4.2.1 BASIC CONCEPTS

The central concept of the theory of Diatomics-In-Molecules (DIM), is the partitioning of the total electronic Hamiltonian into a sum of atomic and diatomic Hamiltonians. In common with virtually all theories the Born-Oppenheimer approximation is assumed, and normally

spin-orbit coupling is neglected.

The total Hamiltonian is expressed as a sum:

$$H_{total} = \sum_a \sum_{a<b} H_{ab} - (N-2) \sum_a H_a \qquad [II.4.1]$$

where H_a is an atomic Hamiltonian depending only on the co-ordinates and electrons of atom 'a', and H_{ab} depends on the co-ordinates and electrons of the diatomic 'bc'. The term (N-2) corrects for the inclusion of the atomic factors in the diatomics terms.

The normal basis set for DIM calculations is a set of polyatomic valence-bond type wavefunctions comprising atomic wavefunctions coupled together in various schemes. The molecular wavefunctions are then expressed as a linear combination of the basis functions, i.e.

$$M_k(r) = \sum_m c_{mk}(r) B_m \qquad [II.4.2]$$

where B_m are the basis functions, M_k the molecular wavefunctions, and c_{mk} the coefficients.

Given such a basis set, if the integrals between all basis functions are known then the coefficients c_{mk}, and more importantly the energies, can be found. This is acheived in the usual way by transforming the problem into a secular equation expressed in matrix form:

$$\underline{H} \cdot \underline{c} = \underline{S} \cdot \underline{c} \cdot \underline{E} \qquad [II.4.3]$$

where H is the Hamiltonian matrix, and S the overlap matrix such that

$$H_{nm} = \langle B_n \mid H \mid B_m \rangle, \text{ and } S_{nm} = \langle B_n \mid B_m \rangle \qquad [II.4.4]$$

It is the method of calculating these polyatomic matrix elements that is unique in Diatomics-in-molecules theory. Expanding the Hamiltonian in eqn [II.4.4] according to [II.4.1] gives:

$$H_{nm} = \sum_a \sum_{b>a} {}^{ab}H_{nm} - (N-2) \sum_a {}^{a}H_{nm} \qquad [II.4.5]$$

where ${}^{ab}H_{nm}$ are the diatomic hamiltonian matrix elements in the polyatomic basis defined by eqn. [II.4.7], and ${}^{a}H_{nm}$ the corresponding atomic elements defined by eqn. [II.4.8].

$${}^{ab}H_{nm} = 0.5 * [\langle B_n \mid {}^{ab}H \mid B_m \rangle + \langle B_m \mid {}^{ab}H \mid B_n \rangle \qquad [II.4.7]$$

$${}^{a}H_{nm} = 0.5 * [\langle B_n \mid {}^{a}H \mid B_m \rangle + \langle B_m \mid {}^{a}H \mid B_n \rangle] \qquad [II.4.8]$$

${}^{ab}H_{nm}$ and ${}^{a}H_{nm}$ are defined in this way in order to make them Hermitian. The basic problem is then to calculate the matrix elements ${}^{ab}H_{nm}$ and ${}^{a}H_{nm}$ To do this the basis functions, B_k , are transformed for each diatomic pair in turn, into a set of eigenfunctions of the diatomic spin angular momentum operators, $s^2(ab)$ and $s_z(ab)$. These new functions, ${}^{ab}B_k$, the matrix elements in the polyatomic basis are then expressed as a sum of matrix elements in the diatomic basis, i.e.-

$$\underline{{}^{ab}H} = 0.5 \; \underline{{}^{ab}t}^{+} . (\underline{{}^{ab}h} + \underline{{}^{ab}h}^{+}) . \underline{{}^{ab}t} \qquad [II.4.9]$$

where ${}^{ab}h_{nm}$ is the diatomic matrix element in the diatomic basis defined by eqn. [II.4.10].

$${}^{ab}h_{nm} = \langle {}^{ab}B_n \mid {}^{ab}h \mid {}^{ab}B_m \rangle \qquad [II.4.10]$$

and $^{ab}\underline{T}$ is the matrix which transforms the polyatomic basis to diatomic according to eqn. [II.4.11].

$$^{ab}\underline{B} = {}^{ab}\underline{T} \cdot \underline{B} \qquad \text{[II.4.11]}$$

The $^{ab}B_k$ constitute a set of valence bond wavefunctions over the diatomic "ab". The next step is to assume that the true diatomic eigenfunctions, $^{ab}D_k$, can be represented by a linear combination of the diatomic functions, as represented by eqn. [II.4.12].

$$^{ab}D_k = \sum_m {}^{ab}d_{km} \, {}^{ab}B_m \qquad \text{[II.4.12]}$$

It is this assumption that is the fundemental approximation of DIM theory. It follows immediately from this assumption that the diatomic matrix elements, $^{ab}H_{nm}$ can be calculated from the known diatomic energies, and the matrices ^{ab}d.

If ^{ab}E is the diagonal matrix of exact diatomic energies. Then ^{ab}h is approximated by

$$^{ab}\underline{h} = {}^{ab}\underline{S} \cdot {}^{ab}\underline{d} \cdot {}^{ab}\underline{E} \cdot {}^{ab}\underline{d}^{-1} \qquad \text{[II.4.13]}$$

The matrix ^{ab}d accounts for the mixing of diatomic states of the same symmetry.

The atomic matrix elements $^{a}H_{nm}$ are simply given by

$$^{a}\underline{H} = \underline{S} \cdot {}^{a}\underline{E} \qquad \text{[II.4.14]}$$

where ^{a}E are the exact atomic energies. One of the major problems in DIM theory is the calculation of the overlap matrices, because the wavefunctions are never explicitly calculated.

2.4.2.2 POLYATOMIC TO DIATOMIC TRANSFORMATION

The bulk of effort in any application of DIM theory to a particular system is required to derive the transformation matrices $^{ab}\underline{T}$, Defined in eqn. [II.4.11].

For each diatomic pair this matrix is a product of three matrices as given by eqn.[II.4.15].

$$^{ab}\underline{T} = {}^{a}\underline{R} \cdot {}^{b}\underline{R} \cdot {}^{ab}\underline{Q} \qquad [II.4.15]$$

The matrix $^{a}\underline{R}$ is the rotation matrix which transforms the polyatomic functions centred on atom "a" to the correct orientation with respect to the diatomic "ab". Similarly ^{b}R acts of those functions centred on atom "b".

$^{ab}\underline{Q}$ is a matrix of angular momentum coupling constants. Its function is to transform the polyatomic functions which are eigenfunctions of the total S^2 and S_z operators into eigenfunctions of the diatomic spin operators $^{ab}S^2$ and $^{ab}S_z$.

Normally the polyatomic function is regarded as being formed by a given coupling scheme, e.g. by coupling atoms "b" and "c" to give eigenfunctions of $^{bc}S^2$ and $^{bc}S_z$. $^{bc}\underline{Q}$ in this case will be the unit matrix, but $^{ab}\underline{Q}$ will transform the polyatomic eigenfunctions into eigenfunctions of "ab". Similarly $^{ac}\underline{Q}$ will transform them into eigenfunctions of "ac".

2.4.3 Application to NH_2^+

2.4.3.1 BASIS SET

The starting point for the basis set was the two lowest states of Nitrogen (^2D and ^4S), N^+ (^3P and ^1D) and ground state Hydrogen

and H^+.

Interactions between these states were then considered, to form polyatomic basis functions (PBFS). Those PBFs involving diatomic states of high energy were excluded because their contribution to the ground state energy is minimal. However, it is necessary to ensure that the basis set is a complete one. If a given atomic function is included, then all functions related to it by rotation in the molecular plane must be included. The molecule is usually taken to lie in the XZ plane. This means that the p functions divide into two groups (x,z) and (y), and also the d functions into (z^2, x^2-y^2, xz) and (yz.xy). Therefore if for example a z^2 function is included a x^2-y^2 and xz must be included as well. It is reasonably obvious that if this is not the case then the rotation matrix R_a will not be unitary. The resulting set of PBFs are summarized in Table II.4.1.

2.4.3.2 ESTIMATION OF ATOMIC STATES

It was decided to use the energy of the isolated reactant atoms as a zero energy state, i.e. the energy of $N^+(^3P)$ and $2 \times H^\bullet$, was taken to be zero.

The relative energies of the other atomic states were derived to reproduce the results of Guest and Hirst [43] at 20.00 a.u.. Fixing the energy of H^+ at 0.5 a.u., the atomic energies obtained are shown in table II.4.2.

2.4.3.3 ESTIMATION OF DIATOMIC TERMS (diagonal)

The estimation of diatomic energies is crucial to the success of a DIM calculation as it is primarily from these values that the polyatomic energy is derived. There are four diatomics whose potential

Table II.4.1

Polyatomic basis set for NH_2^+

	N	H_a	H_b	NH_a	NH_b	HH
1	$N^+(^3P_x)$	$H(^2S)$	$H(^2S)$	$^4\Sigma^-$	$^2\Sigma^-$	$^1\Sigma_g^+$
2	$N^+(^3P_x)$	$H(^2S)$	$H(^2S)$	$^2\Sigma^-$	$^4\Sigma^-$	$^1\Sigma_u^+$
3	$N^+(^3P_y)$	$H(^2S)$	$H(^2S)$	$^4\Pi$	$^2\Pi$	$^1\Sigma_g^+$
4	$N^+(^3P_y)$	$H(^2S)$	$H(^2S)$	$^2\Pi$	$^4\Pi$	$^3\Sigma_u^+$
5	$N^+(^1D_{zz})$	$H(^2S)$	$H(^2S)$	$^2\Sigma^+$	$^2\Sigma^+$	$^1\Sigma_g^+$
6	$N^+(^1D_{zz})$	$H(^2S)$	$H(^2S)$	$^2\Pi$	$^2\Pi$	$^3\Sigma_g^+$
7	$N^+(^1D_{zz})$	$H(^2S)$	$H(^2S)$	$^2\Delta$	$^2\Delta$	$^1\Sigma_g^+$
8	$N\ (^4S)$	H^+	$H(^2S)$	$^4\Sigma^-$	$^3\Sigma^-$	$^2\Sigma_g^+$
9	$N\ (^2D)$	H^+	$H(^2S)$	$^2\Sigma^+$	$^3\Sigma^-$	$^2\Sigma_g^+$
10	$N\ (^2D)$	H^+	$H(^2S)$	$^2\Pi$	$^3\Pi$	$^2\Sigma_g^+$
11	$N\ (^2D)$	H^+	$H(^2S)$	$^2\Delta$	$^3\Delta$	$^2\Sigma_g^+$
12	$N\ (^4S)$	$H(^2S)$	H^+	$^3\Sigma^-$	$^4\Sigma^-$	$^2\Sigma_g^+$
13	$N\ (^2D)$	$H(^2S)$	H^+	$^3\Sigma^-$	$^2\Sigma^+$	$^2\Sigma_g^+$
14	$N\ (^2D)$	$H(^2S)$	H^+	$^3\Pi$	$^2\Pi$	$^2\Sigma^+$
15	$N\ (^2D)$	$H(^2S)$	H^+	$^3\Delta$	$^2\Delta$	$^2\Sigma^+$

The columns labelled N, H_a and H_b denote the atomic states which constitute the polyatomic basis. The columns labelled NH_a, NH_b and HH denote the diatomic states formed by the various coupling schemes.

energies are required, NH^+, NH, H_2, H_2^+.

The NH^+ ion has received comparatively little study, but detailed calculations have recently been made by Guest & Hirst [43]. Some of their preliminary calculations were performed using the same basis set and programs as used for the C.I. calculations described herein [44]. These only differed from those described in [43] by the absence of polarization functions. As the C.I. calculations were performed without polarization functions the preliminary figures were used.

The only previous study of the low-lying states of NH^+ was that of Liu & Verhaegen [64] who calculated limited potential energy curves for nine low-lying states. The only other calculation is on the $X^2\Pi$ state using the pseudo-natural orbital CI method by Rosmus & Meyer [92].

In order to utilize calculations of potential energy curves in DIM calculations it is necessary to either express the point energies as an analytical function, or use some interpolation technique. For reasons of economy it is vastly preferable to use an analytical function, especially as most diatomic potentials can be described quite accurately this way.

However the normal form of the Morse potential does not have sufficient flexibility to accurately describe curves with local maxima, or inflections as arise for NH^+. A number of functional forms have been used, but the best results for this type of calculation seem to be those obtained by Baker & Parr [24], using eqn. [II.4.16].

$$E(r) = D_e[\exp(-a.R_e.X)+A.a.f(X).\exp(-R_eX)] \qquad [II.4.16]$$

where

$$X = r - r_0,$$

and

$$f(X) = (1-b.X) \cdot \exp(bX[2-bX]/2),$$

A = +1 for repulsive, -1 for attractive.

Note that if a=2 and b=0 then this reduces to the normal Morse/ anti-Morse function. Also note that at the equilibrium point: $E(r) = D_e[1+A.a]$ rather than just D_e as for the usual Morse potential.

Guest and Hirst have produced potential energy curves for eight of the low-lying states ($^4\Sigma_1^-$, $^4\Sigma_2^-$, $^2\Pi_1$, $^2\Pi_2$, $^4\Pi$, $^2\Sigma^-$, $^2\Sigma_1^+$, and $^2\Delta_1$).

The parameters D_e, B_e, R_o, a and b were determined by least squares optimization for each of these states. The technique is discussed in Chapter 3. The results obtained are shown in Table II.4.2.

This leaves three states ($^2\Sigma_2^+$($^2D_{zz}$), $^2\Pi_2$($^1D_{xz}$) and $^2\Delta_2$ ($^1D_{xx-yy}$)), unknown. All of these states are predicted be high in energy and have repulsive curves, and certainly do not appear in spectroscopic studies [20]. Therefore arbitrary potentials were taken for these states, subject only to the condition that they did not cross any states of the same symmetry. As the only reason for including these states is that the basis set be a complete one under rotation in the molecular plane, this approximation seems reasonable.

The potential energy curves for all NH^+ states used are shown in fig. II.4.2.

For NH rather fewer states are required and they have been used previously in DIM calculations by Tully [108]. The values derived by Tully for the states ($^3\Sigma_1^+$, $^3\Sigma_2^+$, $^3\Pi$, and $^3\Delta$) were used as quoted in

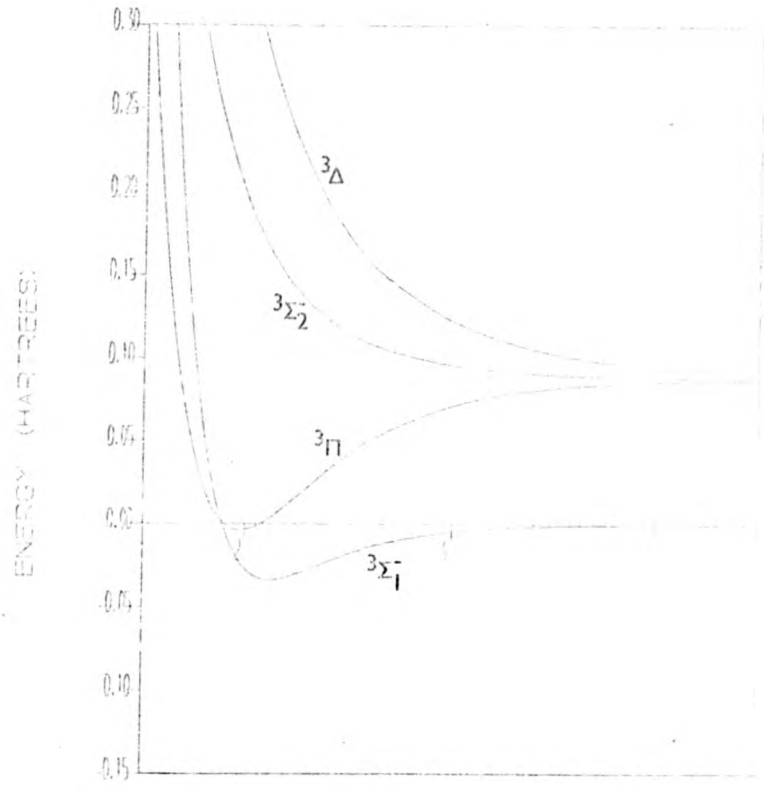

FIG. II.4.1 NH MORSE POTENTIALS.
FROM TULLY [1981]

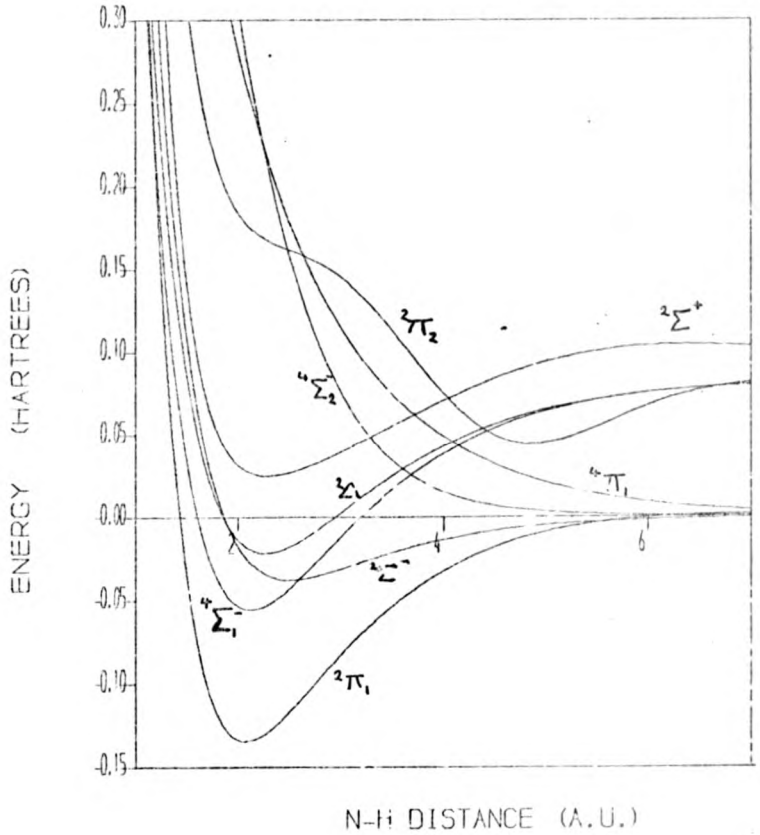

FIG. II.4.2 TRIPLET NH' POTENTIAL ENERGY CURVES

Table II.4.2

Parameters for NH^+ potential energy curves

State	D_e	B_e	R_o	a	b	A
$^2\Pi_1$	0.05297	0.75919	2.07402	3.5464	0.24702	-1.0
$^2\Pi_2$	0.005593	0.23888	2.767219	1.74013	0.89597	1.0
$^2\Delta$	0.081	0.8418	2.2663	2.2991	-0.00011	-1.0
$^2\Sigma^-$	0.03725	1.07267	2.5056	2.0185	0.0	-1.0
$^2\Sigma^+$	0.006288	0.34573	2.2897	11.2697	0.405177	-1.0
$^4\Sigma_1^-$	0.1111	0.8857	2.1249	2.2567	0.00037	-1.0
$^4\Sigma_2^-$	0.4379	0.8381	0.4281	2.2030	0.00904	1.0
$^4\Pi_1$	0.0394	2.0166	3.1145	0.6331	0.68114	1.0
$^4\Pi_2$	0.01064	0.63714	2.9215	3.65895	0.42413	-1.0

Table II.4.3

Extended Morse parameters for H_2

D_e	B_e	R_o	a	b	A
0.032313	0.504889	1.996405	4.219265	0.130596	-1

[108].

The two states of H_2 ($^1\Sigma_g^+$ and $^3\Sigma_u^-$) have been used previously both by Tully and Eaker and Parr[24]. Tully uses the values given by Pedersen and Porter [82], and Eaker and Parr the results of Kolos and Wolniewicz [54].

Eaker and Parr fitted their extended Morse function to the values they used, and the parameters obtained by them are used here. For H_2^+ only the ground state ($^1\Sigma_g$) was found to be needed although the $^1\Sigma_u$ state might be expected to participate. This discrepancy may account for the poor results of the DIM calculations. Two sources of potential energy curves are available, those of Peek [83], and Bates & Reid [2]. The results of these calculations for the internuclear distances of interest here are very close. However the results of Peek [83] are more suitable for least squares optimization, and a modified Morse potential was fitted to these points in the range 1.5 to 10.0 a.u. The same technique was used as for NH^+. The results are shown in Table II.4.3, and a plot of the resulting curve in Fig II.4.3. The results of this fitting were extremely good, showing that the extended Morse function is very suitable for this range of internuclear distances. However it is noticable that this Morse curve does tend to zero too rapidly at large internuclear distances.

2.4.3.4 ESTIMATION OF DIATOMIC TERMS (off-diagonal)

As mentioned earlier the calculation of the coupling terms, i.e. the matrix $\underline{d}$, between diatomic states represents something of a problem in DIM calculations. Since the wavefunctions are never explicitly calculated these off-diagonal matrix elements can not be calculated directly. A variety of methods have been tried for estimating their values. Tully [108] calculates the hamiltonian matrix elements from the diagonal elements using [II.4.17]. Where the $^{ab}v_{nm}$

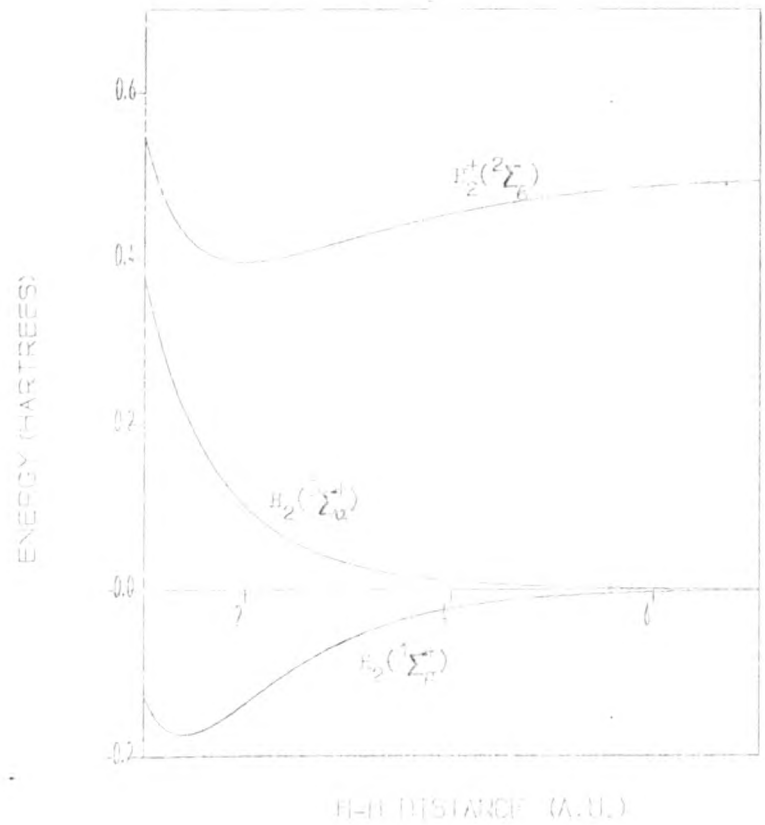

FIG II.4.3 H_2 MORSE POTENTIAL

are the diatomic

$$^{ab}h_{nm} = C_{nm}[^{ab}V_n - {}^{ab}V_m] \qquad [II.4.17]$$

interaction energies, i.e. $^{ab}V_n\ (r_{ab}=\infty) = {}^{ab}V_m\ (r_{ab}=\infty) = 0$, and C is a dimensionless parameter. This parameter, C, is estimated, if possible by molecular orbital arguments, or failing that it is chosen empirically to give the best agreement for the triatomic surface. Once all C_{nm} have been determined the Morse and anti-Morse functions [II.4.18] were used to calculate the diatomic energies. The parameters of these functions were optimised by a least squares

$$^{ab}V_m = D_m\ (\exp[2.B_m(R_m^o - r_{ab})] + 2.\exp[B_m(R_m^o - r_{ab})]) \qquad [II.4.18]$$

procedure such that the eigenvalues of the 2 x 2 matrix defined by equations [II.4.17] and [II.4.18] gave the best fit to known diatomic curves.

This procedure has the advantage that in the asymptotic limit the diatomic energy values are reproduced. However the major disadvantage is that the numerical values of the off-diagonal elements are generally poorly estimated. This is particularly so for very small separations where the off-diagonal term defined by [II.4.17] becomes very large.

Kuntz and Roach [57] in their paper on ArH_2^+ derive the coupling terms for ArH^+ somewhat differently. They performed a minimal basis set calculation on ArH^+ at various internuclear distances. The resulting molecular orbitals were expanded in terms of functions representing the diatomic states. The coefficients in this expansion then provided the necessary coupling constant at each internuclear distance. The value of the coupling constant changed with internuclear distance, and they found that it was well approximated by eqn [II.4.19]. Where X and Y are parameters and R the internuclear distance.

are the diatomic

$$^{ab}h_{nm} = C_{nm}[^{ab}V_n - {}^{ab}V_m] \qquad [II.4.17]$$

interaction energies, i.e. $^{ab}V_n\ (r_{ab}=\infty) = {}^{ab}V_m\ (r_{ab}=\infty) = 0$, and C is a dimensionless parameter. This parameter, C, is estimated, if possible by molecular orbital arguments, or failing that it is chosen empirically to give the best agreement for the triatomic surface. Once all C_{nm} have been determined the Morse and anti-Morse functions [II.4.18] were used to calculate the diatomic energies. The parameters of these functions were optimised by a least squares

$$^{ab}V_m = D_m\ (\exp[2.B_m(R_m^o - r_{ab})] + 2.\exp[B_m(R_m^o - r_{ab})]) \qquad [II.4.18]$$

procedure such that the eigenvalues of the 2 x 2 matrix defined by equations [II.4.17] and [II.4.18] gave the best fit to known diatomic curves.

This procedure has the advantage that in the asymptotic limit the diatomic energy values are reproduced. However the major disadvantage is that the numerical values of the off-diagonal elements are generally poorly estimated. This is particularly so for very small separations where the off-diagonal term defined by [II.4.17] becomes very large.

Kuntz and Roach [57] in their paper on ArH_2^+ derive the coupling terms for ArH^+ somewhat differently. They performed a minimal basis set calculation on ArH^+ at various internuclear distances. The resulting molecular orbitals were expanded in terms of functions representing the diatomic states. The coefficients in this expansion then provided the necessary coupling constant at each internuclear distance. The value of the coupling constant changed with internuclear distance, and they found that it was well approximated by eqn [II.4.19]. Where X and Y are parameters and R the internuclear distance.

$$C^{-1} = X.R^2.\exp(-Y.R) \qquad [II.4.19]$$

Eaker and Parr [24] use the same formula for the diatomic coupling in the CH_2 system. They use a mixing matrix of the form:

$$^{ab}_{d} = \begin{pmatrix} \cos\theta & -\sin\theta \\ \sin\theta & \cos\theta \end{pmatrix} \qquad [II.4.20]$$

where,

$$\cos^2\theta = C^2/(1+C^2)$$

$$\sin^2\theta = 1/(1+C^2)$$

$$\cos\theta \cdot \sin\theta = C/(1+C^2)$$

They generate X and Y however by optimizing the resultant triatomic surface using a least squares method. They found that the triatomic surface is quite sensitive to changes in the parameters, and this enabled them to optimize 12 parameters to yield reasonable agreement with the best ab initio results [103].

The case of NH_2^+ is made more complex if states arising from both the neutral and ionized states of nitrogen are used. Firstly this means that molecular orbital arguments are not at all possible Also the method used by Kuntz and Roach is not suitable because of the size of the basis set required, and the effort involved in the expansion.

It was therefore decided to follow Eaker and Parr and use the formula for the coupling terms developed by Kuntz and Roach, and to fit the parameters by optimizing the resultant surface. From the ATMOL 3 C.I. calculations a set of calculated energies were available that would serve as a "target" surface. The aim therefore was to find the set of parameters that gave the surface closest to the calculated C.I. surface. The C.I. points had not been produced with the intention of using them in any fitting procedure. This meant that their distribution over

configuration space was far from ideal. However the aim was not to produce a surface for dynamic calculations but merely to investigate the capacity of the DIM method to reproduce C.I. results. In any case the correct asymptotic behaviour was assured because of the nature of the DIM method.

The basis set chosen involves three pairs of NH states of the same spin and symmetry. There are therefore 6 parameters to be determined.

To facilitate the optimization only the lowest energy eigenvalues were used in the calculation. These were of course all A" symmetry under the C_s point group. This gave a total of 137 points to be used in the optimization. The values were corrected for the energy of separated N^+ (^3P) and H^*, estimated to be -54.9148 a.u.

The method used was a variation of the method described in section 3.1.3, differing only in the fact that derivatives were not explicitly calculated. A readily available computer routine was used (routine E04FBA, see ref.[78], Powell's 1968 method).

2.4.3.5 SPIN TRANSFORMATION MATRICES FOR NH_2^+

The role of the spin transformation matrices can be best clarified by consideration of the spin eigenfunction for the first pbf for NH_2^+ in Table II.4.1.

Consider first the eigenfunction for the $^4\Sigma_2^-$ state of NH^+. This is formed by coupling the ^3P state of N^+ with the ^2S state of H. If for convienience the three states of $N^+(^3P)$ are labelled by their $\langle s_z \rangle$ values, viz: -1,0,1, and the ^2S state of H likewise: +/- 1/2, then

the spin eigenvectors for $NH^+(^4\Sigma_2^-)$ are:

$<s_z>= 3/2 : \quad (1,1/2)$

$<s_z>= 1/2 : \quad [2^{1/2}(0,1/2) + (1,-1/2)]/3^{1/2}$

Now, if these are coupled with the ^2S state of the second hydrogen to yeild the $^3A''$ state of the triatomic molecule, for the $<s_z>=1$ case one obtains:

$$[3(1,1/2,-1/2) - 2^{1/2}[(0,1/2,1/2) + (1,-1/2,1/2)]]/12^{1/2} \quad [II.4.21]$$

However if the two hydrogens are coupled together first instead to give the spin eigenfunction for $H_2(^1\Sigma_g^+)$:

$$[(1/2,-1/2) - (-1/2,1/2)]/2^{1/2}$$

Coupling this with the $N(^3P)$ yeilds eqn [II.4.22] for the $^3A''$ eigenfuntion:

$$[(1,1/2,-1/2)\cdot(1,-1/2\ 1/2)], \quad <s_z>=1 \qquad [II.4.22]$$

Comparison of equations [II.4.21] and [II.4.22] shows the different representations of the triatomic state that result from different coupling schemes. It is the role of the spin transformation matrices, $\underline{Q}$, to transform from these representations to that of the triatomic.

The triatomic representation is taken to be that of H_2, therefore ${}^{BC}\underline{Q}$ is equal to thee unit matrix.

The other matrices, ${}^{ab}\underline{Q}$ and ${}^{ac}\underline{Q}$ are more complex, their elements being the appropiate Racah coefficients, usually denoted $W(j_1,j_2,j,j_3|j_{12},j_{23})$. However most of the matrix elements can be determined to be zero by inspection, because only the off-diagonal elements connecting pbf's with the same atomic constituents will be non-zero.

The non-zero terms can be determined by use of the formulae given by Landau and Lifshitz [61] page 417. for simplified cases. It

turns out that the only part of $^{ab}\underline{Q}$ that is not equal to the unit matrix is the top-left 4x4 block this is given by eqn. [II.4.23].

$$^{ab}Q_{11}=^{ab}Q_{22}= (2/3)^{1/2} \qquad [II.4.23]$$

$$^{ab}Q_{21}=-^{ab}Q_{12}= (1/3)^{1/2}$$

Note that the case for pbf's 3 and 4 is identical to that of pbf's 1 and 2.

Because of the way in which the basis set was chosen $^{ac}\underline{Q}$ is identical to $^{ab}\underline{Q}$.

2.4.3.6 ROTATION MATRIX

The three rotation matrices are reasonably straight forward for NH_2^+. The hydrogen atomic functions are all spherically symmetrical, and the rotation matrices for the hydrogens therefore equal to the unit matrix.

For the nitrogen the matrix is rather more complex. The molecular co-ordinates are such that the molecule lies in the xz plane One hydrogen lies along the z axis and the second at an angle θ from the z axis. The rotation matrix for nitrogen is then dependent on the behaviour of the atomic basis functions on rotation about the y axis.

For the basis set used the rotation matrix is given by Table II.4.4.

2.4.4 Results of DIM

The optimization of the off-diagonal coupling constants represented a considerable computational problem. In all 137 CI points were taken. To optimize the coupling constants took 37 iterations and approximatly 8 hours processor time on a Burroughs B6700.

Table II.4.4

Matrix for rotation about nitrogen atom.

The matrix has the form:

$$\begin{pmatrix} P & C & 0 & 0 & 0 & 0 \\ 0 & Q & 0 & 0 & 0 & 0 \\ 0 & 0 & 1 & C & 0 & 0 \\ 0 & 0 & 0 & Q & 0 & 0 \\ 0 & 0 & 0 & 0 & 1 & 0 \\ 0 & 0 & 0 & 0 & 0 & Q \end{pmatrix}$$

where:

$$P = \begin{pmatrix} \cos\theta & 0 & -\sin\theta & 0 \\ 0 & \cos\theta & 0 & -\sin\theta \\ \sin\theta & 0 & \cos\theta & 0 \\ 0 & \sin\theta & 0 & \cos\theta \end{pmatrix}$$

and

$$Q = \begin{pmatrix} [1+3.\cos\theta]/2 & -3^{1/2}.\sin\theta.\cos\theta & 3^{1/2}.\sin^2\theta \\ (3^{1/2}.\sin\theta.\cos\theta & \cos^2\theta-\sin^2\theta & -\sin\theta.\cos\theta \\ (3^{1/4}.\sin^2\theta/2 & \sin\theta.\cos\theta & [1+\cos^2\theta]/2 \end{pmatrix}$$

Table II.4.5

Optimized values of off-diagonal coupling constants

State (NH)	A	B
$^4\Sigma^-$	0.2066	1.2735
$^2\Pi$	1.8973	0.4646
$^2\Sigma^+$	undetermined	

The results were disappointing in that the final LSD was 0.04 hartrees (105 KJ mole^{-1}). The values for the coupling constants obtained are given in Table II.4.5.

The most noticeable feature is that the lowest energy eigenvalue was not dependent on the $^2\Sigma^+$ coupling constants. Closer examination revealed that the states arising from the N+ H_2^+ configurations had ,apart from the $^4\Sigma_1^-$ state, little effect on the ground state. Indeed the results would be virtually identical if they had been omitted from the basis set.

In fact the improvement in the least squares deviation ; obtained by optimization of the coupling constants, was slight. Indicating that contrary to the case of Eaker and Parr the least squares deviation of the surface was not very sensitive to the off-diagonal coupling constants. But it is worth noting that they were optimising 12 parameters, and in this calculation only 6 were optimized, and of those only two had any marked effect.

In effect therefore it seems that the basis set is equivalent to a much smaller , rather inflexible basis and the disappointing results not so surprising.

It would be very interesting to know the effect of increasing the basis set to be more comparable with that of Eaker and Parr.

A plot of the area involving the deep potential well is shown in fig II.4.4, with the CI $^3B_1$ state (relative to infinite separation)for comparison. It can be seen that the DIM calculation has failed completely to reproduce the deep well, and has a shape more reminisent of the $^3A_2$ state. Fig II.4.5 shows the approach of N^+ to H_2, again the CI points are included, this time the $^3A_2$ state. here the DIM surface is better behaved but is too attractive at short internuclear

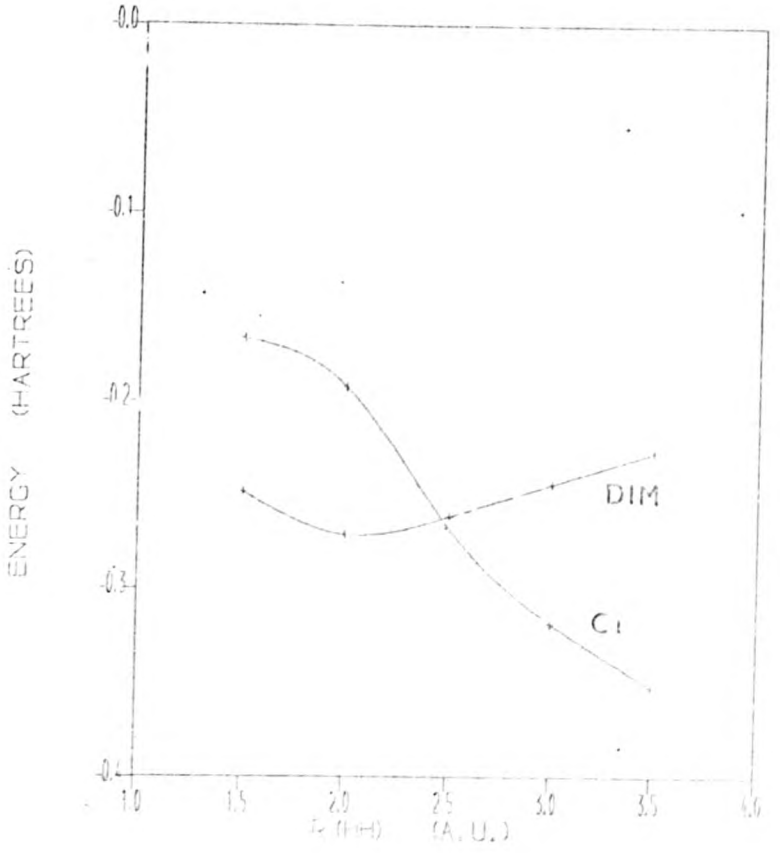

FIG. II.4.4. $E(NH_2)$ DIM AND CI VS. R(N-H)
C_{2v} SYMMETRY; N-H DISTANCE = 2.0 A.U.

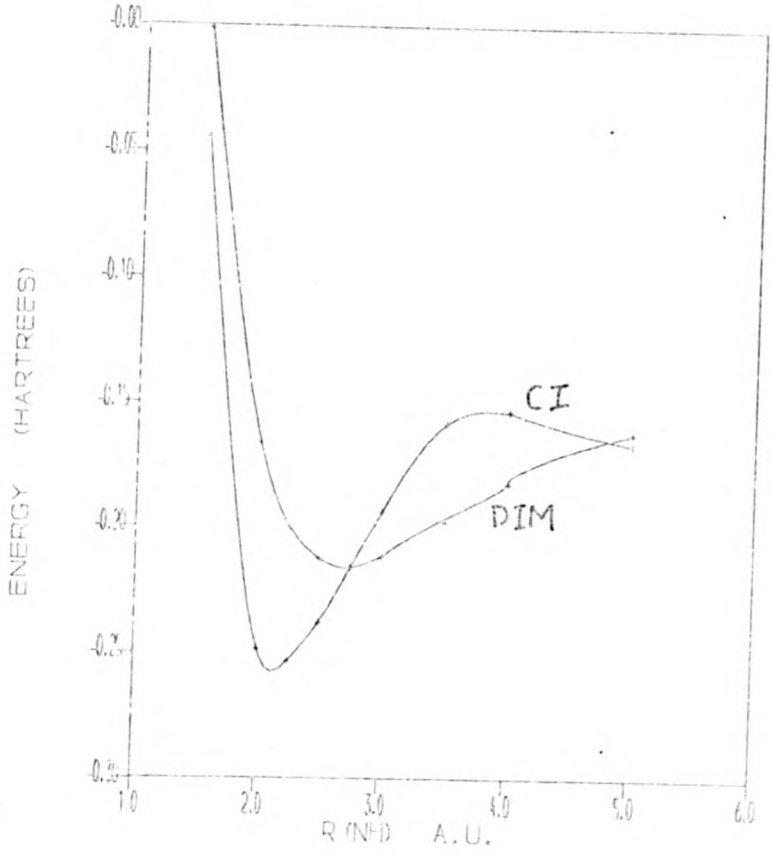

FIG. II.4.5 $E(NH_2)$ DIM AND CI VS. R(NH),
C_{2v} SYMMETRY, H-H DISTANCE = 1.5 A.U.

distances.

Chapter 3.

Surface fitting and Interpolation

3.1 SURFACE FITTING AND INTERPOLATION

3.1.1 Introduction

Before a set of ab initio points can be used in a trajectory calculation, or, indeed, any other dynamical calculation it is necessary to obtain some method to calculate the energy at an arbitrary point. There are two fundamental approaches to this problem; either some form of analytical function is fitted to the points or an interpolation technique is applied.

3.1.2 Techniques of surface fitting

Fitting an analytical surface to a set of points is a special case of an optimization problem. The essential feature of an optimization problem is that given a function, $F(p_1,p_2,\ldots p_n)$ to find the set of parameters, p_i which produce the minimum, or more usually maximum value of F. This problem has recieved a great deal of attention and a whole range of methods have been developed for estimating the best parameters.

In the case of surface fitting the function to be minimized is the "error" in the fit. The usual procedure is to minimise the least square deviation as shown in eqn. [III.1.1].

$$F = (1/n \cdot \sum(V_i - V_i^o)^2)^{1/2} \qquad [III.1.1]$$

where n = number of points

V_i = estimate of potential at point i.

V_i^o = actual potential at point i.

This function is generally regarded as being the best criterion of the quality of a fit. However it does have a failing in some cases. This is that the points with the largest absolute value tend to dominate the function. These are usually the points in the highly repulsive parts of the surface, where the fit is not critical. This means that the situation can arise where the fitting procedure is spending all its effort trying to fit in an unimportant region.

One way in which this problem can be alleviated is to weight each point as shown in eqn [III.1.2].

$$F = (1/n \sum w_i (V_i - V_i^o)^2)^{1/2} \qquad [III.1.2]$$

where w_i = the weight applied to point i.

The difficulty is then to allocate suitable, but also unbiased weights. For diatomic curves this is relatively easy, but not for triatomic surfaces. A better alternative is to have a good distribution of points, with fewer points in the less important regions.

Least squares deviation is not the only function that can be used. Another function commonly used for optimization is the so called minimax function , eqn. [III.1.3]. There are two major disadvantages to this form,

$$F = \max |V_i - V_i^o| \ , i=1,n \qquad [III.1.3]$$

firstly it is worse than LSD for concentrating on the repulsive region, and secondly it is not differentiable.

Some other possibilities considered are shown in eqn. [III.1.4].

$$F = N^{-1} . \sum |V_i - V_i^o| \qquad \text{(average)} \qquad [III.1.4]$$

$$F = (n^{-1} (\sum (100*(V_i - V_i^o)/V_i^o)^2)^{1/2 \quad \text{(rel.least squares)}}$$

$$F = \max |100*(V_i - V_i^o)/V_i^o| \quad \text{(percentage minimax)}$$

$$F = n^{-1}\sum|100*(V_i-V_i^o)/V_i| \quad \text{(average percent)}$$

But in practice virtually all published fits have used a least squares error, however Alexander and Berard have considered the other functions mentioned here [122].

The simplest method for minimization is the direct search, where from some initial estimate, each parameter is varied in turn. If a lower value of the error function is obtained then the new value is retained, and the search continues with the next parameter. In practice this method usually starts well, but the improvement quickly falls off. In the "hill climbing" analogy it descends into a valley, but requires large numbers of iterations to follow the valley to the true minimum. Many methods exist which are extensions of direct search which attempt to improve the convergence.

A somewhat pleasing variation on the direct search is the simplex method [79]. A simplex in n-dimensional space is a solid having plane faces and n+1 vertices, e.g. for 2-dimensions a triangle, and for 3-dimensions a tetrahedron. At each iteration the simplex is reflected through one face, so that the position of one vertex moves. The vertex which moves is usually the one with the greatest value of the error function. Extensions of the method allow for expansion or contraction of the simplex at each iteration [102].

Certainly one of the oldest approaches dates back to 1847 [79]. This method, the steepest descent, is occasionally, with modifications, still used today. The basis of the method is that, given an initial estimate of the parameters, p_j, a better estimate is given by $p_i + d_i$ where the d_i are defined by eqn. [III.1.5].

$$-d_i(\underline{p}) = \partial F(\underline{p})/\partial p_i \qquad \text{[III.1.5]}$$

It has been shown [37] that repeated application of this formula will converge to the correct solution if the function, F, satisfies certain conditions. However, the rate of convergence is usually between poor and abysmal.

Much better methods are based on a Taylor series expansion of the error function. If only the terms up to second order are retained then eqn. [III.1.6] results. This equation is of course only exact for

$$F(\underline{p}+\underline{d}) = F(\underline{p}) + \sum_{i=1} d_i g_i + (1/2) \sum_{i,j} d_i G_{ij} d_i \qquad \text{[III.1.6]}$$

where $g_i = \partial F(\underline{p})/\partial p$

and $G_{ij} = d^2F(\underline{p})/dp_i dp_j$

quadratic functions. If it assumed to be exact then the step is given by eqn. [III.1.7]

$$d_i = -\sum_{j=1}^{n} (G^{-1})_{ij} g_j \quad , \quad i=1,2,..n \qquad \text{[III.1.7]}$$

bearing in mind that all first derivatives are zero at a minimum. Using eqn [III.1.4] to calculate the step leads to second-order convergence and is hence very efficient. However it is apparent that if the hessian $\underline{G}$ is not positive definite then the step can lead to divergence. It turns out in practice to be positive definite close to the minimum. This is not always the case however, and for direct minimization of LCAO-MO-SCF functions it has been shown [106] that this is not the case. Usually this class of method works well if a good initial estimate of the parameters is available. However that is not the usual case. The simplest extension to this method to improve the convergence properties is to use eqn [III.1.7] to define a search direction only, and to perform a one-dimensional optimization along this direction. This is possible even if $\underline{G}$ is singular. The trouble with this approach is that it can lead to many function evaluations per iteration step, thereby losing a lot of the second order efficiency.

An alternative class of methods attempts to combine the second order convergence with the guaranteed convergence of the steepest descent by using a step given by eqn [III.1.8].

$$d_1 = -\sum_{j=1}^{n}[a.\underline{I} - \underline{G}]^{-1}_{ij}g_j \qquad i=1,2..n \qquad [III.1.8]$$

where a is a constant, and $\underline{I}$ the unit matrix

Note that if a=0 then eqn. [III.1.8] reduces to eqn. [III.1.7], and as 'a' tends to infinity, eqn. [III.1.8] tends to [III.1.5]. The problem then of course is to determine the best value of a. One method due to Goldfeld, Quandt and Trotter [33] makes 'a' the maximum of: zero and (R+the largest eigenvalue of G), where R is used to control the step length so that $F_{i+1}<F_i$. This method seems to work well, but has the disadvantage of requiring a solution for the largest eigenvalue at each iteration. However, if the error function is very time consuming to calculate this will be an important overhead.

A class of methods that use a rather different approach are those based on conjugate directions. Two vectors ,$\underline{d}$ and $\underline{p}$, are regarded as conjugate if:

$$\underline{d}^t.\underline{G}.\underline{p} = 0 \qquad [III.1.9]$$

These are useful because, if a linear search is made successively along a set of mutually conjugate directions, then the function is minimized in the space spanned by those directions if the function is quadratic [30]. It is not usually possible to obtain such a conjugate set of vectors, and error functions are rarely exactly quadratic. There are many different methods based on this idea varying in the algorithms used to estimate the required directions, and the size of step to be taken.

For the special case of "sum of squares" problems, as for least squares deviation, some special techniques are available. The general sum of squares problem is one given by eqn. [III.1.10]

$$F = \sum_{j=1}^{m} f_j(\underline{p})^2 = \underline{f}^t.\underline{f} \qquad [III.1.10]$$

The gradient ,$\underline{g}$, is usually given in terms of eqn. [III.1.11], where $\underline{J}$ is the Jacobian matrix, $J_{ij}=df_i/dp_j$.

$$\underline{g} = 2.\underline{J}^t.\underline{f} \qquad [III.1.11]$$

The hessian is therefore given by eqn. [III.1.12].

$$\underline{G} = 2.\underline{J}^t.\underline{J} + 2.\sum_j f_j.\underline{K}^j \qquad [III.1.12]$$

where $K^j_{rs} = d^2f_j/dp_r dp_s$

The simplest approximation to make is that the hessian is given by III.1.13 instead.

$$\underline{G} = 2.\underline{J}^t.\underline{J} \qquad [III.1.13]$$

The f_i are either assumed to be all negligibly small, or that they are nearly linear so that the $\underline{K}^i$ are small. If this approximation is used in eqn [III.1.7], then the method is known as Gauss-Newton or generalized least squares. In practice eqn. [III.1.7] is frequently used as a search direction only, rather than a fixed step, because eqn. [III.1.13] is often a poor approxiamtion.

Marquartd [66] considers the case of using eqn.[III.1.13] in eqn.[III.1.8] in place of $\underline{G}$, to obtain eqn. [III.1.14].

$$d_i = -\sum_{j=1}^{n} [a.\underline{I} - 2\underline{J}^t.\underline{J}]^{-1}_{ij}.g_i \quad ,i=1,2..n \qquad [III.1.14]$$

He shows that this will give the best step in some maximum neirbourhood of $\underline{p}$. The constant 'a', is varied dynamically as the calculation progresses. Its value being decreased if $F(\underline{p}+\underline{d}) < F(\underline{p})$ or increased otherwise. This method is very attractive for this type of problem, because of its comparative simplicity and good convergence properties.

3.1.2 Functions for triatomic surfaces

Before surface fitting can begin, it is necessary to decide on one or more trial surfaces whose parameters are to be varied in order to reproduce the ab initio points. Somewhat surprisingly the choice of

surfaces is fairly limited, especially for attractive surfaces.

A function must fulfill the following criteria before it can be considered:

1.It must contain a sufficient number of parameters to make it flexible enough to fit a variety of surfaces, but not so many parameters that the fitting becomes impractical.

2.It must be continuous with respect to the parameters,and it is highly desirable that it is differentiable as well.

3.It must be reasonably rapid to evaluate.

4.It must "dissociate" properly, that is at the diatomic limits it must describe the diatomics themselves accurately.

Of these criteria it is usually the last that seems to cause the greatest problems.

The functions used can be grouped, albeit somewhat loosely, into three groups; those derived from Valence bond considerations; those from extended Morse potentials; and, thirdly, those based on the sum of n-body potentials.

3.1.2.1 VALENCE BOND RELATED FUNCTIONS

It is possible, in principle, to apply valence bond arguments to any triatomic, and derive an expression for the energy in terms of Coulomb and Exchange integrals. These integrals can then be expressed in terms of the diatomic potentials, i.e. the Cashion & Hersbach technique [13], and the diatomic parameters estimated to give a semi-empirical surface or optimized.

The oldest, and still much used example is the London-Eyring-Polanyi -Sato (LEPS) surface. This started as an expression for the

energy of three hydrogen atoms (London [65]). It has been used extensively as a semi-empirical surface, e.g. [75,50,115], extended to include overlap parameters [95,96], and used as a function for surface fitting [116]. The most complex form is that used extensively by Polanyi's group as a semi-empirical surface [87], see for example [80]. It has also been extended to fit four-atom surfaces, e.g. 2(HF) [119].

The most usual form of the function is given by eqn [III.1.15].

$$V = Q_1 + Q_2 + Q_3 - [J_1^2 + J_2^2 + J_3^2 - J_1J_2 - J_1J_3 - J_2J_3]^{1/2} \qquad \text{[III 1.15]}$$

where $Q_i = q_i/(1+S_i^2)$, $i=1,2,3$

$J_i = J_i/(1+S_i^2)$

$q_i = [{}^1E_i(r_i) + {}^3E_i(r_i)]/2$

$J_i = [{}^1E_i(r_i) - {}^3E_i(r_i)]/2$

Q_i and J_i are conceptually Coulomb and exchange integrals respectively, ${}^1E_i$ and ${}^3E_i$ the bonding and anti-bonding potentials, and S_i the overlap integrals (Sato parameters). The most common practice is to use Morse and anti-Morse potentials for ${}^1E_i$ and ${}^3E_i$.

This function has been used in a number of different ways. If the overlap is taken to be zero, and the Morse parameters estimated from diatomic curves, then the function has no unknowns and provides a semi-empirical surface. Alternatively, the Morse and anti-Morse parameters are taken from diatomic data and the overlap values, (which are independent of r_i) are fitted to give a least squares fit to some reference points, or attribute of the surface, such as barrier height [75,100]. This approach has one shortcoming that is sometimes unappreciated. This is concerned with the asymptotic diatomic limits.

If the overlap parameters are zero, then the limit of, say, $r_2 = \infty$, $r_3 = \infty$, then $Q_2 = Q_3 = J_2 = J_3 = 0$, and $V = {}^1E_1(r_1)$ as expected. However if S_1 is non-zero then in the limit $V = {}^1E_1(r_1^2)/(1+S_1)$. Therefore, the asymptotic diatomic energies are dependent on the parameters being optimised when they should only depend on the Morse parameters. The best way to avoid this problem is to use:

$$Q_i = (1+S^2)[{}^1E_i(r_i) + {}^3E_i(r_i)] \qquad [III.1.16]$$

$$J_i = (1+S^2)[{}^1E_i(r_i) - {}^3E_i(r_i)]$$

for the Coulomb and exchange integrals.

Taking the fitting one stage further, it is possible to optimise the anti-Morse and overlap parameters, but estimate the Morse from diatomic data, e.g. [116].

Or, in the limit, optimize all the parameters and have no empirical parameters at all. This is rarely the best policy, as the diatomic potentials are better handled separately to ensure that the limits are correct.

A more recent application of valence bond principles is that of Blais and Truhlar [5], who derive expressions for the energy for H_3 and use them as semi-empirical surfaces.

A similar, but much more complex type, of surface has been fitted by Yates and Lester [120,48] to H_3. They use a slightly modified version of the Porter and Karplus [88] potential function. However, Choi and Tang [16] have pointed out that this function has the wrong asymptotic behaviour at dissociation. Neither of these functions is of generally applicability, although analagous functions could be derived for any particular case.

3.1.2.2 ROTATED MORSE FUNCTIONS

This type of function was originally proposed by Wall and Porter [112], who for a collinear geometry suggest a rotated Morse potential of the form:

$$V(r_x,r_y,\theta)=q(\theta).([1-\exp(-b(\theta)\rho)^2-1) \qquad [III.1.17]$$

where $q(\theta)=D_1(\cos\theta)^l + D_2(\sin\theta)^m$

$b(\theta)=b_1(\cos\theta)^p + b_2(\cos\theta)^r$

$\theta=\tan^{-1}(r_2-r_y)/(r_1-r_x)$

$$\rho=([\{r_1-[(r_2-y_0)^2+(r_1-x_0)^2]^{1/2}\cos\theta)$$
$$-(r_1-[(r_2-r_y)^2+(r_1-r_x)^2]^{1/2}\cos\theta)]$$
$$+[\{r_2-[(r_2-y_0)^2+(r_1-x_0)^2]^{1/2}\sin\theta)$$
$$-(r_2-[(r_2-r_y)^2+(r_1-r_x)^2]^{1/2}\sin\theta)])^{1/2}$$

D_1, D_2 = dissociation energy of AB and BC

x_0, y_0 = equilibrium distance of AB and BC

b_1, b_2 = Morse curvature for AB and BC

r_x, r_y = internuclear distance

r_1, r_2 = distance at which interaction becomes negligible

This function has been extended to three dimensions by Csizmadia et al. [22].

This type of function has been used occasionally in a somewhat different manner. Instead of using functions for the b(θ) etc., they have been calculated by one-dimensional spline interpolation. This seems to give good flexible surfaces for collinear geometries.

A similar type of function is the Hyperbolic Map function proposed by Bunker and Elais [4], and later extended by Bunker and Parr [11]. The basic idea is that the surface is defined from a reaction

co-ordiate, in fact a hyperbole is used. The function is, in its general form:

$$V=F(\partial).D(v).\{\exp[-2b(v)S]-2.\exp[-b(v)S]\} \qquad [III.1.18]$$

where $v=(y^2-x^2)/2$

$$S=+/-\ [(x-x_o)^2 + (y-y_o)^2]^{1/2}$$

$$x=r_{ab}-r_{ab}^{eq},\ y = r_{bc}-r_{bc}^{eq}$$

The success of this function has been limited and at least one case it has failed to give as good a fit as a LEPS function [87].

3.1.2.3 SUM OF N-BODY POTENTIALS

This type of potential is specified as a sum of terms, each term describing the potential involving n members of the system. For triatomic systems it consists of three two-body terms and one three body term. The three body term is always designed to be negligiably small at large internuclear distances. One early potential in this form was that of Anderson [173] for co linear geometries:

$$V(r_1,r_2)=V_1(r_1)+V_2(r_2)+A.E \qquad [III.1.19]$$

where $E=\exp(-B(r_1-c.D_2-D_1)^2/(r_1+r_2)^2$

r_1, r_2 = internuclear distances

V_1, V_2 = ground state diatomic functions

Here, because of the restricted geometry, one of the two-body terms is missing.

Chang and Karplus [15] used the following function for H_2O:

$$V=F(r_1,r_2,r_3)+V_{OH}(r_1)+V_{OH}(r_2)+V_{HH}(r_3) \qquad [III.1.20]$$

where $F(r_1,r_2,r_3)=$

$$\exp[-a_1(r_1+r_2-b)-a_3r_3].P_1(r_1,r_2,r_3)$$

$$+\exp[-a_2(r_1+r_2-b)-a_4r_3].P_2(r_1,r_2,r_3)$$

P_1 and P_2 are polynominals involving powers of r_1, r_2 and r_3 from -1 to 3.

This function has a total of 25 parameters.

Sorbie and Murrell [101] have proposed an analytical function, the parameters of which they obtain from spectroscopic data. The function is suitable for fitting, and seems especially appropiate for attractive potentials.

The potential is given by eqn. [III.1.2].

$$V(r_1,r_2,r_3)=V_1(r_1)+V_2(r_2)+V_3(r_3)+V_{123}(r_1,r_2,r_3) \qquad \text{[III.1.2]}$$

$$V_{123}(r_1,r_2,r_3)=V_s(r_1-r_1^{eq},r_2-r_2^{eq},r_3-r_3^{eq})$$

$$V_s(s_1,s_2,s_3)=A.P(s_1,s_2,s_3).(1-\tanh q_1.s_1/2).(1-\tanh q_2.s_2/2).(1-\tanh q_3.s_3/2)$$

where A is a constant

P is a polynomial up to quartic terms

r_i^{eq} = i^{th} internuclear distance of equilibrium geometry.

Subsequently this function has been applied to ozone [77] and extended to H_n systems [110].

It has also been used by Herbst [47] to fit the $^2A'$ of CH_2^+, calculated by DIM. Using over 1,200 points, he obtained a LSD of 5.7 Kcal mol^{-1} (23.8 kJ mol^{-1}). He used a double iteration method to optimise the parameters. The linear parameters, polynomial coefficients, were optimized by linear least squares at each iteration of the non-linear parameters. The method used for the non-linear parameters is not specified. This composite technique is only suitable for functions having a large number of linear parameters.

Sorbie and Murrell point out that it is not only necessary for the three-body potential to become zero at large separations, but it must also be finite at short internuclear distances. Consider the case

where $r_1 << r_2, r_3$, if V_{123} is based on, say, a negative exponential function, then at very short values of r_1 it will become very large and dominate the diatomic function V_1. But for this geometry the potential should be virtually all due to V_1.

They also describe how to handle the case of two intersecting dissociation channels which lead to a cusp in the surface at infinite separation.

3.1.3 Results of surface fitting

Work on surface fitting was commenced prior to the function of Sorbie and Murrell being published. At that time the most successful function published was the LEPS function. Initial work was therefore performed using the LEPS surface.

Surface fitting went in four stages:

i) Initial experimentation using LEPS surface.

ii) Attempt to obtain reasonable LEPS fit.

iii) Fit of Sorbie and Murrell function to UHF data.

iv) Fit of Sorbie and Murrell function to CI data.

3.1.3.1 INITIAL DEVELOPMENT

The first attempts at surface fitting were done with a simple steepest descent method, using a small number of UHF points. The classic steepest descent behaviour was observed. The least square deviation dropped rapidly at first, but stopped changing after only a few iterations. Restarting the calculation with a different initial estimate of the parameters failed to give agreement. A modification to steepest descent due to Forsythe and Motzkin [32] was tried. In this modification every n^{th} iteration (n = 5 , was taken in practice) instead of

where $r_1 << r_2, r_3$, if V_{123} is based on, say, a negative exponential function, then at very short values of r_1 it will become very large and dominate the diatomic function V_1. But for this geometry the potential should be virtually all due to V_1.

They also describe how to handle the case of two intersecting dissociation channels which lead to a cusp in the surface at infinite separation.

3.1.3 Results of surface fitting

Work on surface fitting was commenced prior to the function of Sorbie and Murrell being published. At that time the most successful function published was the LEPS function. Initial work was therefore performed using the LEPS surface.

Surface fitting went in four stages:

i) Initial experimentation using LEPS surface.

ii) Attempt to obtain reasonable LEPS fit.

iii) Fit of Sorbie and Murrell function to UHF data.

iv) Fit of Sorbie and Murrell function to CI data.

3.1.3.1 INITIAL DEVELOPMENT

The first attempts at surface fitting were done with a simple steepest descent method, using a small number of UHF points. The classic steepest descent behaviour was observed. The least square deviation dropped rapidly at first, but stopped changing after only a few iterations. Restarting the calculation with a different initial estimate of the parameters failed to give agreement. A modification to steepest descent due to Forsythe and Motzkin [32] was tried. In this modification every n^{th} iteration (n = 5 , was taken in practice) instead of

searching along the current gradient, a search is performed along the direction:

$$(p_i^{(k-2)} - p_i^{(k)})$$

where the superscript refers to the iteration number. The idea in this method is that the calculation becomes lodged in a narrow valley, and this new search direction points down the valley. This modification certainly improved the results, decreasing the best least square deviation by a factor of 10. However convergence was still not obtained. Then Broyden's method [10] was tried, as an algorithm was available [29]. This method is a quasi-Newton method, i.e. it is a second order method but the derivatives are estimated, rather than explicitly calculated. The results were better and approximate convergence obtained, but the rate of convergence was very slow. Therefore a general least squares program was written using the approximate Hessian given by eqn. [III.1.13], and the increment, $\underline{d}$, given by eqn. [III.1.4]. If this approximate Hessian was singular, or nearly so, $\underline{d}$ was taken to be the steepest descent direction. At each step if $F(\underline{p} + \underline{d}) > F(\underline{p})$ then a one-dimensional search along the direction was made to optimize $F(\underline{p} + s.\underline{d})$, where s is the step length. This program worked much better than any tried previously. Also, because of the LEPS functions basically repulsive nature an attempt was made to add an attractive three body potential to the function as shown in eqn. [III.1.22]

$$V = V(\text{LEPS}) + \text{EXP}(-a.r_1.r_2.r_3) \qquad [\text{III.1.22}]$$

This gave very poor results because the minimum appeared to be at a value of infinity for one of the parameters, D_{HH} in fact. The value of this parameter increased until the function became swamped by rounding error. The LEPS function tends to $\infty - \infty$ in these conditions, i.e. the difference between two large numbers.
This three body function was abandoned.

3.1.3.2 SURFACE I

With an optimization program working an attempt was made to fit the UHF points that had been calculated at this time using an LEPS surface.

In order to ensure that the correct behaviour occured on dissociation the two diatomics were treated separately.

Firstly a set of UHF points for $NH^+(^4\Sigma)$ was calculated, and a Morse potential fitted to those points using the program descibed above. The points calculated and the values obtained are shown in Table III.1.1. The Morse parameters obtained, after ?? iterations are shown in Table III.1.2. The least square deviation was 2.75 10^{-5} hartrees. For the second diatomic, H_2, a set of points from the edge of the UHF surface was used. After 40 interations a least square deviation of (1.75 10^{-5}) hartrees was obtained. The parameters are shown in Table III.1.3. The excited state parameters were then optimized together with the two overlap parameters,making a total of 8 parameters. 241 UHF points were used, and the best result obtained was a least square deviation of 0.0286 hartrees. The optimized parameters are shown in Table III.1.4. However, when a contour plot was performed on the resulting function, it was apparent that the surface was far from satisfactory. Closer examination of the points used revealed that the trouble was a lack of points on the inside edge of the potential well (see fig.III.1.1). This illustrates well the fact that, in order to obtain a dynamically useful fit, a grid of points over the entire surface is necessary.

3.1.3.3 SURFACE 2.

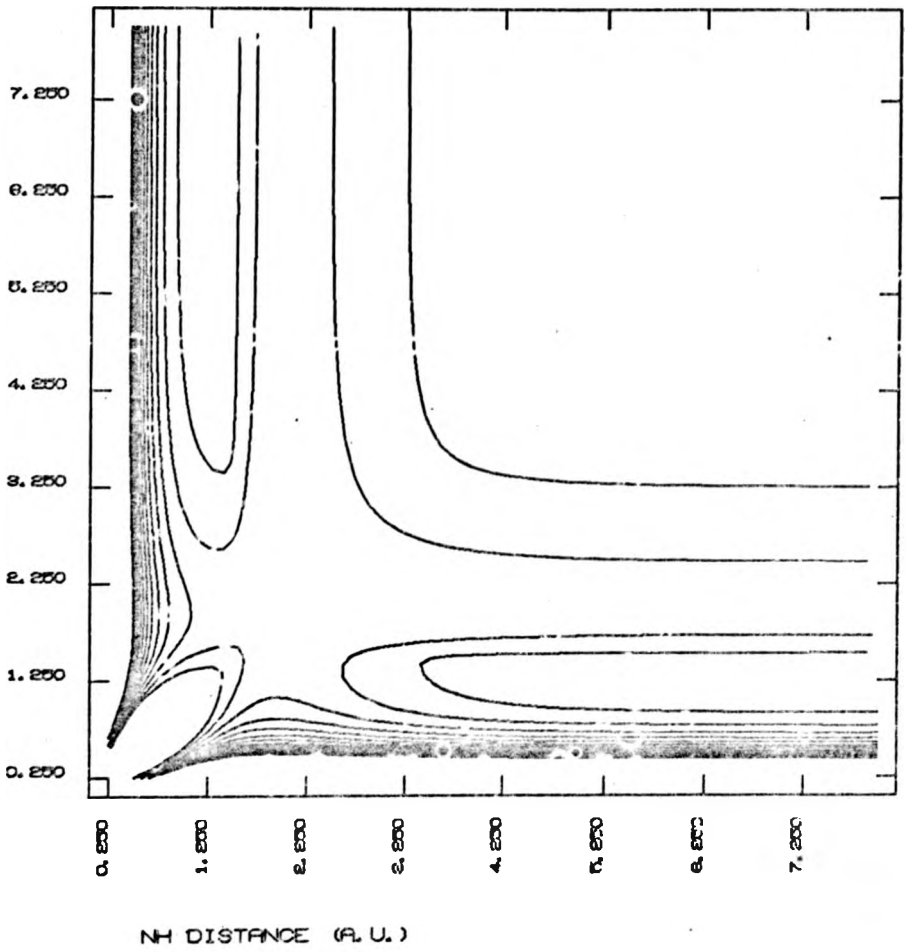

FIG. III.1.1. NH_2^+: Surface 1; Contour plot for linear H-N-H geometries.

Table III.1.1

UHF potential for NH^+, and values from Morse potential.

$R(NH^+)$	E(UHF)-E(∞)	E(Morse)
1.0	0.59807	0.5689
1.5	-0.04694	-0.0392
1.75	-0.11454	-0.1171
2.0	-0.13025	-0.1362
2.25	-0.12407	-0.1286
2.5	-0.10995	-0.1109
3.0	-0.07941	-0.0725
4.0	-0.03574	-0.0253
5.0	-0.01187	-0.0081
6.0	-0.00350	-0.0025
7.0	-0.00128	-0.0008

E(∞) = -53.39737 hartrees

Table III.1.2

Morse parameters for NH^+, UHF.

D_e = 0.136147 hartrees

r_o = 2.02070 a.u.

b = 1.17574 $a.u.^{-1}$

Table III.1.3

Morse parameters for H_2 (UHF).

D_e = 0.116468 hartrees

r_o = 1.64038 a.u.

b = 0.794987 $a.u.^{-1}$

Table III.1.4

LEPS parameters for surface 1.

NH	D_e	-3.64927	hartrees
	r_o	0.45023	a.u.
	b	10.03207	$a.u.^{-1}$
	s^2	0.10739	(no units)
H_2	D_e	1074.7842	hartrees
	r_o	-196.08885	a.u.
	b	14.2658	$a.u.^{-1}$
	s^2	-0.22829	(no units)

This was fitted in the same way as surface 1 except that some points were added with a N-H distance of 1.0 a.u. Initially a large number of such points were added. However, because of the comparatively large magnitude of these points they tended to dominate the fitting procedure. Therefore the number of points was reduced to include about half of those with an N-H distance of 1.0 a.u., i.e. 33 points giving a total of 274 points.

The best fit obtained for this surface had a LSD of 0.129 hartrees (338 kJ mol $^{-1}$). The parameters are given in table III.1.5.

A plot of the linear [N-H-H] geometry is shown in fig.III.1.2. While this result is reasonable, the parameters do appear to be rather unexpected , and are certainly nothing like the semi-empirical values. This would seem to indicate the unsuitable nature of the LEPS function for attractive surfaces. To try to overcome this shortcoming some trials fits were done with an extra three body term of the form: $\exp(-c.r_1.r_2.r_3)$. These gave very poor results for reasons discussed in the section on Sorbie and Murrell function (3.1.2.3.).

3.1.3.4 SURFACE 3

This was the same as surface 2 except that a variation of Marquartd's method, due to Fletcher [31], was used as implemented in the NAG library [78]. Since the surface had been fitted already the emphasis was on comparing the rate of convergence, rather than obtaining the best fit. In fact the best fit achieved was slightly worse than surface 2 ,with a LSD of 0.132 hartees (347 kJ mol $^{-1}$) The parameters are shown in table III.1.6. Although the actual fit obtained was slightly worse, the convergence was very good. Particularly as the this method was not prone to stopping at stationary points other than the minimum, as the

Table III.1.5

LEPS parameters for surface 2.

	NH	HH	
D_e	4.9493	5.89E-13	hartrees
r_o	-2.9288	29.8622	a.u.
b	0.8495	10.2066	$a.u.^{-1}$
S^2	-0.1649	73.2121	(no units)

Table III.1.6

LEPS parameters for surface 3.

	NH	HH	
D_e	0.6136	-8.1245	hartrees
r_o	0.8809	-66.016	a.u.
b	1.7341	5.3069	$a.u.^{-1}$
S^2	0.4586	18.1152	(no units)

previous non-linear least squares routine was prone to doing. Because of this all subsequent work was done with this method.

3.1.3.5 SURFACE 4: SORBIE AND MURRELL FUNCTION

This surface was based on the function of Sorbie and Murrell.

The diatomic potentials were the Morse potentials used for surface 1. The equilibrium geometry was taken to be linear H-N-H with both N-H distances = 2.0 a.u. The position of this point was not optimized.

From the nature of the potential it would be possible to fix the parameter, A, such that the equilibrium point is fitted exactly. Although removing this parameter from the fitting routine would make the fitting slightly easier it would remove considerable freedom for fitting the other points. This is especially true if there is any error on the equilibrium geometry.

In practice it was found that the fitting procedure was very sensitive to the value of this parameter, as might be expected. The best policy appeared to be to give A an initial value such that the equilibrium point is fitted exactly, but then allow it to vary. On a number of occasions results were obtained where one or more of the polynominal coefficients tended to $+/-\infty$ and the A parameter diverged from its expected value. It appears, therefore, that the error hypersurface for this function has various valleys leading to infinite parameters as well as the main global minimum.

The best LSD obtained was 0.00813 hartrees (21.35 kJ mol^{-1}), i.e. the improvement compared to the LEPS function was more than an order of magnitude. The parameters are shown in Table III.1.7. Note

Table III.1.7

Parameters for Sorbie and Murrell function for surface 4.

q_{NH}	1.3405	c_{210}	-6.5713
q_{HH}	1.1119	c_{111}	-13.946
c_{100}	-1.1088	c_{202}	-0.3862
c_{010}	2.2840	c_{040}	-0.1773
c_{200}	-7.8754	c_{301}	-0.7620
c_{020}	-3.6064	c_{202}	-1.2315
c_{110}	11.1780	c_{310}	0.3394
c_{101}	-15.251	c_{220}	-1.6210
c_{300}	0.4997	c_{130}	0.9303
c_{030}	-1.6003	c_{121}	-2.4171
c_{201}	2.5012	c_{211}	1.0922
c_{120}	6.2705	A	-0.015993

N.B. c_{ijk} is the coefficient in the polynominal of $s_1^i.s_2^j.s_3^k$

$c_{ijk} = c_{kji}$

(all quantities in atomic units)

that the polynominal coefficients are reduced by symmetry, i.e. $c_{ijk} = c_{kji}$. This is very similar to the LSD obtained by Herbst [47] of 23.8 kJ mol $^{-1}$.

3.1.3.6 SURFACE 5: CI POINTS

This was the same as surface 4 except that 118 points on the lowest energy A" state were fitted. As pointed out above, the CI points were not calculated with a view to using them in a fitting procedure and therefore the fit was treated with caution. The best fit obtained had a LSD of 0.0197 hartrees (51.7 kJ mol $^{-1}$) and the parameters are shown in Table III.1.8.

3.1.3.7 SURFACE 6: CI DIABATIC

Since transitions to the higher A" state were considered to be important in the dynamics of the reaction at relative energies above 2.0 eV. An attempt was made to define a diabatic surface consisting of the lower points on the A" surface at geometries greater than the avoided crossing, and the higher points at geometries less than the avoided crossing. This gave a total of 108 points. For C_{2V} symmetry the selection of the correct points is of course simple, but for C_s geometries it is sometimes difficult. This composite set of points was then fitted with the Sorbie and Murrell potential. The results were fairly good considering the artificial nature of the surface and the uneven distribution of points. The best LSD was 0.0247 Hartees (62 kJ mol $^{-1}$), and the parameters are given in table III.1.9. The equilibrium geometry was taken to be the lowest point on the $^3A_2$ surface, estimated to be N-H distance = 2.75 a.u.,H-H distance = 1.5 a.u.

The results of this trial fit indicate that it may be possible

Table III.1.8

Parameters for Sorbie and Murrell function for surface 5.

q_{NH}	0.7785	c_{210}	-15.0979
q_{HH}	-0.8172	c_{111}	-32.7981
c_{100}	-4.5932	c_{202}	0.0098
c_{010}	1.6531	c_{040}	2.1093
c_{200}	3.1776	c_{301}	1.4487
c_{020}	-3.4919	c_{202}	-3.5358
c_{110}	15.779	c_{310}	3.7144
c_{101}	-18.0631	c_{220}	-0.9316
c_{300}	-1.7070	c_{130}	-2.9881
c_{030}	13.4615	c_{121}	-6.7150
c_{201}	6.5071	c_{211}	3.1807
c_{120}	-7.0959	A	-0.008156

Morse parameters used:

	NH	HH
D_e	0.15919	0.16094
r_o	2.05	1.4015
b_e	1.17	0.79

(all quantities in atomic units)

Table III.1.9

Parameters for Sorbie and Murrell function for surface 6.

q_{NH}	1.7642	c_{210}	2.3825
q_{HH}	1.7752	c_{111}	-4.3339
c_{100}	0.2120	c_{202}	-0.5435
c_{010}	-2.2954	c_{040}	1.9705
c_{200}	1.1510	c_{301}	1.7043
c_{020}	7.9414	c_{202}	-1.6825
c_{110}	-1.4167	c_{310}	1.8841
c_{101}	-1.9475	c_{220}	0.0949
c_{300}	0.0949	c_{130}	-0.8525
c_{030}	-5.8849	c_{121}	2.3918
c_{201}	0.4286	c_{211}	-1.2656
c_{120}	3.3501	A	0.1809

N.B. c_{ijk} is the coefficient in the polynominal of $s_1^i.s_2^j.s_3^k$

$c_{ijk} = c_{kji}$

(all quantities in atomic units)

to define an upper surface in this way for use with a trajectory "hopping" model.

3.2.1 Interpolation

Interpolation represents the alternative to surface fitting for using pointwise surfaces in dynamic calculations. The interpolation that has been used most for surfaces of this kind is spline interpolation [41,51].

The general spline function of order k, is given by eqn. [III.3.1]:

$$S_i(x) = \sum_{j=1}^{k} c_{ji}(x-x_i)^j \quad , \quad x_i \leq x < x_{i+1} \qquad \text{[III.2.1]}$$

The set of points, x_i, are referred to as the knots or nodes of the function, and normally are the known values, $f(x_i)$. The coefficients, c_{ij}, are determined by the requirements that the function be continuous, and that the derivatives up to order k-1 also be continuous.

The most common order to use is cubic, and all work for chemical systems has used cubic splines. The continuity requirements mean that the graph of $S''(x)$ consists of connected straight line segments. From this an interpolation formula can be derived in terms of the function values and the second derivatives [41,73]:

$$\begin{aligned} S_i(x) = {} & f(x_i)+[(x-x_i)/(x_{i+1}-x_i)][f(x_{i+1})-f(x_i)] \\ & +(x-x_i)(3(x-x_{i+1}).S''(x_i) \\ & +[(x-x_i)^2-(x_{i+1}-x_i)^2]\{[S''(x_{i+1})-S''(x_i)]/ \\ & (x_{i+1}-x_i)\})/6 \end{aligned} \qquad \text{[III.2.2]}$$

Before this formula can be used it is necessary to calculate the $S''(x_i)$. From the constraint that the first derivatives be continuous, i.e. $S'_{i-1}(x_i) = S'_i(x_i)$, for i=2,3,..n-1, the following equations can

be derived:

$$S''(x_{i+1})(x_{i+1}-x_i)/6 + S''(x_i)(x \qquad \text{[III.2.3]}$$

$$S''(x_i-1)(x_i-x_{i+1})/6 = (f(x_{i+1})-f(x_i)/(x_{i+1}-x_i)$$

$$-(f(x_i)-f(x_{i-1}))/(x_i-x_{i-1}),\ i=2,3,..n-1$$

These are n-2 linear equations in n unknowns, S''_i. Therefore there are two undefined values, or more generally two degrees of freedom. Normally the two end values, $S''(x_1)$ and $S''(x_n)$ are specified by external constraints or simply taken to the zero [73]. The two degrees of freedom can be expressed in terms of the first derivatives, and Sathyamurthy and Raff [94] use a four point Langrangian interpolation to estimate the values of $S'(x_1)$ and $S'(x_n)$.

Another possibility is to optimise the two end second derivatives so that the 'best' interpolation is achieved. Some experimentation was carried out along this approach and the two end second derivatives chosen to minimize:

$$\sum_{i=1}^{n-1} S((x_i+x_{i+1})/2)-[f(x_i) + f(x_{i+1})-f(x_i)/2] \qquad \text{[III.2.4]}$$

i.e. the interpolation is made as close as possible to straight line segments. A number of the figures presented here were prepared using interpolation in this way, (see Figs II.2.1 to II.3.6 inclusive). Although in some cases the values obtained were adjusted by inspection to improve the smoothness.

As an example see fig.III.2.1, This is the same as fig II.2.1 but with differing values of the two end second derivatives. In practice the whole success of spline interpolation may rest on the handling of these two degrees of freedom.

Spline interpolation can be readily extended to more than one dimension [26,73]. The basis of the extension to two dimensions is that the value S(x,y) is obtained from the second derivatives $S''(x,y_j)$.

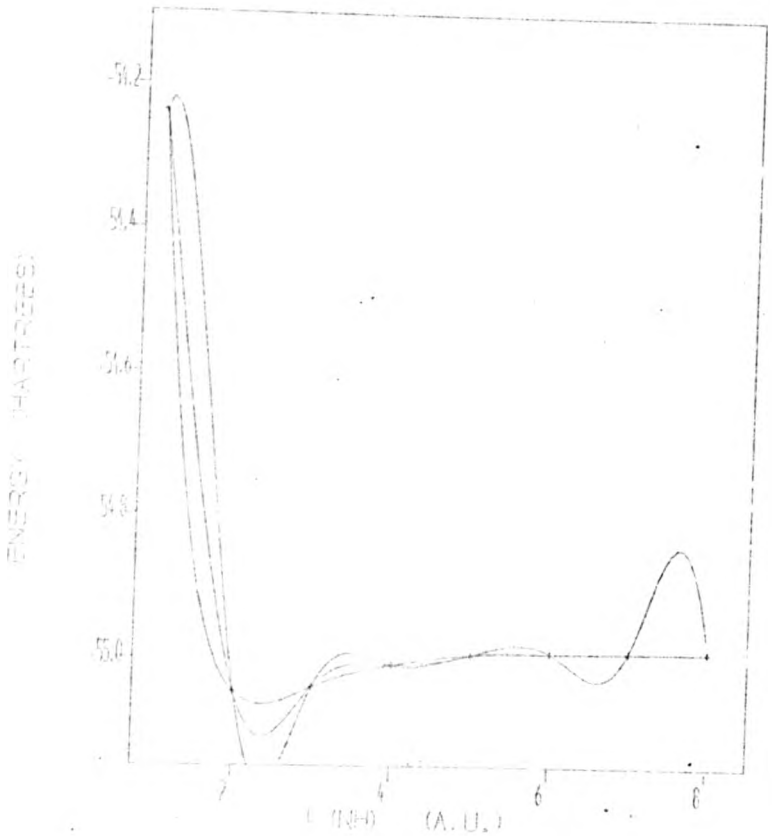

FIG. II.2.1 EXAMPLE OF SPLINE INTERPOLATION

DERIVED FROM FIG. II.2.1

These are in turn derived from the fourth derivatives $S''''(x_i, y_j)$. The second (partial) derivatives are calculated in the same manner as the one dimensional case, for each line of constant x or y. The fourth derivatives are then similarly calculated from the second derivatives.

Extension to three dimensions requires the calculation of derivatives up to the sixth. Explicit formulae for the three-dimensional case are given by Sathyamurthy and Raff[94].

The accuracy of Spline interpolation has been investigated by Sathyamurthy and Raff[94]. They find that in general the accuracy is good, but that it becomes poorer for two and three dimensional cases. They also find that the accuracy is very dependent on the number of nodes used. As the number increases the accuracy increases rapidly, but beyond a certain point the increase slows up, indicating that there is an optimum number of nodes. They also compare the effect on trajectory calculations of using a spline interpolation instead of a semi-empirical surface. They find that on an individual trajectory basis there is no agreement because the trajectories diverge early in the calculation. However, for the overall properties of a batch there was reasonable agreement. It is worth noting that they were not comparing an analytical fit to a set of points with spline interpolation, but rather comparing spline interpolation with the function that generated the points.

It is also worth noting that trajectories using interpolation took approximately 5 times as long, in terms of computer processor time, as those using the semi-empirical function.

McLaughlin and Thompson [73] have used two dimensional spline interpolation for the $HeH^+ + H_2$ -> He + H_3^+ reaction, for C_{2v} symmetry

only.

3.2.2. The co-ordinate problem

Given the comparative success of the results desribed above an attempt was made to interpolate the UFH points described in section 2.2.

Immediately the problem arose of a suitable co-ordinate system in which to perform the interpolation. Multi-dimensional spline interpolation requires a full rectilinear grid, the grid lines do not have to be regular however. If the three internuclear distances are used (r_1,r_2,r_3), as Sathyamurthy and Raff have done, then an attempt to generate such a grid requires the energy to be known at complex geometries. Some methods of calculation work reasonably well for such geometries, e.g. DIM, and indeed such values may be used in semi-classical calculations. UHF potentials were not obtainable for such geometries, and so this simple co-ordinate system was excluded. It is not known whether Sathyamurthy and Raff used complex geometries.

An alternative co-ordinate system is to use (r_1,r_2,θ) where θ is the HNH angle. One major problem with these co-ordinates is that the UHF points calculated did not lie on a grid. Apart from this, to obtain a reasonable representation of the surface at large r_1 and r_2 would require many small values of θ leading to a disproportional number of points at smaller r_1 and r_2 values. Also the potential at r_1=r_2,θ=0 is essentially infinite and this futher complicates the interpolation. The obvious way to handle this would be to use a large value of the energy for such 'infinite' points. However the continuity requirements of the spline equations will require that this is interpolated not as a cusp but a 'hill', i.e. S' will be zero at this point. This will mean that the intervals adjacent to such a cusp will be very poorly interpolated.

To avoid this one could either: split the calculation of second derivatives each time such a cusp was reached, using different values for the S'' on either side of the cusp and treating them the same as the end points;or: have grid points sufficiently close so that the intervals next to the cusp are not dynamically significant. Neither approach is satisfactory.

Similar problems are encountered for other co-ordinate systems.

Normal co-ordinates, (q_1,q_2,θ), $q_1=r_1+r_2$, $q_2=r_1-r_2$, involve θ and hence the problems above.

Another possibility is the perimeter co-ordinates (p,f,q) where $p= r_1+r_2+r_3$, $f=r_1/p$ and $q=r_2/p$. However these show the triangle inequality in a slightly different guise, viz: $f+q> 1/2$.

Prolate spheroid co-ordinates do have some advantages, (ζ,η,a), $a=r_3$, $\zeta=(r_1+r_2)/2a$, $\eta=(r_1-r_2)/2a$, in as much as the complete grid is real. However there is a cusp at $\zeta= 1/2$, $\eta= +/- 1/2$.

Also a large number of physically unimportant points would need to be included in an interpolation. When a is small then $\zeta=8$, is a reasonable maximum, but when a is large $\zeta=1$ would be reasonable. If a is say, 8 then $\zeta=8$ corresponds to internuclear distances of 64. This is not too unpleasant as these values can always be estimated accurately by means other than ab initio calculation, e.g. by extrapolation.

Finally note that a package for one, two, or three dimensional spline interpolation is available from Q.C.P.E. [90]. The techniques it uses are very similar to those discussed here. It does however allow for alternative choices of the remaining two degrees of freedom,

including a four point Langragian interpolation at the end points.

Chapter 4.

Trajectory calculations

METHODS FOR CALCULATING REACTION DYNAMICS

There are basically three methods for calculating reaction dynamics: classical, semi-classical, and quantal. Of these only classical trajectory methods have gained widespread use and acceptance.

4.1.1 Classical

The basis of the method is the numerical integration of the motion from some set of specified starting conditions. The integration is continued until the system is well into some product channel. It is therefore possible to compute the outcome of any particular collision, given the initial conditions, and assuming that the motion is classical. Given a particular surface the accuracy of the method is determined by how accurate an approximation classical mechanics is to the "real" behaviour. Classical mechanics is certainly reasonable because the nuclei are reasonably heavy. In practice it depends what quantity is desired, macroscopic quantities such as reaction rates seem to be well described, but others , such as threshold behaviour are not described adequately. The method has been widely used since the paper of Karplus,Porter and Sharma [53].

4.1.1.2 STARTING CONDITIONS

For each trajectory the exact positions and momenta have to be of the atoms have to be defined. Usually these are not defined in the actual co-ordinates used for the calculation, but in terms of suitable variables (see [53] for a suitable set).

Only one variable is worthy of special note, and that is the vibrational phase of the diatomic. This could be specified directly and the bond length calculated along with the momenta of the two atoms. This is a complex calculation however, firstly to specify the phase, and secondly to calculate the momenta. Instead, the method of Karplus et al. [53] is frequently used. This involves fixing the diatomic bond length at one of its classical turning points, thus giving zero vibrational kinetic energy. The phase distribution is then introduced by varying the initial separation, i_o, over a range of i_o to $i_o + Vt/2$, where V is the relative velocity, and t the time of one vibration of the diatomic. If the separation is sampled linearly over this range then the correct classical phase distribution is obtained. This method is valid if i_o is large enough for the pertubation of the diatomic by the other compoments to be small. This phase distribution is consistent with the method, but is, of course, very unlike the true distribution. This led Careless and Hyatt [12] to try a quantal distribution. They discovered that doing this gave a plot of reaction probability versus energy the oscillatory character of quantal calculations. Further investigation by Bowmann et al [8] showed that using quantum initial conditions was invalid. In particular, the reaction probability was found to be a rapidly varying function of the initial separation. They also showed that any distribution other than the classical is also invalid.

Trajectory calculations are generally done in batches, and in any batch some starting parameters are held constant and some varied from trajectory to trajectory. The nature of the variation of the trajectories depends on the purpose of the calculations. Virtually always some parameters are varied randomly for Monte Carlo analysis [45]. The basis of Monte Carlo methods is that to remove the dependence on some parameter random values of that parameter are taken, and the

results of the calculation averaged. Usually the starting parameters are defined in such a way that they have a uniform distribution within a given range. Non-uniform distributions create special problems unless the distribution function can easily be transformed to a linear form.

An important question with Monte Carlo methods is the accuracy of the averaged results. The fractional error for some quantity which depends linearly on the number of, say, reactive trajectories, N_r, to the total number, N, is given by eqn [IV.1.1].

$$\text{Error} = [(N-N_r)/(N.N_r)]^{1/2} \qquad [IV.1.1]$$

It is apparent from this that a large number of trajectories are required to attain high accuracy.

4.1.1.2 INTEGRATION OF THE EQUATIONS OF MOTION

Having specified the starting conditions it is then necessary to calculate the actual trajectory. This is done by numerical integration of, usually, Hamilton's equations of motion [38]. Sometimes other formalisms such as Lagrange's [38] are used [59].

The end of the integration is usually tested on the basis of interpartical distance, i.e. when the atoms have separated a specified distance. Leasure and Bowman [62] have suggested that, because changes in vibrational state are confined to one area of the surface, the trajectory could be terminated on exit from that area.

The actual integration method used depends on many factors. Early work used Runge-Kutta methods almost exclusively. But multi-step methods quickly gained ground, and now fourth or higher order predictor-corrector methods seem to be most commonly used. Muckerman uses an 11-th order method [74]. One disadvantage of predictor-corrector methods is that the step size can not be changed

easily in the course of an integration. For this reason self adjusting methods such as Nordsiek's are attractive, but an attempt to use this method failed because the step size was not controlled sufficiently well.

4.1.3 Alternate Methods

4.1.3.1 QUANTAL METHODS

Few quantal calculations have been reported for full three-dimensional reactive collisions, and a well proven technique does not exist that can be applied with confidence to a previously unknown reaction.

The main problem with quantal methods arises from the choice of co-ordinates and basis sets. Consider the collision of an atom, A, and diatomic BC, in which the partners are transformed from state 'n' to state 'm'. Let ${}^{o}H_n$ be the Hamiltonian for the internal motions of state 'n', and θ_{in} the i^{th} eigenfunction:

$$ {}^{o}H_n \; \theta_{in}(r_n) = E_{in} \; \theta_{in}(r_n) \qquad [IV.1.2] $$

The non-interacting (or asymptotic) Hamiltonian can then be written in two possible ways:

$$ H = {}^{o}H_n + T_n + V_n \qquad [IV.1.3] $$

$$ H = {}^{o}H_m + T_m + V_m $$

where T_k and V_k are the kinetic energy operator and potential for the initial or final states. Expanding the Hamiltonian in terms of the initial state gives:

$$ H = -(h^2/2u_{A,BC})\nabla_R^2 - (h^2/2u_{BC})\nabla_r + V_{BC}(r) + V(R,r) \qquad [IV.1.4] $$

where r = BC bond length,

R = distance from centre mass BC bond to A

$u_{A,BC}$, u_{BC} are the appropiate reduced masses

From formal scattering theory the solution to this asymptotic equation must also satisfy the Lippman-Schwinger integral equation.

$$X_m^+ = X_m + [E_m - H_m - ei]^{-1}.V.X_m^+ \qquad [IV.1.5]$$

where X_m is the initial in asymptote,

V is the potential, and

the term in square brackets represents the general Green's function for outgoing waves in all states of the channel m.

The most obvious approximation to make in eqn. [IV.1.5] is to use the asymptotic solution, i.e. the plane wave eigenvectors of the non-interacting Hamiltonian:

$$X_n(R,r) = \exp(ik_n.R).Q_n(r) \qquad [IV.1.6]$$

where $Q_n(r)$ is the n^{th} internal state of the products. This approxiamtion is known as the first Born approximation, and the accuracy of the results is low. The general class of methods which replace X_m^+ by some approximate function are called distorted wave Born (DWB) methods. A more sophisticated version of this approach has been used by Choi and Tang [116] for the $D + H_2$ reaction.

Another important approach to the problem is to use numerical methods. These fall into two types, both of which have been almost exclusively applied to collinear geometries. In the finite difference method the Schrodinger equation is written as a set of diffence equations on a grid of points, and these difference equations then solved. The other method known as the close-coupling [98], involves expanding the wave function on to a complete basis set for one variable, and solving the resultant coupled equations. Both methods are limited in the number of channels they can handle by the time and storage requirements on the computer used.

Schatz and Kupperman [99] have recently published a method

and applied it to the H + H_2 reaction where the Schrodinger equation is expressed in body-fixed co-ordinates, the wavefunction expanded in a set of vibration- rotation functions. The resultant set of coupled equations are then integrated for each arrangement channel, and the solutions combined to enable the scattering matrix to be calculated.

4.1.3.2 SEMI-CLASSICAL METHODS

The other alternative is to use Semi-classical methods developed mainly by the efforts of Miller [71,70,69], and Marcus [68,67,55]. They have derived similar methods from different starting foundations.Both methods apply action-angle variables, [38, page 209] Marcus from an extension of WKB theory, and Miller from the Feynman propagator. The basic idea of semi-classical theory is to develop the classical limit of quantum theory. It has been amply shown that classical mechanics is a reasonable description of the behaviour of atoms during collisions, but atoms actually obey quantum mechanics. Therefore such purely quantal effects as interference, tunnelling, and threshold behaviour can not be calculated by using classical mechanics. Semi-classical theory hopes to include these effects. For example, consider a transition from state n to m. In quantum theory one calculates a transition amplitude, S_{nm}, which is the corresponding element of the S-matrix. The transition probability is then

$$P_{nm} = |S_{nm}|^2 \quad . \qquad [IV.1.7]$$

Suppose that classically two paths from n to m exist, then the total classical probability is ${}^{t}p_{nm} = {}^{1}p_{nm} + {}^{2}p_{nm}$. The semi-classical approximation to S_{nm} is given by equation [IV.1.8].

$$S_{nm}^{cl} = {}^{1}p^{1/2}.\exp(i.A_1) + {}^{2}p^{1/2}.\exp(i.A_2) \qquad [IV.1.8]$$

(where A is the classical action along the path)

Therefore one can define the semiclassical probability as being

$$P^{sc}_{nm} = |S^{cl}_{nm}|^2 = {}^1p + {}^2p \quad 2({}^1p, {}^2p).\cos(A_1 - A_2) \qquad [IV.1.9]$$

$$= P^{cl}_{nm} + \text{interference}$$

The Feynman propagator on which Miller's approach is based is concerned with the causal development of quantal systems. If one considers a state at time t, i.e. $|t\rangle$, then its state at a later time, t_2, is given by eqn. [IV.1.10]:

$$|t_2\rangle = U(t_2,t).|t\rangle \qquad [IV.1.10]$$

Where $U(t_2,t)$ is the time evolution operator, which can be written explicitly as eqn. [IV.1.11].

$$U(t_2,t_1) = \exp(-iH(t_2-t_1)/h) \qquad [IV.1.11]$$

The basis of Feynman's formulation of quantum mechanics is that matrix elements of the time evolution operator, or propagator can be expressed as eqn. [IV.1.12]:

$$\langle R_2|U(t_2,t_1)|r_1\rangle = \sum \exp(iA\,[r(t)]/h) \qquad [IV.1.12]$$

Where the matrix element is the transition amplitude that a particle at r_1 t_1 will be r_2 at t_2, and $A[r(t)]$ is the Action functional. If the classical limit of equation [IV.1.12] is now taken, then only those paths for which the action functional is an extremum will contribute, and equation [IV.1.12] becomes [IV.1.13], and the summation becomes over all classical paths.

$$\langle r_2|U|r_1\rangle = \sum \exp(iA(r_2,r_1)/h) \qquad [IV.1.13]$$

The scattering operator, S, is now the propagator with the unperturbed time dependence subtracted out in the correct manner, and is given by equation [IV.1.14].

$$S = \exp(iH_o t_o/H) \cdot \exp(-iH(t_2-t_1)/h) \cdot \exp(-iH_o t_1/h) \qquad [IV.1.14]$$

The unperturbed time dependence is due to the non-interacting Hamiltonian, H. The classical S-matrix is the matrix of the S operator in the momentum representation of action angle variables. The resulting expresion for the S-matrix elements is given equation [IV.1.15].

$$S_{nm} = \langle n|S|m\rangle = 2\,(dJ_n/dw_m)^{-1/2}_{J_m} \cdot \exp(iA(m,n)) \qquad [IV.1.15]$$

An important aspect of semi-classical theory is that part which attempts to account for quantum tunneling. This is equivalent to finding trajectories that are classially forbidden, and such trajectories do exist if the co-ordinates and time are allowed to become complex. Semi-classical theory can be seen to account very well for many quantal features. However, with the increase of full three-dimensional calculations it appears that the quantal effects in these systems are not as pronounced as in linear cases. That is to say the quantal features appear to be partially quenched by the increase in dimensionality.

4.2 RESULTS OF TRAJECTORY CALCULATIONS

Trajectories were calculated on the Sorbie and Murrell fit to the UHF points. For C_s symmetry this is the lowest adiabatic surface. The purpose was to determine how much of the dynamics could be explained by collisions on this surface alone. This is necessary before the importance of diabatic effects can be estimated.

Batches of 200 or 300 trajectories were calculated for relative velocities between 13,200 and 24,806m s^{-1} (energies of 0.79 to 2.04 eV), and H_2 vibrational states 0,1, and 2, as well as rotational states (J) of 0,1, and 2. In addition two extra batches of 200-300 trajectories were calculated at 5,000 and 9,000 m s^{-1}, with vibrational state 0, and rotational state 1. This was to investigate the behaviour of cross section at very low energies.

The calculations were performed using a specially written computer program using the method of Karplus,Porter and Sharma [53].

4.2.1 Method

Explicit details of the method used are given by Karplus et al.[53], and it follows closely that described in section 4.1.1.

The co-ordinate system used for the calculations is as follows: If (q_1,q_2,q_3) are the cartesian co-ordinates for atom A of mass, m_A, (q_4,q_5,q_6) for B with mass, m_B,and (q_7,q_8,q_9) for atom C with mass m_C, and P_i the conjugate momenta. then the co-ordinates used $Q_j(j+1,2...9)$, are given by:

$$Q_j = q_{j+6} - q_{j+3} \qquad \text{[IV.2.1]}$$

$$Q_{j+3} = q_j - (m_B q_{j+3} + m_C q_{j+6})/(m_B+m_C)$$

$$Q_{j+6} = (1/M)(m_A q_j + m_B q_{j+3} + m_C q_{j+6})$$

where $M = m_A+m_B+m_C$

In these co-ordinates the equations of motion become [53]

$$dQ_j/dt = (1/u_{BC})\, p_j \quad , \quad j=1,2,3 \qquad \text{[IV.2.2]}$$

$$dQ_j/dt = (/u_{A,BC})\, P_j \qquad j=4,5,6$$

$$dQ_j/dt = (1/M)\, p_j \qquad j=7,8,9$$

$$-dP_j/dt = (1/r_1)[m_C/(m_B+m_C)][Q_j m_C/(m_B+m_C)+Q_{j+3}](dV/dr_1)$$
$$+(1/r_3)[m_B/(m_B/(m_B+m_C)][Q_j \cdot m_B/(m_B+m_C)-Q_{j+3}](dV/dr_3)$$
$$j=1,2,3$$

$$-dP_{j+3}/dt = (1/r_1)[m_C Q_j/(m_B+m_C) + q_{j+3})(dV/dr_1) -$$
$$(1/r_3)[m_B Q_j/(m_B+m_C)\cdot Q_{j+3}](dV/dr_3) \quad , \quad j=1,2,3$$

(note that ref [53] has a slight indexing error in this equation)

These equations were integrated using a fourth order predictor-corrector method, which was started by a Runge-Kutta-Gill method. Integration was continued until the products had separated by more than a specified distance. This distance varied slightly with the value of b_{max}, but was typically 7.0 A.

The program written to calculate the trajectories prints the inital and final states of each trajectory, and also writes them to a file for later analysis. It also calculates the average values of the scattering angles, the vibrational and rotational energy of the resultant diatomic, and reaction probability and cross section. Each trajectory took between 10 and 30 seconds of processor time on a Burroughs B6700, depending on the initial relative velocity and the length of time spent in the collision.

Before trajectories can be calculated it is necessary to determine two parameters for the calculation. These are the stepsize to

be used in the integration, and the value of b_{max}, the maximum impact parameter. The choice of stepsize is determined by two factors: the accuracy of the integration and the computer time required. The accuracy is usually monitored by requiring that the total energy of the system remains within a specified limit of the starting energy. For all calculations the relative change in energy was less than 0.01%. The maximum stepsize to achieve this was $1.5\ 10^{-16}$ seconds. For some calculations it was necessary to reduce this to $1.125\ 10^{-16}$ seconds. Before full batches were calculated some trial trajectories were calculated using different stepsizes, on a LEPS surface for $He+H_2^+$. The results for one particular type are summarized in Table IV.2.1. The scattering angle, θ, was found to be the final condition most sensitive to inaccurate integration, and the values for this are contained in the table. Note that with a stepsize of $2.0\ 10^{-16}$ seconds the same result is obtained as with the smallest stepsize used.

To determine the maximum impact parameter a large value, 3 Å, was taken and a batch of trajectories calculated with this value. The highest impact parameter which could give rise to a reactive collision was then obtained by inspection. This value varies markedly with relative velocity. For velocities of 24,806 and 18,902 m s^{-1}, 2.25 Å was found to be suitable. For relative velocities below 18,902 m s^{-1} the value was increased to 2.75 Å. The value used was checked by calculating a small batch with the impact parameter fixed at the maximum value. All of these trajectories were non-reactive. Indeed all had a scattering angle of less than 20 degrees indicating only slight interaction. For the single batches calculated at 5,000 and 9,000 m s^{-1} a value of 4.5 Å was used.

Table IV.2.1

Relationship of stepsize to energy conservation and scattering angle

Stepsize ($secs.10^{-16}$)	ΔE (%)	no. of steps	θ (degrees)
5.00	2.91	92	18.776
4.00	1.09	114	19.072
3.00	0.30	190	19.217
2.00	0.059	284	19.229
1.60	0.026	355	19.229
1.05	0.0075	555	19.229
0.50	0.0014	1136	19.229
0.40	0.00084	1420	19.229

4.2.2 Results

A summary of all batches calculated is shown in Table IV.2.4. The values shown are the reaction cross-section, average rotational and vibrational energies of NH^+ product, and the average and maximum intensity values of the scattering angle (in centre of mass co-ordinates).

4.2.2.1 REACTION CROSS SECTION

The variation of reaction cross section with velocity is shown in fig IV.2.1 The most obvious feature is that the reaction cross section falls with increasing relative velocity. This is true for all values of V and J. The typical variation of cross section shows a sharp increase with relative velocity till some maximum value is reached. For reactions with little or no barrier it then decreases again due to kinetic effects. This is due to the maximum impact parameter becoming smaller at high velocities. This type of behaviour has been clearly observed in the reaction of K+NaCl by Kwei et al. [58].

Thermodynamically, the reaction is slightly exothermic, but the absence of a barrier is more significant. This means that, in principle, reaction can occur at any relative energy. Therefore a high reaction cross section is to be expected at very low relative energies. The decrease in cross section seems very pronounced, and it is possible that some other effect is enhancing the decrease.

The most likely possibility arises from the nature of the surface. For a fixed H-H distance of 1.5 a.u., i.e. close to the H_2 equilibrium value, the surface has only a shallow minimum (see Fig. II.3.2). Although for C_s symmetry this leads without a barrier, to a

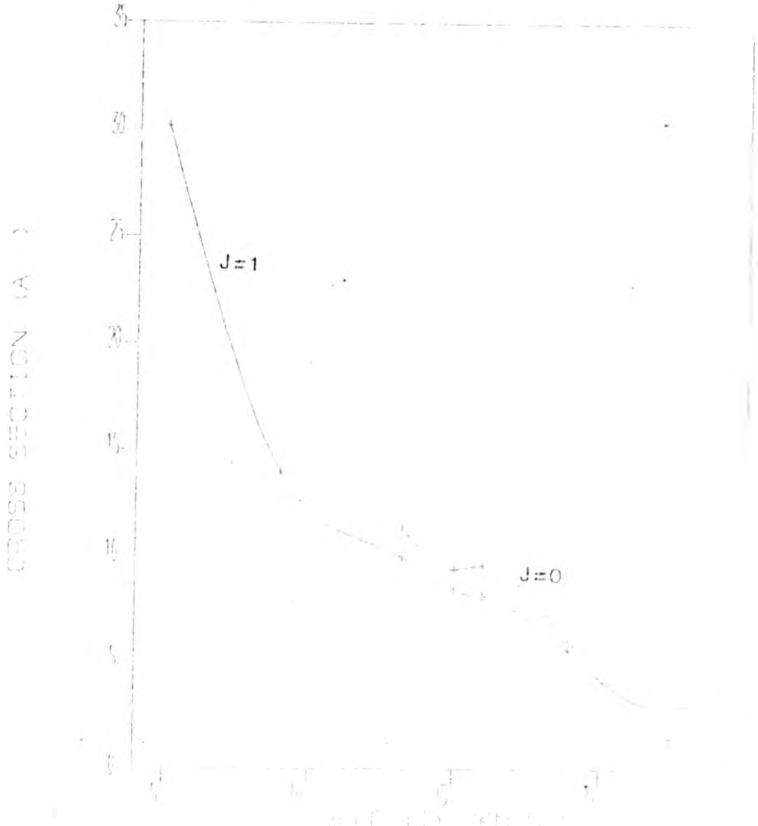
J=1
J=0

Table IV.2.2

Summary of trajectory calculations on UHF surface.

(S_r in A^2; E_{vib} and E_{rot} in $J.10^{-19}$; θ in degrees)

V_{rel} = 5000 m s^{-1} (0.11 eV); b_{max} = 4.5 A; batch size =200

V	J	S_r	$\langle E_{rot} \rangle$	$\langle E_{vib} \rangle$	$\langle \theta \rangle$	θ_{max}	Err
0	1	30.22	2.62	2.09	93	145	7.4

V_{rel} = 9,000 m s^{-1} (0.11 eV); b_{max} = 4.5 A; batch size =300

V	J	S_r	$\langle E_{rot} \rangle$	$\langle E_{vib} \rangle$	$\langle \theta \rangle$	θ_{max}	Err
0	1	13.93	4.66	2.07	112	125	4.8

V_{rel} = 13,200 m s^{-1} (0.79 eV); b_{max} = 2.75 A; batch size =300

V	J	S_r	$\langle E_{rot} \rangle$	$\langle E_{vib} \rangle$	$\langle \theta \rangle$	θ_{max}	Err
0	0	11.32	6.60	5.84	111	145	6.0
0	1	9.98	6.83	4.14	117	125	6.8
0	2	10.42	7.58	2.99	112	135	6.5
1	0	12.43	6.51	4.02	124	175	5.5
1	1	11.72	7.73	4.26	126	175	5.9
1	2	11.80	8.77	4.23	127	135	5.8
2	0	16.16	11.96	4.97	131	165	4.0
2	1	13.22	11.37	4.62	131	175	5.2
2	2	12.20	10.67	4.94	136	165	5.6

Table IV.2.2 contd.

V_{rel} = 15,000 m s^{-1} (1.02 eV); b_{max} = 2.75 A; batch size =300

V	J	S_r	$\langle E_{rot} \rangle$	$\langle E_{vib} \rangle$	$\langle \theta \rangle$	θ_{max}	Err
0	0	9.42	7.72	3.40	121	145	7.1
0	1	8.39	8.13	4.46	116	135	7.8
0	2	8.31	6.80	4.29	111	105	7.9
1	0	11.16	9.94	5.16	135	155	6.1
1	1	10.61	9.69	4.33	132	155	6.4
1	2	8.47	10.80	4.55	124	145	7.8
2	0	14.10	12.72	6.09	139	155	4.8
2	1	11.80	13.11	5.97	130	155	5.8
2	2	11.32	13.64	5.38	139	175	6.0

V_{rel} = 15,995 m s^{-1} (1.16 eV); b_{max} = 2.75 A; batch size =300

V	J	S_r	$\langle E_{rot} \rangle$	$\langle E_{vib} \rangle$	$\langle \theta \rangle$	θ_{max}	Err
0	0	9.58	7.75	4.17	120	145	7.0
0	1	8.16	7.45	5.01	118	135	8.0
0	2	6.73	7.31	4.62	113	125	9.2
1	0	11.01	8.13	4.52	132	155	8.2
1	1	10.06	8.22	5.30	136	165	6.7
1	2	8.39	10.95	5.00	124	165	7.8

Table IV.2.2 contd.

V_{rel} = 18,902 m s^{-1} (1.62 eV); b_{max} = 2.25 A; batch size =200

V	J	S_r	$\langle E_{rot} \rangle$	$\langle E_{vib} \rangle$	$\langle \theta \rangle$	θ_{max}	Err
0	0	6.20	9.53	6.44	118	165	8.8
0	1	5.64	9.71	6.92	120	145	9.5
0	2	4.53	11.47	7.60	121	135	11.2
1	0	8.11	10.04	5.48	135	165	8.9
1	1	7.39	10.52	5.36	123	155	7.6
1	2	6.84	13.54	6.76	124	155	8.1
2	0	9.70	13.44	4.35	134	165	5.7
2	1	7.63	15.46	5.58	127	165	7.4
2	2	7.63	13.96	4.75	128	175	7.4

V_{rel} = 24,806 m s^{-1} (2.79 eV); b_{max} = 2.25 A; batch size =200

V	J	S_r	$\langle E_{rot} \rangle$	$\langle E_{vib} \rangle$	$\langle \theta \rangle$	θ_{max}	Err
0	0	3.58	11.40	6.86	108	145	13.1
0	1	1.59	12.17	5.13	102	105	17.3
0	2	2.94	14.80	8.20	118	145	14.6
1	0	3.18	9.57	8.37	122	155	14.1
1	1	3.74	11.56	8.12	116	155	12.8
1	2	5.01	11.52	7.47	125	165	10.4
2	0	5.01	11.71	9.25	127	165	10.4
2	1	4.93	9.10	8.64	132	165	10.5
2	2	5.65	10.80	7.09	136	170	9.5

deep well, the H-H distance has to more than double before the well is attained. At low velocities the H_2 is going to have time to relax and enter the deep well. As the velocity is increased the time available will decrease and eventually the point will be reached at which the collision is over before the H_2 bond has time to expand.

The variation of cross section with rotational quantum number is comparatively small, and is shown in fig IV.2.2. The variation is probably not significant.

The variation of cross section with vibrational quantum number is much more pronounced and is shown in fig IV.2.3 for three different velocities, all are with J=0. Such an increase is to be expected with the increase in internal energy , especially as the energy will be in the correct mode to facilitate the necessary increase in H-H distance.

4.2.2.2 ANGULAR DISTRIBUTION

The experimental work of Fair and Mahan [27] shows a symmetric distribution at 0.79 eV, which becomes asymmetric at higher energies, reaches a maximum asymmetry and becomes slightly less asymmetric as the relative energy increases further. The angular distribution obtained for V_{rel}=5,000 m s^{-1} (0.11 eV) ($v(H_2)$=0,J=1) is shown in fig IV.2.4. It is apparent from this, and the fact that the average scattering angle is 93 degrees, that the distribtion is totally symmetric at this very low energy.

For V_{rel} = 13,200 m s^{-1} (0.79 eV) the distribution, as shown in Fig IV.2.5, is shifted towards the forward direction. The average scattering angle is now 117 degrees. It is, of course, at this relative energy that Fair and Mahan obtain a symmetric distribution. We, therefore, observe the same type

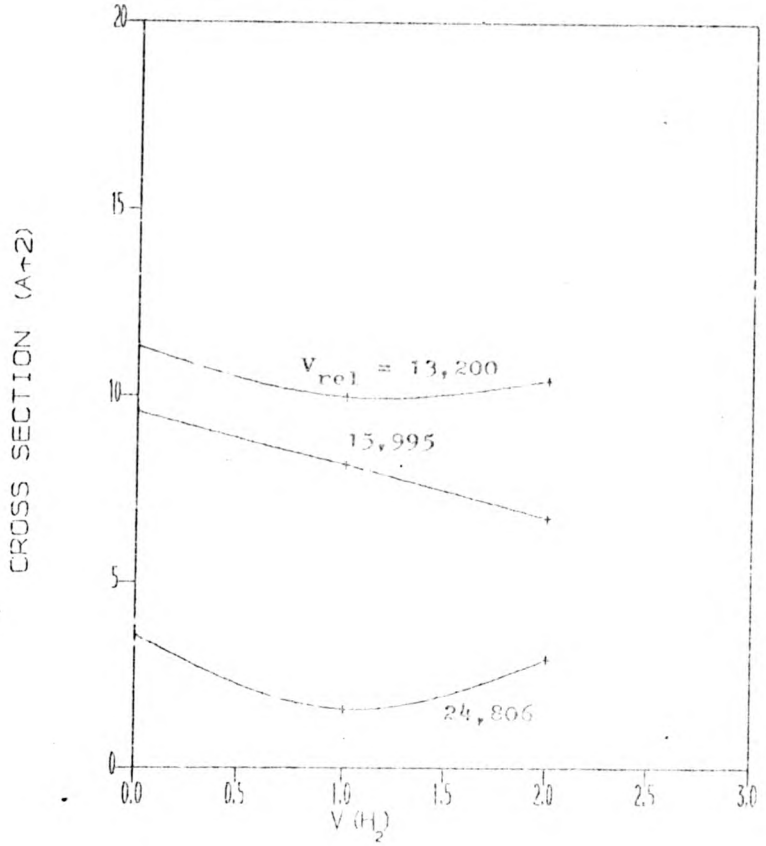

FIG. IV.2.2 REACTION CROSS SECTION VS. J(H_2)

V(H_2) = 0

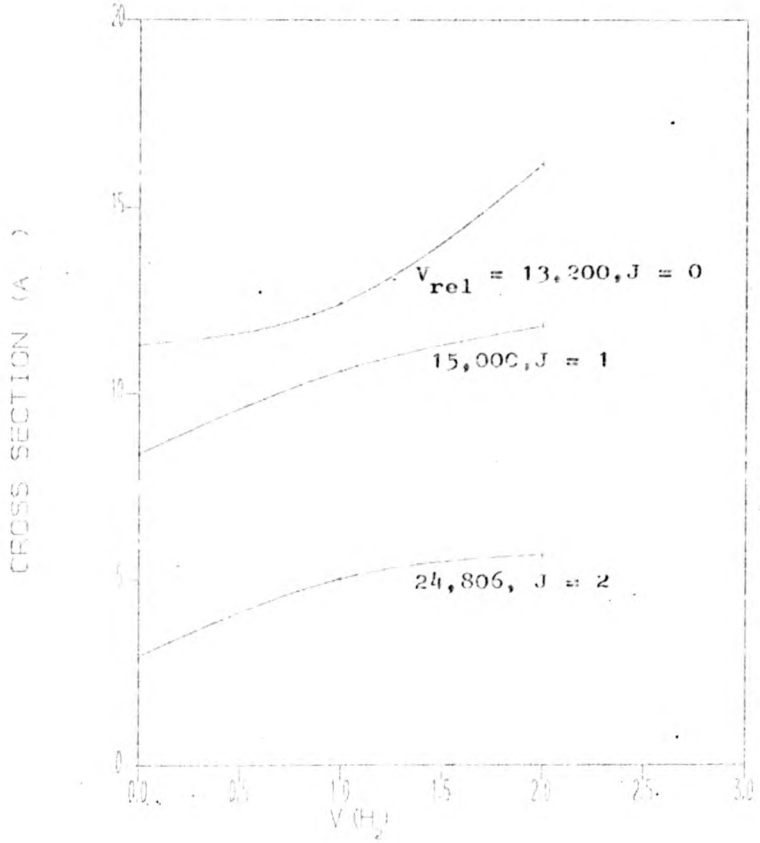

FIG. IV.2.3 REACTION CROSS SECTION VS. V(H)

FIG. IV.2.4 ANGULAR DISTRIBUTION OF NH^+

$V_{REL} = 5,000$ M S^{-1}, $V(0_2) = 0$, $J(0_2) = 1$

of shift from symmetric to asymmetric as Fair and Mahan, but the shift occurs at a lower relative energy. This difference is probably due to the fact that the surface used is not of "chemical accuracy". However, it does demonstate clearly that forward scattering can occur, at quite low energies, on a surface with a deep well.

At higher velocities the distribution becomes slightly more symmetric.

4.2.2.3 INDIVIDUAL TRAJECTORIES

In order to determine whether reactive collisions were in fact occuring via a direct mechanism or collision complex, groups of trajectories were examined. This was done by displaying the three internuclear distances at every 20^{th} integration step to produce a crude plot of internuclear distance against time. In this way a relatively large number of trajectories could be examined in a short time. Those which showed interesting characteristics were re-calculated to produce more refined plots.

Four basic types of collision were easily identified, direct reaction, direct non-reaction, complex reaction and complex non-reaction.

A direct reaction is regarded as one where the internuclear distance of the non-reacting diatomic pair, i.e. A and C if A + BC -> AB + C, has only one minimum. A typical direct non-reaction is shown in fig IV.2.6, a direct reaction in fig IV.2.7, and a complex reaction in fig IV.2.8.

At 15,000 m s^{-1} less than 10% of the reactive collisions were

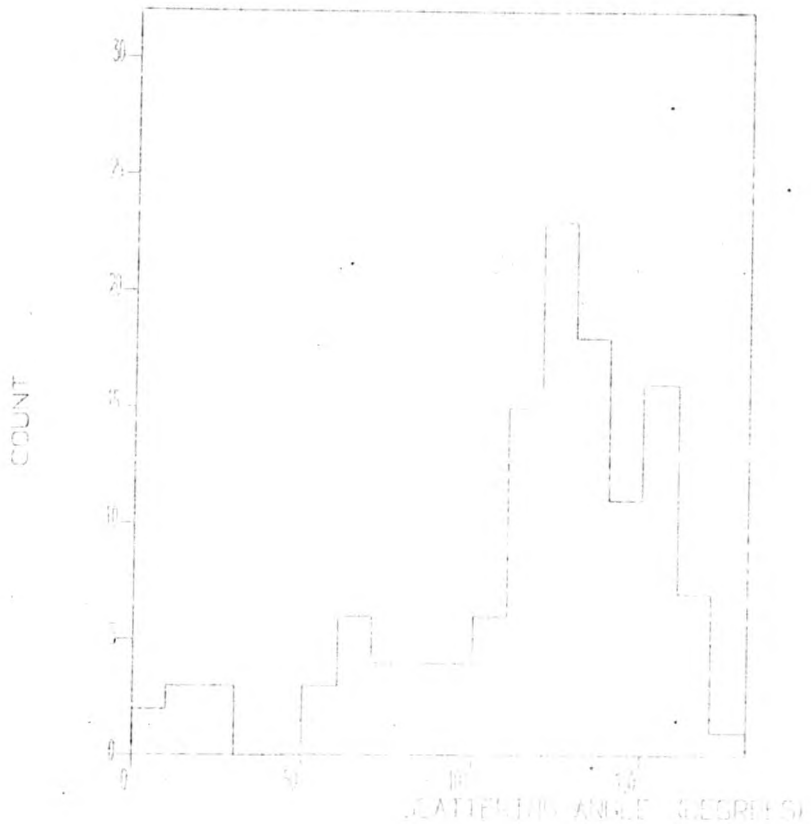

FIG. IV.2.5 ANGULAR DISTRIBUTION OF NH$_3^+$
V_{rel} 13,200 M S^{-1}, V (E$_T$) C. J (E$_T$) 1

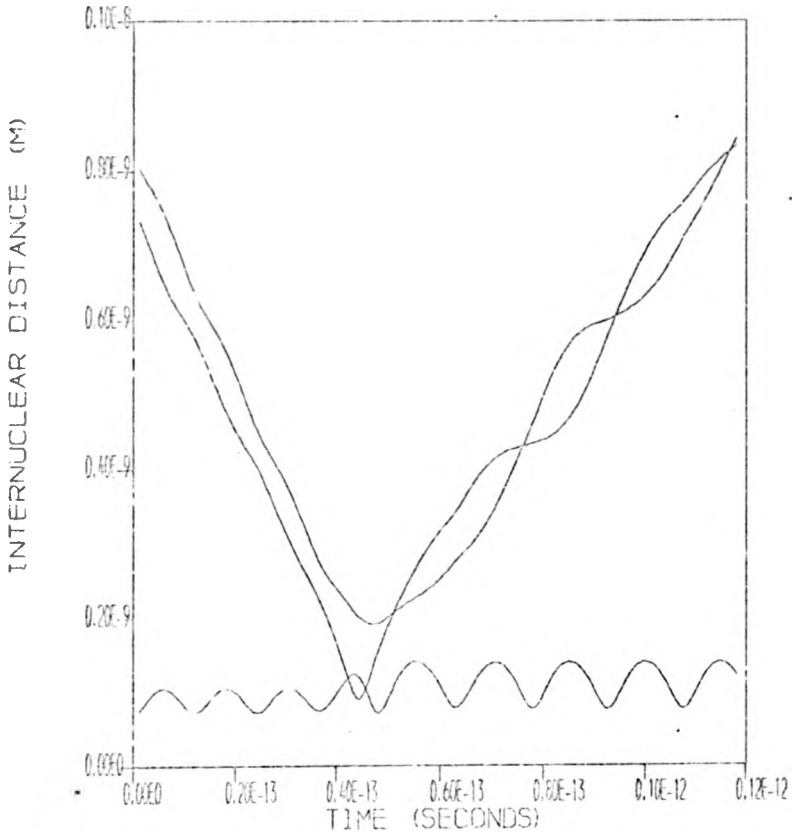

FIG IV.2.6 TYPICAL UN-REACTIVE TRAJECTORY;

$V(H_2) = 0$; $J(H_2) = 1$

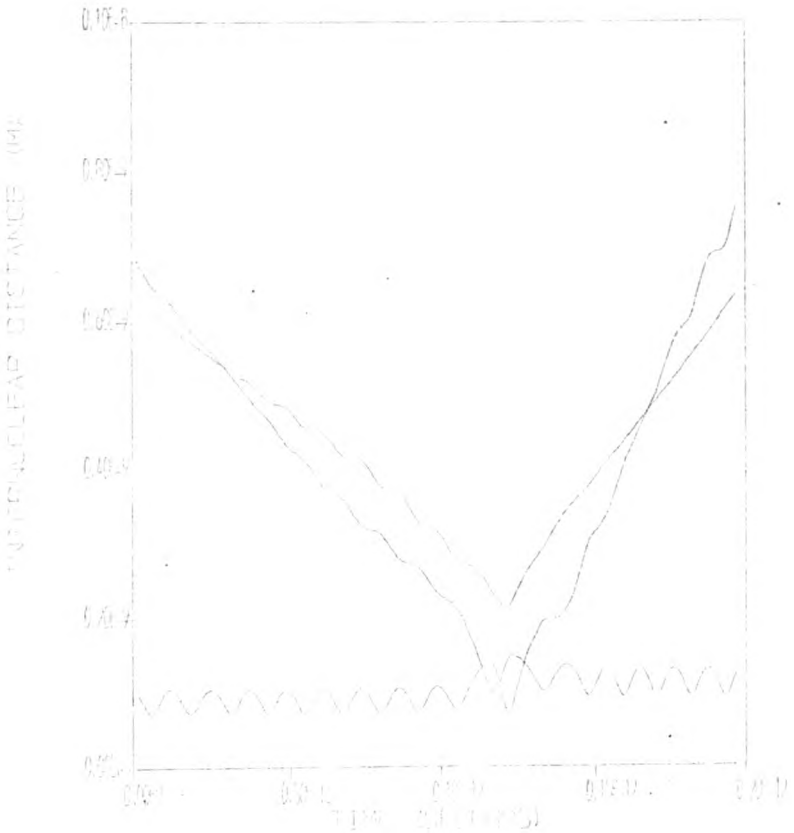
INTERNUCLEAR DISTANCE (M)

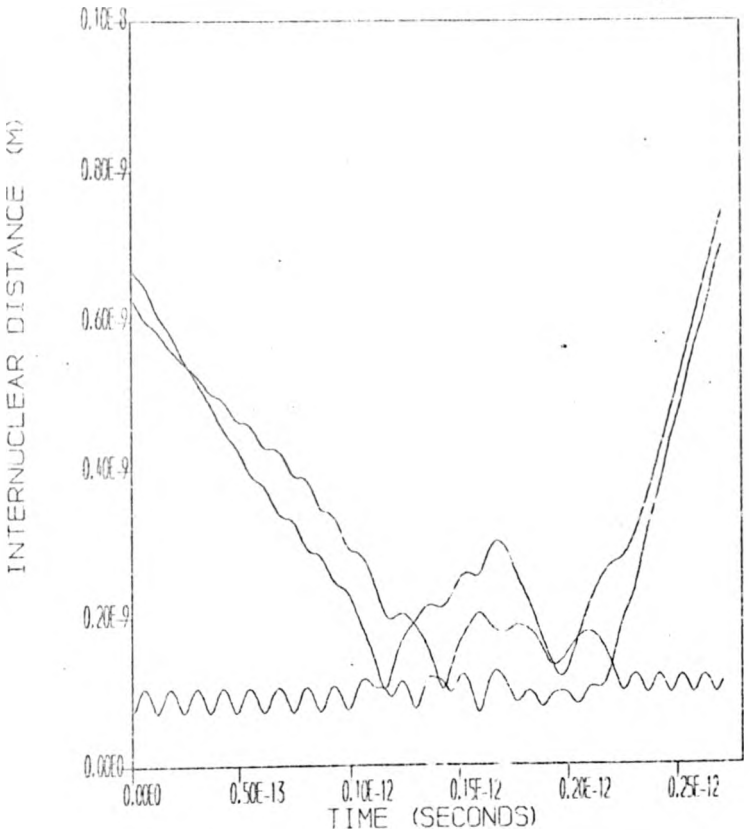

FIG IV.2.8 REACTIVE TRAJECTORY VIA COMPLEX,

V_{REL} = 5,000 M S^{-1}; $V(H_2)=0$; $J(H_2)=1$

of the complex type, and even for these the collision complex lasted for no more than one vibration. This shows clearly that the deep well does not cause collision complex formation at this relative velocity, and that it is not necessary to invoke electronic transitions to a higher state to explain the experimentally observed forward scattering.

At 5,000 m s^{-1} the situation is completely different, as one might expect. Here virtually all collisions give rise to a collision complex that vibrates a number of times before eventually breaking up to either the reactants or $NH^+ + H$.

Chapter 5.

5.1 SUMMARY

The main results obtained are summarized below.

The UHF surface appears, at least for NH_2^+ to be a good qualitative description of the surface compared with the CI. The CI results themselves appear to be as expected, and to be an accurate description of the true surface, with the exception of the $^3A_2$, state where polarization functions are important.

The application of DIM to this system has produced rather disappointing results, which appear to be due to a rather small basis set, although it may be due to the DIM formalism being inadequate for NH_2^+.

The transition from ab initio points to a form suitable for dynamical calculations is probably the area most prone to failure. The direct use of spline interpolation is subject to problems for the three dimensional triatomic case ,as well as incurring overheads in time. The use of rotated Morse functions coupled with spline interpolation seems to be useful for collinear, and even planar geometries, but the extension to three dimensions does not seem straightforward. For NH_2^+, the best approach by far is the use of the function of Sorbie and Murrell,with optimization of the parameters. This method is dependent on the function being well behaved. i.e..to reproduce the diatomic limits reasonably well, and to be suitable for the type of surface concerned. The LEPS function, although used for attractive surfaces with various additional terms included does not seem suitable for this

type of surface.

Trajectory calculations proceed with no difficulty on the Sorbie and Murrell function, the derivatives are easy to calculate.

It is difficult to draw very much in the way of conclusions from comparison of the trajectory results with the experimental data until more detailed experimental results become available. It is manifest that the UHF surface does reproduce the gross features observed in the kinetics, which at first sight is rather surprising considering the deep well and the presence of a conical intersection. It appears that the forward scattering observed at energies in excess of 2 eV is due as much to kinetic effects as to diabatic effects.

5.2 CONCLUSION

The questions arising from the work described here are mainly as follows:

Would increasing the basis set for the DIM calculations improve its abilitiy to reproduce the deep well as expected, or is the failure due to some shortcoming of the DIM formalism.

Does the Sorbie and Murrell function provide such a good fit for a set of CI energies spread over a wide range of geometries.

To what extent do diabatic effects alter the dynamics of the reaction. To answer this the application of a surface hopping model [105] may prove useful, or one of the quantal techniques recently described [16,99].

In conclusion, therefore, we can say that the methods investigated here provide a reasonable picture of the dynamics, even for

such an interesting and complex reaction as $N^+ + H_2 \rightarrow NH^+ + H$. However, the application of more sophisticated, and futher experimental work is required before this reaction will be fully understood.

APPENDIX A.

UHF Energies for NH_2^+.

(all items in a.u. except <NHN which is in degrees).

R(NH)	R(NH')	R(HH)	<HNH	ENERGY	$<S^2>$	STATE[†]
1.0	0.736813	0.736813	47.27	-52.15087	2.0	1A"
1.0	1.0	1.0	60.0	-53.36908	2.01	A"
1.0	1.0	1.5	97.18	-53.73746	2.0	1A"
1.0	1.0	2.0	180.0	-53.83375	2.01	1A"
1.0	1.242128	1.242128	66.26	-54.02992	2.0	1A"
1.0	1.322870	1.0	48.59	-53.97149	2.01	1A"
1.0	1.5	1.0	41.41	-54.04130	2.01	1A"
1.0	1.5	1.5	70.53	-54.26123	2.01	1A"
1.0	1.5	2.0	104.48	-54.39307	2.01	1A"
1.0	2.0	1.0	0.0	-54.11513	2.01	A"
1.0	2.0	1.5	46.57	-54.23389	2.03	1A"
1.0	2.0	2.0	75.52	-54.38112	2.09	1A"
1.0	2.0	2.5	108.21	-54.47190	2.01	1A"
1.0	2.0	3.0	180.0	-54.50443	2.02	1A"
1.0	2.5	2.0	49.46	-54.26101	2.02	1A"
1.0	2.5	2.5	78.46	-54.37160	2.05	1A"
1.0	2.5	3.0	110.49	-54.43773	2.03	1A"
1.0	3.0	2.0	0.0	-54.23706	2.76	1A"
1.0	3.0	2.5	51.32	-54.26645	2.07	1A"
1.0	3.0	3.0	80.41	-54.34232	2.29	1A"
1.0	3.0	4.0	180.0	-54.41315	2.1	1A"
1.0	3.5	3.0	52.62	-54.29387	2.83	1A"
1.0	3.5	3.5	81.79	-54.30496	2.01	1A"

1.0	4.0	3.0	0.0	-54.28749	2.97	1A"
1.0	4.0	4.0	82.82	-54.28988	2.08	1A"
1.0	5.0	4.0	0.0	-54.29794	3.0	1A"
1.0	5.0	4.5	54.9	-54.25176	2.41	1A"
1.0	5.0	5.0	84.26	-54.30285	2.95	1A"
1.0	5.0	5.5	115.15	-54.30671	2.89	1A"
1.0	5.0	6.0	180.0	-54.31228	2.79	1A"
1.0	5.5	5.0	55.38	-54.30671	2.89	1A"
				-54.24929	2.46	A"
1.0	5.5	6.0	115.58	-54.30247	2.95	1A"
1.0	6.0	5.0	0.0	-54.29909	3.0	1A"
1.0	6.0	6.0	85.22	-54.29970	2.99	1A"
1.0	6.0	6.5	115.94	-54.30039	2.98	1A"
1.0	6.0	7.0	180.0	-54.30146	2.96	1A"
1.0	6.5	6.0	56.1	-54.29898	3.0	1A"
				-54.23206	2.01	A"
1.0	6.5	7 0	116.25	-54.29941	2.99	1A"
1.0	7.0	6.0	0.0	-54.29887	3.0	1A"
1.0	7.0	6.5	56.39	-54.29882	3.0	1A"
1.0	7.0	7.0	85.9	-54.29886	3.0	1A"
1.0	7.0	7.5	116.51	-54.29896	3.0	1A"
1.0	7.0	8.0	180.0	-54.29914	3.0	1A"
1.0	7.5	8.0	116.74	-54.29876	3.0	1A"
1.0	7.527610	7.022460	56.32	-54.29871	3.0	1A"
1.0	7.805410	7.326280	58.1	-54.23471	2.01	A"
1.0	8.0	7.0	0.0	-54.29869	3.0	1A"
1.0	8.0	7.5	56.85	-54.29865	3.0	1A"
1.0	8.0	8.0	86.42	-54.29865	3.0	1A"
				-54.24205	2.02	A"

1.0	8.0	8.5	116.94	-54.29866	3.0	1A"
1.0	8.0	9.0	180.0	-54.29869	3.0	1A"
1.0	8.5	8.0	57.04	-54.29862	3.0	1A"
				-54.23547	2.01	A"
1.0	8.5	9.0	117.12	-54.24842	2.01	A"
				-54.29862	3.0	1A"
1.0	9.0	8.0	0.0	-54.23060	2.01	A"
				-54.29861	3.0	1A"
1.0	9.0	8.5	57.2	-54.29860	3.0	1A"
1.0	9.0	9.0	86.82	-54.29872	3.0	1A"
1.0	9.0	10.0	180.0	-54.29860	3.0	1A"
				-54.25347	2.01	A"
1.0	9.5	9.0	57.35	-54.23669	2.01	A"
				-54.29859	3.0	1A"
1.0	10.0	9.0	0.0	-54.29859	3.0	1A"
				-54.23272	2.01	A"
1.0	10.0	10.0	87.13	-54.29859	3.0	1A"
1.0	10.0	11.0	180.0	-54.12047	2.01	A"
				-54.29858	3.0	1A"
1.0	11.0	10.0	0.0	-54.23430	2.01	A"
				-54.29858	3.0	1A"
1.5	6.0	5.0	42.6	-54.95113	2.9	1A"
1.5	6.0	7.0	126.67	-54.94521	2.98	1A"
1.750000	1.750000	2.0	69.7	-55.04239	2.01	1A"
				-54.94430	2.0	2A"
				-54.84869	2.0	1A'
2.0	1.5	3.5	180.0	-55.13692	2.03	1A"
2.0	2.0	1.0	28.96	-54.75549	2.02	2A"
2.0	1.5	3.5	180.0	-54.75783	2.0	A'

2.0	2.0	1.0	28.96	-54.59229	2.0	3A"
2.0	2.0	1.5	44.05	-55.00953	2.01	1A"
				-54.93010	2.02	2A"
				-54.84213	2.0	1A'
				-54.61784	2.0	3A"
2.0	2.0	2.0	60.0	-55.02953	2.02	1A"
				-55.01744	2.01	2A"
				-54.88993	2.01	1A'
2.0	2.0	2.5	77.36	-55.10452	2.02	1A"
				-55.00744	2.01	2A"
				-54.91427	2.01	1A'
				-54.86081	2.0	A'
				-54.26790	2.0	A'
2.0	2.0	3.0	97.18	-54.98567	2.01	2A"
				-54.92524	2.01	1A'
				-55.16056	2.02	1A"
2.0	2.0	3.5	122.09	-55.19620	2.02	1A"
				-54.94444	2.01	2A"
				-54.74549	2.0	A'
				-54.56814	2.0	A'
2.0	2.0	4.0	180.0	-55.20663	2.03	1A"
2.0	2.5	4.5	180.0	-55.17032	2.06	1A"
				-54.87794	2.0	1A'
				-54.88293	2.0	A'
				-54.77977	3.01	A"
2.0	2.750000	4.750000	180.0	-55.14612	2.09	1A"
				-54.87271	2.01	A'
2.0	3.0	1.0	0.0	-54.95082	2.04	1A"
2.0	3.0	2.0	41.41	-55.02430	2.16	1A"

2.0	3.0	3.0	70.53	-55.03061	2.52	1A"
				-55.02899	2.05	1A'
2.0	3.0	4.0	104.48	-55.09151	2.11	1A"
2.0	3.0	5.0	180.0	-55.12336	2.15	1A"
				-54.86561	2.01	A'
2.0	3.5	5.5	180.0	-55.08666	2.33	1A"
				-54.85142	2.0	A'
2.0	4.0	2.0	0.0	-55.04576	2.65	1A"
2.0	4.0	3.0	46.57	-55.02466	2.86	1A"
				-54.99629	2.34	A"
2.0	4.0	4.0	75.52	-55.02922	2.89	1A"
				-55.00584	2.13	A"
2.0	4.0	5.0	108.21	-55.04462	2.73	1A"
2.0	4.0	6.0	180.0	-55.06136	2.55	1A"
2.0	5.0	3.0	0.0	-55.03865	2.89	1A"
2.0	5.0	4.0	49.46	-55.02786	2.97	1A"
2.0	5.0	5.0	78.46	-55.02825	2.93	1A"
				-54.99326	2.34	A"
2.0	5.0	6.0	110.49	-55.03129	2.94	1A"
2.0	5.0	7.0	180.0	-55.03562	2.87	1A"
2.0	6.0	4.0	0.0	-55.03156	2.97	1A"
2.0	6.0	5.0	51.32	-55.02768	3.0	1A"
2.0	6.0	6.0	80.41	-55.02740	3.0	1A"
				-54.98912	2.42	A"
2.0	6.0	7.0	112.02	-55.02789	2.99	1A"
2.0	6.0	8.0	180.0	-55.02867	2.98	1A"
2.0	7.0	5.0	0.0	-55.02844	3.0	1A"
2.0	7.0	6.0	52.62	-55.02721	3.0	1A"
2.0	7.0	7.0	81.79	-55.02706	3.0	1A"

2.0	7.0	8.0	113.13	-55.02712	3.0	1A"
2.0	7.0	9.0	180.0	-55.02725	3.0	1A"
2.0	8.0	6.0	0.0	-55.02735	3.0	1A"
2.0	8.0	7.0	53.58	-55.02700	3.0	1A"
2.0	8.0	8.0	82.82	-55.02694	3.0	1A"
2.0	8.0	9.0	113.97	-55.02695	3.0	1A"
2.0	8.0	10.0	180.0	-55.02697	3.0	1A"
2.0	9.0	7.0	0.0	-55.02703	3.0	1A"
2.0	9.0	8.0	54.31	-55.02693	3.0	1A"
2.0	9.0	9.0	83.62	-54.95491	2.02	A"
				-55.02691	3.0	1A"
2.0	9.0	10.0	114.62	-55.02691	3.0	1A"
2.0	10.0	8.0	0.0	-55.02693	3.0	1A"
2.0	10.0	9.0	54.9	-55.02690	3.0	1A"
2.250000	2.250000	1.5	38.94	-55.03922	2.01	1A"
				-54.89620	2.02	2A"
2.250000	2.250000	2.0	52.78	-55.04019	2.01	1A"
				-54.98208	2.03	2A"
				-54.88293	2.01	1A'
				-54.68606	2.0	A'
2.5	2.5	1.5	34.92	-55.05038	2.02	1A"
				-54.85857	2.03	3A"
2.5	2.5	2.0	47.16	-55.04413	2.02	1A"
				-54.92683	2.03	2A"
				-54.86071	2.02	2A'
2.5	2.5	5.0	180.0	-55.13516	2.07	1A"
				-54.89011	2.04	A"
				-54.87451	2.0	A'
				-54.78505	3.0	A"

				-54.51101	2.0	A′
				-54.40966	2.01	A"
2.750000	2.750000	1.5	31.65	-55.05316	2.04	1A"
				-54.83275	2.04	3A"
2.750000	2.750000	2.0	42.65	-55.04258	2.07	1A"
				-54.38259	2.03	3A"
				-54.84138	2.04	2A′
3.0	3.0	1.0	19.19	-54.98026	2.02	1A"
3.0	3.0	1.5	28.96	-55.05153	2.05	1A"
				-54.95022	2.01	1A′
				-54.94629	2.01	2A"
				-54.81981	2.04	A"
3.0	3.0	2.0	38.94	-55.03960	2.18	1A"
3.0	3.0	3.0	60.0	-54.98688	2.25	1A"
				-54.98026	2.02	A"
3.0	3.0	4.0	83.62	-54.98072	2.37	1A"
				-54.95024	2.11	2A"
3.0	3.0	5.0	112.89	-54.92888	3.32	A"
				-55.01961	2.21	1A"
3.0	3.0	6.0	180.0	-55.04174	2.17	1A"
				-54.85080	3.0	2A"
				-54.83170	2.0	A"
3.0	4.0	1.0	0.0	-54.97534	2.02	1A"
3.0	4.0	1.5	18.57	-55.04305	2.24	1A"
3.0	4.0	2.0	28.96	-55.00366	2.49	1A"
3.0	4.0	3.0	48.19	-54.99540	2.69	1A"
3.0	4.0	4.0	67.98	-54.95636	2.49	2A"
				-54.94344	2.42	A"
				-54.97738	2.87	1A"

3.0	4.0	5.0	90.0	-54.94783	2.48	A"
				-54.97890	2.89	1A"
				-54.94783	2.49	2A"
3.0	4.0	6.0	117.28	-54.98535	2.81	1A"
3.0	4.0	7.0	180.0	-54.99316	2.73	1A"
3.0	5.0	2.0	0.0	-55.03912	2.66	1A"
3.0	5.0	3.0	33.56	-55.00359	2.8	1A"
3.0	5.0	4.0	53.13	-54.98219	2.91	1A"
3.0	5.0	5.0	72.54	-54.97696	2.97	1A"
3.0	5.0	6.0	93.82	-54.97703	2.98	1A"
3.0	5.0	7.0	120.0	-54.97828	2.96	1A"
3.0	5.0	8.0	180.0	-54.98006	2.94	1A"
3.0	6.0	3.0	0.0	-55.00860	2.85	1A"
3.0	6.0	4.0	36.34	-54.98538	2.93	1A"
3.0	6.0	5.0	56.25	-54.97791	2.98	1A"
3.0	6.0	6.0	75.52	-54.97644	3.0	1A"
3.0	6.0	7.0	96.38	-54.97637	3.0	1A"
3.0	6.0	8.0	121.86	-54.97658	3.0	1A"
3.0	6.0	9.0	180.0	-54.97693	2.99	1A"
3.0	7.0	4.0	0.0	-54.98736	2.94	1A"
3.0	7.0	5.0	38.21	-54.97859	2.98	1A"
3.0	7.0	6.0	58.41	-54.97656	3.0	1A"
3.0	7.0	7.0	77.63	-54.97619	3.0	1A"
3.0	7.0	8.0	98.21	-54.97615	3.0	1A"
3.0	7.0	9.0	123.2	-54.97618	3.0	1A"
3.0	7.0	10.0	180.0	-54.97625	3.0	1A"
3.0	8.0	5.0	0.0	-54.97906	2.99	1A"
3.0	8.0	6.0	39.57	-54.97667	3.0	1A"
3.0	8.0	7.0	60.0	-54.97618	3.0	1A"

3.0	8.0	11.0	180.0	-54.97610	3.0	1A"
3.0	9.0	7.0	40.6	-54.97606	3.0	1A"
3.0	9.0	6.0	0.0	-54.97676	3.0	1A"
3.0	10.0	7.0	0.0	-54.97622	3.0	1A"
3.0	10.0	13.0	180.0	-54.97605	3.0	1A"
3.0	11.0	8.0	0.0	-54.97609	3.0	1A"
3.0	12.0	9.0	0.0	-54.97606	3.0	1A"
3.0	13.0	10.0	0.0	-54.97605	3.0	1A"
3.0	15.0	12.0	0.0	-54.97605	3.0	1A"
3.9	4.0	5.0	78.52	-54.93673	2.89	1A"
4.0	2.645751	3.0	48.59	-55.00898	2.73	1A"
4.0	3.464102	2.0	30.0	-55.02603	2.48	1A"
4.0	3.900804	5.934330	97.36	-54.93787	2.9	1A"
4.0	4.0	1.0	14.36	-54.96996	2.01	1A"
				-54.95364	2.0	1A'
4.0	4.0	1.5	21.61	-55.02942	2.07	1A"
				-55.00056	2.01	1A'
				-55.00004	2.01	2A"
4.0	4.0	1.750000	25.27	-55.02492	2.31	1A"
				-54.98597	2.01	1A'
				-54.82724	2.01	2A'
4.0	4.0	2.0	28.96	-55.01720	2.54	1A"
				-54.83120	2.01	2A'
				-54.96409	2.01	1A'
4.0	4.0	2.5	36.42	-54.99687	2.71	1A"
				-54.91638	2.01	1A'
				-54.82328	2.01	2A'
4.0	4.0	3.0	44.05	-54.97548	2.75	1A"
				-54.87473	2.02	1A'

				-54.81119	2.01	2A'
4.0	4.0	4.0	60.0	-54.94152	2.79	1A"
4.0	4.0	5.0	77.36	-54.90355	2.91	2A"
				-54.91905	2.82	1A"
4.0	4.0	6.0	97.18	-54.90474	2.87	2A"
				-54.91753	2.86	1A"
4.0	4.0	7.0	122.09	-54.89536	2.93	2A"
				-54.92505	2.86	1A"
4.0	4.0	8.0	180.0	-54.93014	2.72	1A"
				-54.82647	3.0	A"
4.0	5.0	1.0	0.0	-54.96633	2.0	1A"
				-54.95816	2.0	1A'
4.0	5.0	1.5	14.36	-55.02043	2.05	1A"
4.0	5.0	2.0	22.33	-55.00928	2.7	1A"
4.0	5.0	3.0	36.87	-54.97457	2.86	1A"
4.0	5.0	4.0	51.32	-54.94502	2.82	1A"
4.0	5.0	5.0	66.42	-54.93422	2.96	1A"
4.0	5.0	6.0	82.82	-54.93284	2.98	1A"
				-54.90836	2.91	2A"
4.0	5.0	7.0	101.54	-54.93297	2.98	1A"
				-54.90577	2.9	2A"
4.0	5.0	8.0	125.1	-54.93346	2.98	1A"
4.0	5.0	9.0	180.0	-54.93419	2.97	1A"
4.0	6.0	2.0	0.0	-55.00762	2.79	1A"
4.0	6.0	3.0	26.38	-54.97560	2.9	1A"
4.0	6.0	4.0	41.41	-54.94732	2.92	1A"
4.0	6.0	5.0	55.77	-54.93509	2.97	1A"
4.0	6.0	6.0	70.53	-54.93293	3.0	1A"
4.0	6.0	7.0	86.42	-54.93259	3.0	1A"

4.0	6.0	8.0	104.48	-54.93259	3.0	1A"
4.0	6.0	9.0	127.17	-54.93268	3.0	1A"
4.0	6.0	10.0	180.0	-54.93283	3.0	1A"
4.0	7.0	3.0	0.0	-54.97677	2.92	1A"
4.0	7.0	4.0	28.96	-54.94860	2.94	1A"
4.0	7.0	5.0	44.42	-54.93558	2.98	1A"
4.0	7.0	6.0	58.81	-54.93302	3.0	1A"
4.0	7.0	7.0	73.4	-54.93254	3.0	1A"
4.0	7.0	8.0	88.98	-54.93246	3.01	1A"
4.0	7.0	9.0	106.6	-54.93246	3.01	1A"
4.0	7.0	10.0	128.68	-54.93248	3.01	1A"
4.0	7.0	11.0	180.0	-54.93250	3.01	1A"
4.0	8.0	4.0	0.0	-54.94953	2.94	1A"
4.0	8.0	5.0	30.75	-54.93589	2.98	1A"
4.0	8.0	6.0	46.57	-54.93308	3.0	1A"
4.0	8.0	7.0	61.03	-54.93254	3.01	1A"
4.0	8.0	8.0	75.52	-54.93243	3.01	1A"
4.0	8.0	9.0	90.9	-54.93241	3.01	1A"
4.0	8.0	10.0	108.21	-54.93241	3.01	1A"
4.0	9.0	5.0	0.0	-54.93617	2.98	1A"
4.0	9.0	6.0	32.09	-54.93313	3.0	1A"
4.0	9.0	7.0	48.19	-54.93254	3.0	1A"
4.0	9.0	8.0	62.72	-54.93242	3.01	1A"
4.0	9.0	9.0	77.16	-54.93240	3.01	1A"
4.0	9.0	10.0	92.39	-54.93240	3.01	1A"
4.0	10.0	6.0	0.0	-54.93318	3.0	1A"
4.0	10.0	7.0	33.12	-54.93255	3.01	1A"
4.0	10.0	8.0	49.46	-54.93242	3.01	1A"

4.0	10.0	7.0	33.12	-54.93256	3.0	1A"
4.1	4.0	5.0	76.22	-54.93328	2.91	1A"
5.0	5.0	1.0	11.48	-54.96325	2.0	1A"
5.0	5.0	1.5	17.25	-55.01397	2.01	1A"
				-55.00718	2.01	1A'
				-55.00704	2.0	2A"
5.0	5.0	2.0	23.07	-54.99721	2.87	1A"
5.0	5.0	3.0	34.92	-54.96745	2.94	1A"
				-54.87450	2.01	1A'
				-54.69327	2.87	A'
5.0	5.0	4.0	47.16	-54.93841	2.95	1A"
5.0	5.0	5.0	60.0	-54.91916	2.96	1A"
				-54.85288	2.92	A"
				-54.83980	3.0	A"
				-54.78830	2.01	A'
5.0	5.0	8.0	106.26	-54.85366	2.96	A"
				-54.85104	2.93	A"
5.0	6.0	1.0	0.0	-54.96250	2.0	1A"
				-54.96099	2.0	2A"
5.0	6.0	1.5	11.72	-55.01731	2.0	1A"
5.0	6.0	2.0	18.19	-54.99392	2.94	1A"
5.0	6.0	3.0	29.93	-54.94810	2.99	1A"
5.0	6.0	4.0	41.41	-54.93795	2.98	1A"
5.0	6.0	6.0	65.38	-54.90981	2.99	1A"
5.0	6.0	7.0	78.46	-54.90871	3.0	1A"
5.0	7.0	2.0	0.0	-54.99329	2.96	1A"
5.0	7.0	3.0	21.79	-54.96595	2.98	1A"
5.0	7.0	4.0	34.05	-54.93803	2.98	1A"
5.0	7.0	5.0	45.57	-54.91965	2.99	1A"

4.0	10.0	7.0	33.12	-54.93256	3.0	1A"
4.1	4.0	5.0	76.22	-54.93328	2.91	1A"
5.0	5.0	1.0	11.48	-54.96325	2.0	1A"
5.0	5.0	1.5	17.25	-55.01397	2.01	1A"
				-55.00718	2.01	1A'
				-55.00704	2.0	2A"
5.0	5.0	2.0	23.07	-54.99721	2.87	1A"
5.0	5.0	3.0	34.92	-54.96745	2.94	1A"
				-54.87450	2.01	1A'
				-54.69327	2.87	A'
5.0	5.0	4.0	47.16	-54.93841	2.95	1A"
5.0	5.0	5.0	60.0	-54.91916	2.96	1A"
				-54.85288	2.92	A"
				-54.83980	3.0	A"
				-54.78830	2.01	A'
5.0	5.0	8.0	106.26	-54.85366	2.96	A"
				-54.85104	2.93	A"
5.0	6.0	1.0	0.0	-54.96250	2.0	1A"
				-54.96099	2.0	2A"
5.0	6.0	1.5	11.72	-55.01731	2.0	1A"
5.0	6.0	2.0	18.19	-54.99392	2.94	1A"
5.0	6.0	3.0	29.93	-54.94810	2.99	1A"
5.0	6.0	4.0	41.41	-54.93795	2.98	1A"
5.0	6.0	6.0	65.38	-54.90981	2.99	1A"
5.0	6.0	7.0	78.46	-54.90871	3.0	1A"
5.0	7.0	2.0	0.0	-54.99329	2.96	1A"
5.0	7.0	3.0	21.79	-54.96595	2.98	1A"
5.0	7.0	4.0	34.05	-54.93803	2.98	1A"
5.0	7.0	5.0	45.57	-54.91965	2.99	1A"

5.0	8.0	3.0	0.0	-54.96607	2.99	1A"
5.0	8.0	4.0	24.15	-54.93817	2.99	1A"
5.0	8.0	6.0	48.51	-54.91028	2.99	1A"
5.0	8.0	7.0	60.0	-54.90880	3.0	1A"
5.0	9.0	4.0	0.0	-54.93834	2.99	1A"
5.0	9.0	5.0	25.84	-54.91998	2.99	1A"
5.0	10.0	6.0	27.13	-54.91046	2.99	1A"
5.0	10.0	7.0	40.54	-54.90882	3.0	1A"
5.0	11.0	6.0	0.0	-54.91053	2.99	1A"
6.0	6.0	1.0	9.56	-54.96124	2.0	1A"
6.0	6.0	1.5	14.36	-55.00860	2.0	1A"
6.0	6.0	2.0	19.19	-54.99044	2.98	1A"
				-54.97294	2.06	2A"
				-54.95871	2.0	3A"
6.0	6.0	3.0	28.96	-54.96398	2.99	1A"
6.0	6.0	4.0	38.94	-54.80240	2.01	A"
				-54.93631	2.99	1A"
6.0	6.0	5.0	49.25	-54.91798	2.99	1A"
6.0	7.0	1.0	0.0	-54.96121	2.0	1A"
				-54.96092	2.0	2A"
6.0	7.0	2.0	15.36	-54.96837	2.0	1A'
6.0	7.0	1.5	9.9	-55.00774	2.0	1A"
6.0	7.0	2.0	15.36	-54.97032	2.02	A"
6.0	7.0	3.0	25.21	-54.96340	3.0	1A"
				-54.89805	2.67	A'
6.0	7.0	4.0	34.77	-54.88338	2.93	A'
				-54.93590	3.0	1A"
6.0	7.0	5.0	44.42	-54.84539	2.99	A"
				-54.91760	3.0	1A"

6.0	8.0	2.0	0.0	-54.96970	2.02	2A"
6.0	8.0	3.0	18.57	-54.89914	2.68	A'
				-54.89714	2.68	A"
				-54.96323	3.0	1A"
6.0	8.0	4.0	28.96	-54.93577	3.0	1A"
				-54.86262	3.0	A"
6.0	8.0	5.0	38.62	-54.91759	3.0	1A"
				-54.83740	2.98	A'
6.0	9.0	3.0	0.0	-54.89728	2.68	A"
				-54.96320	3.0	1A"
6.0	9.0	4.0	20.74	-54.93573	3.0	1A"
				-54.88462	2.92	3A"
				-54.83169	2.98	A'
6.0	9.0	5.0	31.59	-54.91755	3.0	1A"
				-54.88074	2.99	A'
6.0	10.0	4.0	0.0	-54.93572	3.0	1A"
				-54.78911	2.0	A"
7.0	7.0	1.0	8.19	-54.96076	2.01	1A"
				-54.96069	2.0	1A'
				-54.96068	2.0	2A"
7.0	7.0	1.5	12.3	-55.00716	2.0	1A"
				-54.96923	2.98	3A"
7.0	7.0	2.0	16.43	-54.96892	2.01	2A"
7.0	7.0	3.0	24.75	-54.96269	3.0	1A"
				-54.88936	3.0	A"
				-54.80613	3.0	A'
				-54.81662	2.0	A'
7.0	7.0	4.0	33.2	-54.93532	3.0	1A"
				-54.86264	3.0	A"

				-54.83009	2.25	A′
				-54.79297	2.01	1A′
				-54.69758	2.94	A′
7.0	7.0	5.0	41.85	-54.91726	3.0	1A"
				-54.83652	3.0	A′
				-54.75687	2.0	A′
7.0	7.0	6.0	50.75	-54.90677	3.0	1A"
7.0	7.0	7.0	60.0	-54.90148	3.0	1A"
7.0	8.0	1.5	8.57	-55.00675	2.0	1A′
				-55.00688	2.0	1A"
7.0	8.0	1.0	0.0	-54.96075	2.0	1A"
7.0	8.0	2.0	13.29	-54.96825	2.0	1A"
7.0	8.0	3.0	21.79	-54.96245	3.0	1A"
				-54.89736	2.68	A"
				-54.89711	2.66	A′
7.0	8.0	4.0	29.99	-54.93511	3.0	1A"
				-54.83027	3.0	A′
				-54.78995	2.0	A′
7.0	8.0	5.0	38.21	-54.91702	3.0	1A"
				-54.88108	2.99	A′
				-54.83650	3.0	A′
7.0	8.0	8.0	64.06	-54.89895	3.0	1A"
				-54.88092	3.0	A′
7.0	9.0	2.0	0.0	-54.98821	3.0	1A"
				-54.96787	2.01	2A"
				-54.96755	2.0	1A′
7.0	9.0	2.5	10.84	-54.92029	2.34	1A′
				-54.91543	2.0	A′
				-54.92014	2.31	A′

7.0	9.0	3.0	16.2	-54.89730	2.68	A'
				-54.89730	2.68	A"
				-54.96235	3.0	1A"
7.0	9.0	4.0	25.21	-54.93501	3.0	1A"
				-54.86198	3.0	A"
				-54.88473	2.93	A"
7.0	9.0	5.0	33.56	-54.91693	3.0	1A"
				-54.88124	2.99	A"
				-54.84412	3.0	A"
				-54.83657	3.0	A'
7.0	10.0	3.0	0.0	-54.96231	3.0	1A"
				-54.89739	2.69	A'
				-54.89719	2.69	A"
				-54.72866	2.0	A'
7.0	10.0	4.0	18.19	-54.93497	3.0	1A"
				-54.88368	2.93	A'
				-54.86219	3.0	A"
7.0	10.0	5.0	27.66	-54.91688	3.0	1A"
				-54.83666	3.0	A'
7.0	11.0	4.0	0.0	-54.93494	3.0	1A"
				-54.88372	2.93	A'
				-54.75113	2.0	A'
7.0	11.0	5.0	19.69	-54.91685	3.0	1A"
				-54.84406	3.0	A"
				-54.83675	3.0	A'
7.0	12.0	5.0	0.0	-54.91683	3.0	1A"
				-54.84405	3.0	A"
				-54.83682	3.0	A"
8.0	8.0	1.0	7.17	-54.96061	2.0	1A'

8.0	8.0	1.5	10.76	-55.00676	2.0	1A"
				-55.00670	2.0	1A'
				-54.96832	3.0	3A"
8.0	8.0	2.0	14.36	-54.96786	2.0	2A"
8.0	8.0	3.0	21.61	-54.96218	3.0	1A"
				-54.86687	2.0	1A'
8.0	8.0	4.0	28.96	-54.93487	3.0	1A"
				-54.88369	2.93	A"
				-54.83010	3.0	A'
8.0	8.0	5.0	36.42	-54.91681	3.0	1A"
				-54.83635	3.0	A'
8.0	9.0	1.0	0.0	-54.96057	2.0	1A'
				-54.96058	2.0	1A"
8.0	9.0	1.5	7.55	-55.00657	2.0	1A'
				-54.96819	3.0	3A"
8.0	9.0	2.0	11.72	-54.96752	2.0	1A'
8.0	9.0	3.0	19.19	-54.88905	3.0	A"
				-54.96206	3.0	1A"
				-54.86661	2.0	1A'
8.0	9.0	4.0	26.38	-54.86078	3.0	A"
				-54.83081	3.0	A'
8.0	9.0	5.0	33.56	-54.91670	3.0	1A"
				-54.88122	2.99	A"
8.0	10.0	2.0	0.0	-54.98780	3.0	1A"
				-54.96727	2.0	3A"
8.0	10.0	3.0	14.36	-54.96201	3.0	1A"
				-54.89698	2.68	A'
8.0	10.0	4.0	22.32	-54.83038	3.0	A'
				-54.93471	3.0	1A"

				-54.83032	3.0	A'
8.0	10.0	5.0	29.69	-54.88104	2.99	A'
8.0	11.0	3.0	0.0	-54.89698	2.69	A'
				-54.96197	3.0	$1A''$
8.0	11.0	4.0	16.21	-54.93467	3.0	$1A''$
				-54.79109	2.0	A'

† The column labelled state is the representation, under the C_s point group to which the wavefunction belongs (A' or A''). The number prefixing the state denotes the order of the states with regard to energy, viz. 1 is the ground state etc. Where a prefix is absent insufficient information is available to make a definite assignment, this does not imply that the state is the ground state.

				-54.83032	3.0	A'
8.0	10.0	5.0	29.69	-54.88104	2.99	A'
8.0	11.0	3.0	0.0	-54.89698	2.69	A'
				-54.96197	3.0	1A"
8.0	11.0	4.0	16.21	-54.93467	3.0	1A"
				-54.79109	2.0	A'

† The column labelled state is the representation, under the C_s point group to which the wavefunction belongs (A' or A"). The number prefixing the state denotes the order of the states with regard to energy, viz. 1 is the ground state etc. Where a prefix is absent insufficient information is available to make a definite assignment, this does not imply that the state is the ground state.

APPENDIX E.

CI energies for NH_2^+.

(all items in atomic units)

C_{2v} Geometries.

R(NH)	R(HH)	$E(^3B_1)$	$E(^3B_2)$	$E(^3A_2)$
1.5	2.0	-55.02208	-54.69553	-54.81334
1.5	2.5	-55.09772	-54.69520	-
1.5	3.0	-55.12554	-	-
1.52	1.5	-54.91611	-54.68277	-54.83779
1.60078	2.5	-55.15134	-	-54.88274
1.625	1.25	-54.88862	-	-54.90386
1.73656	1.75	-55.05717	-	-55.00302
1.82003	3.5	-55.26520	-	-55.19974
1.86278	3.0	-55.24116	-	-55.17260
1.75	2.0	-55.10917	-54.85364	-55.00427
2.0	1.25	-54.93643	-54.83493	-54.98682
2.0	1.5	-55.00685	-54.85721	-55.05662
2.0	2.0	-55.16067	-54.89995	-55.19909
2.0	2.5	-55.17954	-54.90322	-55.17941
2.0	3.0	-55.13260	-54.90333	-55.13003
2.0	3.5	-55.20604	-54.90790	-55.20452
2.0	4.0	-55.27439	-54.88888	-55.23899
2.06155	4.0	-55.27307	-	-55.26674
2.09538	1.25	-54.93077	-	-54.97268
2.12132	3.0	-55.21356	-	-55.18509
2.18503	1.75	-55.03899	-	-55.03376
2.23607	4.0	-55.25082	-	-55.23867
2.25	1.5	-54.97954	-54.86581	-54.97669

2.25	2.0	-55.06922	-54.89798	-55.11934
2.30489	3.5	-55.21313	-	-55.07723
2.35856	2.5	-55.11279	-	-55.11253
2.5	1.5	-54.94521	-54.93509	-55.12708
2.5	2.0	-55.02190	-54.90988	-55.12670
2.5	2.5	-55.08171	-54.89798	-55.11260
2.5	3.0	-55.13007	-54.91640	-55.09932
2.5	3.5	-55.16752	-54.93201	-55.08481
2.57694	1.25	-54.93846	-	-55.10793
2.61008	1.5	-54.94683	-	-55.12903
2.64870	1.75	-54.96379	-	-55.13183
2.75	1.5	-54.97378	-54.98643	-55.12941
2.75	2.0	-54.97812	-54.95884	-55.12510
2.79508	2.5	-55.02052	-	-55.10501
2.85048	1.5	-54.98975	-	-55.12859
3.0	1.5	-55.00884	-55.01699	-55.12613
3.0	2.0	-54.97620	-54.99119	-55.11957
3.0	3.0	-55.02368	-54.92352	-55.07807
3.0	2.5	-54.98492	-54.95357	-
3.06481	1.25	-55.01123	-	-55.10630
3.175	1.75	-55.00868	-	-55.12360
3.5	1.5	-55.04408	-55.05171	-55.11223
3.5	2.0	-55.01384	-55.02431	-55.10295
3.5	2.5	-54.97294	-	-55.07850
3.54	5.0	-55.02525	-54.89996	-
4.0	1.5	-55.05617	-55.06348	-55.09692
4.0	2.0	-55.02618	-55.03558	-55.08499
4.47	8.0	-54.96819	-	-
5.0	1.5	-55.05931	-55.06768	-55.07627

5.0	2.0	-55.02734	-55.03784	-55.05659
6.0	1.25	-55.05377	-55.06218	-55.06313
6.0	1.5	-55.05377	-	-55.06890
6.0	2.0	-55.02465	-55.03629	-55.04184
6.0	2.5	-54.97993	-54.99530	-55.01098
6.0	3.0	-54.94077	-54.96126	-54.99796
6.0	3.5	-54.91039	-54 91164	-54.97026
6.0	4.0	-54.88828	-54.89228	-54.95649
17.0	20.0	-54.80494	-54.81574	-54.90634

Linear NHH geometries.

R(NH)	R(HH)	$E(^3\Sigma^-)$	$E(^3\pi)$
1.5	1.25	-54.94271	-
1.5	1.5	-54.96976	
1.5	2.0	-54.98386	-
1.5	2.5	-54.98328	-
1.5	3.0	-54.98033	-
1.5	3.5	-54.97752	-
1.5	4.0	-54.97530	-
1.5	5.0	-54.97265	-
1.75	2.5	-55.07004	-
1.75	3.0	-55.06107	-
2.0	1.25	-55.08782	-
2.0	1.5	-55.10873	-54.99630
2.0	2.0	-55.11170	-
2.0	2.5	-55.09912	-
2.0	3.0	-55.08659	-
2.0	3.5	-55.07708	-
2.0	4.0	-55.07056	-
2.0	5.0	-54.06406	-
2.5	1.25	-55.10727	-
2.5	1.5	-55.12544	-55.04050
2.5	2.0	-55.12045	-
2.5	2.5	-55.10128	-
2.5	3.0	-55.08314	-
2.5	3.5	-55.06928	-
2.5	4.0	-55.05962	-
2.5	5.0	-55.04977	-

3.0	1.25	-55.09743	-
3.0	1.5	-55.11302	-55.05498
3.0	2.0	-55.10411	-
3.0	2.5	-55.08803	-
3.0	3.0	-55.06400	-
3.5	1.25	-55.08432	-
3.5	1.5	-55.09739	-55.06100
4.0	1.25	-55.07456	-
4.0	1.5	-55.08496	-55.06355
4.0	2.0	-55.06948	-
5.0	1.25	-55.06531	-
5.0	1.5	-55.07176	-55.06431
5.0	2.0	-55.04849	

REFERENCES

[1]. H.E.Perry & W.L.Thompson. [illegible] Phys.,66,2545,(1977)

[2]. D.R.Bates & A.E.G.Reid. Adv.At.Mol.Phys.,4,13,(1968)

[3]. C.F.Roothaan, [illegible] & H.F.Schaefer.
Far.Disc.Chem.Soc.,62, [illegible] 49,(1977)

[4]. N.C.Blais & D.G.Truhlar. J.Chem.Phys.,41,2377,(1964)

[5]. N.C.Blais & D.G.Truhlar. J.Chem.Phys.,58,1090,(1973)

[6]. N.C.Blais & D.G.Truhlar. J.Chem.Phys. 61,4186,(1974),[ecratum
65,2303,(1976)].

[7]. N.C.Blais & D.G.Truhlar. J.Chem.Phys.,66,772,(1977)

[8]. J.M.Bowman, A.Kuppermann & G.C.Shatz. Chem.Phys,Lett.,19,21,(1973)

[9]. J.M.Bowman, S.C.Leasure & A.Kuppermann.
Chem.Phys.Lett.,43,375,(1976)

[10]. C.G.Broyden. Math.Comp.,24,365,(1970)

[11]. D.L.Bunker & C.A.Parr. J.Chem.Phys.,52,5709,(1970)

[12]. P.M.Careless & D.Lyatt. Chem.Phys.Lett.,14,358,(1972)

[13]. J.K.Cashion & D.R.Herschbach. J.Chem.Phys.,40,2358,(1964)

[14]. A.Cauchy. C.R.Acad.Sci.Paris,25,536,(1847)

[15]. T.Y.Cheng. Private communication.

[16]. B.H.Choi & Tang. J.Chem.Phys.,63,2854,(1975)

[17]. S.I.Chu,A.C.Q.Cha & E.H.Hayes. J.A.C.S.,94,2069,(1972)

[18]. A.G.Clarke & G.Burns. J.Chem.Phys.,55,4717,(1971)

[19]. A.G.Clarke & G.Burns. J.Chem.Phys.,58,1908,(1973)

[20]. R.Colin & A.E.Douglas. Can.J.Phys.,46,61,(1968)

[21]. H.W.Crowe,P.J.Dagdigian & R.N.Zare. Far.Disc.Chem.Soc.,55,277
,(1973)

[22]. L.C.Colzmadu, J.C.Polanyi, A.C.Roach & W.H.Wong. Can.J.Chem.,

47,4027,(1969)

[23]. G.H.F.Diercksen. Theor. Chim. Acta. 33,1, (1974)

[24]. C.W.Baker & C.A.Parr. J.Chem.Phys. 64, 1322, (1976)

[25]. F.O.Ellison. J.A.C.S. 85, 3540, (1963)

[26]. F.O.Ellison & J.C.Patel. J.A.C.S. 86, 2115, (1964)

[27]. J.A.Weil & B.H.Mahan J.Chem.Phys 62, 515, (1975)

[28]. J.M.Farrar,S.G.Hanson & B.H.Mahan. J.Chem.Phys.,65,2908,(1976)

[29]. K.Fielding. Collected Algorithms From C.A.C.M., No.397,(1969)

[30]. R.Fletcher & C.M.Reeves. Comput. J.,7,149,(1964)

[31]. R.Fletcher. U.K.A.E.A. Research Group Report No.AERE-R6799,(1971)

[32]. G.E.Forsythe & T.S.Motzkin. Bull.Amer.Math.Soc.,57,183,(1951)

[33]. S.M.Goldfeld,R.E.Quandt & H.F.Trotter,Econometrica,34,541,(1966)

[34]. M.A.Gislason, B.H.Mahan, C-W.Tsao & A.S.Werner. J.Chem.Phys,54,3897,(1971)

[35]. M.A.Gitcins & D.M.Hirst. Chem.Phys.Lett.,35,534,(1975)

[36]. M.A.Gitcins, D.M.Hirst & M.F.Guest. Far.Disc.Chem.Soc.,62, 67,(1977)

[37] A.A.Goldstein. Numer. Math.,4,146,(1962)

[38]. H.Goldstein. Classical Mechanics ,Addison-Wesley,Reading (Mass),(1950)

[39]. S.K.Gray & J.S.Wright. J.Chem.Phys.,66,2867,(1977)

[40]. A.R.Gregory. Chem. Phys. Lett., 11,(1971)

[41]. T.N.E Grenville (Ed.). Theory and applications of spline functions , Academic,New York, (1969)

[42]. M.F.Guest & V.R.Saunders. SPLICE.,S.R.C.,Atlas Computing Division, R.H.E.L..

[43]. M.F.Guest & D.M.Hirst. Mol. Phys. ,34,1611, (1977)

[44]. M.F.Guest & D.M.Hirst. Private communication

[45]. J.M.Hammersley & D.C.Handscomb. Monte Carlo Methods ,Wiley&Sons, New York,(1964)

[46]. J.F.Harrison & C.W.Eaker. J.A.C.S.,95,3467,(1973)

[47]. E.Herbst. Chem.Phys.Lett.,47,517,(1977)

[48]. R.E.Howard, A.C.Yates & W.A.Lester. J.Chem.Phys.,66,1960,(1977)

[49]. A.C.Hurley. Introduction to the Electron Theory of small Molecules. Academic Press, London. (1976) .

[50]. R.L.Jaffe & A.B.Anderson. J.Chem.Phys.,54,2224,(1971)

[51]. T.L.Jordan, Smoothing and multivariate interpolation with splines, Los Alamos Scientific Laboratory Report LA-3137,(1965)

[52]. J.Karplus & L.M.Raff. J.Chem.Phys.,41,1267,(1964)

[53]. M.Karplus, R.N.Porter& R.D.Sharma. J.Chem.Phys.,43,3259,(1965)

[54]. W.Kolos & L.Wolniewicz. J.Chem.Phys.,43,2429,(1965)

[55]. H.Kreek & R.A.Marcus. J.Chem.Phys.,61,3308.(1974)

[56]. J.R.Krenos, R.K.Preston, Wolfgang & J.C.Tully. J.Chem.Phys.,60,1634,(1973)

[57]. P.J.Kuntz & A.C.Roach. J.C.S.Far.Trans.2., 68, 43, (1972)

[58]. G.H.Kwei et al., J.Chem.Phys., 58,1722,(1973)

[59]. L.A.LeBuddle & R.A.Bernstein. J.Chem.Phys.,55,5499,(1971)

[60]. L.A.LeBuddle, P.J.Kuntz, R.A.Bernstein& R.D.Levine, C.P.L.,19,7,(1973)

[61]. L.D.Landau & E.M.Lifshitz. Quantum Mechanics (second edition) Pergamon Press,London. (1965)

[62]. S.C.Leasure & J.M.Bowman. J.Chem.Phys.,64,4229,(1976)

[63]. S.T.Lee & K.Morokuma. J.A.C.S.,93,6863,(1971)

[64]. H.P.D.Liu & G.Vethaegen. J.Chem.Phys.,53,735,(1970)

[65]. F.London. Z.Electrochem.,35,552,(1929)

[66]. D.W.Marquardt. J.Soc Appl.Math.,11,431,(1963)

[67]. R.A.Marcus. J.Chem.Phys.,54,3965,(1971)

[68]. R.J.Cvetanovic. [illegible]. 7,1035,(1970)

[69]. D.J.Miller. Chem.Phys.Lett., 7,431,(1970)

[70]. W.H.Miller. J.Chem.Phys., 54,1643,(1970)

[71]. W.H.Miller. Acc.Chem.Res., 4,161,(1971)

[72]. C.E.Moore. Atomic Energy Levels. NBS circular No. 407.,(U.S. Govt. Printing Off. Washington D.C.) (1949)

[73]. D.R.McLaughlin & D.L.Thompson. J.Chem.Phys., 59, 4393, (1973)

[74]. J.T.Muckerman. J.Chem.Phys., 54,1155,(1971)

[75]. J.T.Muckerman. J.Chem.Phys., 56,2997,(1972)

[76]. J.T.Muckerman. J.Chem.Phys., 57,3388,(1972)

[77]. J.N.Murrell, K.S.Sorbie & A.J.C.Varandas. Mol.Phys., 32,1359,(1976)

[78]. NAG Library Manual. (Mk 8), NAG Ltd.,(1976)

[79]. J.A.Nedler & R.Mead. Comput.J., 7,308,(1965).

[80]. C.A.Parr, J.C.Polanyi & W.H.Wong. J.Chem.Phys., 58, 5, (1973)

[81]. P.J.Pearson & R.Roueff. J.Chem.Phys. 64, 1240, (1976)

[82]. L.Pedersen & R.N.Porter. J.Chem.Phys., 50,478,(1969)

[83]. J.M.Peek. J.Chem.Phys., 43,3004,(1965)

[84]. A.Persky. J.Chem.Phys., 66,2932,(1977)

[85]. J.D.Poyerlmeff, R.J.Buenker & L.C.Allen. J.Chem.Phys., 45,736,46,1764,(1970)

[86]. C.V.Pfeiffer, M.T.Huff, L.M.Greenwalt & F.O.Ellison. J.Chem.Phys. 46, 84', (1967)

[87]. J.C.Polanyi & J.L.Schreiber. Chem.Phys.Lett., 29, 319, (1974)

[88]. R.N.Porter & M.Karplus. J.Chem.Phys., 40,1105,(1964)

[89]. R.K.Preston & R.T.Pack. J.Chem.Phys., 66,2480,(1977)

[90]. Quantum Chemistry Program Exchange, Program No. 322, Chemistry department, Indiana University.

[91]. C.C.Rankin & W.H.Miller. J.Chem.Phys., 55,3150,(1971)

[92]. P.[illegible] & [illegible]. J.Chem.Phys.,65,13,(1977)

[93]. M.Rubin. Göttinger Nachr., 247, (1932)

[94]. M.Sathyamurthy & L.M.Raff. J.Chem.Phys.,63,464,(1975)

[95]. S.Sato. Bull.Chem.Soc.Japan.,28,450,(1955)

[96]. S.Sato. J.Chem.Phys.,23,592 & 2465,(1955)

[97]. V.R.Saunders & M.F.Guest. ATMOL3 MANUAL, Atlas computing division,R.R.E.L. [1976].

[98]. H.F.Schaefer & W.A.Lester. Chem.Phys.Lett.,20,575,(1973)

[99]. C.C.Schatz & A.Kuppermann. J.Chem.Phys.,65,4642,(1976)

[100]. D.M.Smith & P.J.Wood. Mol.Phys.,25,441,(1973)

[101]. K.S.Sorbie & J.N.Murrell. Mol.Phys.,22,1387,(1975)

[102]. W.Spendley, G.R.Hext & F.R.Himsworth. Technometrics,4,441,(1962).

[103]. V.Staemmler. Theor. Chim. Acta. 31,39, (1973)

[104]. J.I.Steinfeld. Far.Disc.Chem.Soc.,53,155,(1972)

[105]. J.R.Stine & J.T.Muckerman. J.Chem.Phys.,62,3975,(1976)

[106]. B.T.Sutcliffe & D.Garton. Quantum Chemistry,The State of the Art,SRC ATLAS 4,195,(1974)

[107]. J.C.Tully & R.K.Preston. J.Chem.Phys.,55,562,(1971)

[108]. J.C.Tully. J.Chem.Phys. 58, 1396, (1973)

[109]. J.C.Tully. Berichte der Bunserges.Ges.fur Phys.Chem.,77,397,(1973)

[110]. A.C.Varandas & J.N.Murrell. Far.Disc.Chem.Soc.,62, [illegible],(1976)

[111]. T.E.H.Walker. Chem. Phys. Lett.,9,174,(1971)

[112]. F.T.Wall & R.N.Porter. J.Chem.Phys.,36,3256,(1962)

[113]. J.C.Whitehead. Mol.Phys.,31,549,(1976)

[114]. M.M.Whitton & P.J.Kuntz. J.Chem.Phys.,64,3642,(1976)

[115]. R.L.Wilkins. J.Chem.Phys.,58,3038,(1973)

[116]. R.L.Wilkins. J.Chem.Phys.,58,2326,(1973)

[117]. R.B.Woodward & R.Hoffmann. The Conservation of Orbital Symmetry.,Verlag Chemie,Weinheim/Bergstr.,(1970)

[118]. A.A.Wu & E.O.Ellison. J.Chem.Phys. 48, 727, (1968)

[119]. D.R.Yarkony, S.V.O'Neil, H.F.Schaefer, C.P.Baskin & C.F.Bender J.Chem.Phys.,60,855,(1974)

[120]. A.C.Yates & W.A.Lester. Chem.Phys.Lett.,24,395,(1974)

[121]. D.M.Hirst. Chem.Phys.Lett.,(in press)

[122]. M.H.Alexander & E.V.Benard. J.Chem.Phys.,60,3950,(1974) ,61,3867 & 3868, (1974)

[123]. A.B.Anderson. Chem.Phys.Lett.,18,303,(1973)

[124]. F.H.Dunning. J.Chem.Phys.,53,2823,(1970)